Final Report for NASA Grant No. NSG 5341

(NASA-CR-168964) EVALUATION AND DEVELOPMENT OF SATELLITE INFERENCES OF CONVECTIVE STORM INTENSITY USING COMBINED CASE STUDY AND THUNDERSTORM MODEL SIMULATIONS Final Report, 1 May 1979 - 30 Apr. 1982 (Colorado

N82-24795

HC A05/MF A01

Unclas

G3/47 27916

Evaluation and Development of Satellite Inferences of Convective Storm Intensity Using Combined Case Study and Thunderstorm Model Simulations

William R. Cotton and
Gregory J. Tripoli

May 1, 1979 to April 30, 1982

Prepared for :
National Aeronautics and Space Administration, Washington, DC
Severe Storms Research

COLORADO STATE UNIVERSITY 1870

Final Report for

NASA Grant No. NSG 5341

EVALUATION AND DEVELOPMENT OF SATELLITE INFERENCES OF CONVECTIVE STORM INTENSITY USING COMBINED CASE STUDY ANALYSIS AND THUNDERSTORM MODEL SIMULATIONS

William R. Cotton

and

Gregory J. Tripoli

Co-Principal Investigators

Department of Atmospheric Science
Colorado State University
Fort Collins, CO 80523

May 1, 1979 to April 30, 1982

Prepared for
National Aeronautics and Space Administration, Washington, DC
Severe Storms Research

TABLE OF CONTENTS

SUMMARY

Major research accomplishments under NASA Grant No. NSG 5341 are described in this report. The major conclusions of our research are as follows:

1) Numerical simulation of convective storms in a number of differing environments suggest that the time evolution of storm dynamics and storm movement are sensitive to the description of initial and evolving environmental fields. Also, details in microphysical parameterizations affecting growth of precipitation have a significant influence on the intensity and dynamics of the storm.

2) As a result of our first conclusion we speculate that the consistent accurate production of individual convective clouds will require three-dimensional observations of the environment with detail sufficient to initialize a numerical model on scales of 1 km. over the region to be modeled. Also evolving forcing at the lateral boundaries of a limited area model must be provided in some manner as well.

3) Our simulation of the Heymsfield (1981) Northern Illinois storm has again supported conclusions (1) and (2) although some observed features were simulated.

4) Our past studies in which we have simulated overshooting tops indicate no direct linkage to surface wind gusts. We do find, however, that overshooting tops may lead to strong stretching at mid-levels which may locally enhance entrain-

ment and force a downdraft. Such a downdraft would then lead to surface wind gusts.

5) Our modeling results show a poor correspondence between anvil expansion rate and horizontal velocity divergence.

6) The morphology of mature MCC's have been analyzed and the following features have been documented.

   i) the interaction of the MCC with the remains of the previous day's MCC

   ii) the intrusion of dry, high momentum air into the back of the storm at 500 mb

   iii) a broad region of high momentum outflow from the storm just below the tropopause

   iv) a significant meso-anticyclone at 200 mb which was not present prior to the formation of the MCC

   v) lack of direct interaction with the polar front jet well to the north

   vi) divergence profiles similar to tropical clusters

   vii) virtually no evidence of poleward meridional heat transport associated with the MCC as one would expect in a baroclinic system.

1.0 INTRODUCTION

In this report we summarize major research accomplishments that have been achieved under support of NASA Grant No. NSG 5341. The research has concentrated in the following areas:

i) an examination of observational requirements for predicting convective storm development and intensity as suggested by recent numerical experiments

ii) interpretation of recent 3D numerical experiments with regard to the relationship between overshooting tops and surface wind gusts

iii) the development of software for emulating satellite-inferred cloud properties using 3D cloud model-predicted data

iv) simulation of Heymsfield (1981) Northern Illinois storm

v) the development of a conceptual/semi-quantitative model of eastward propagating, mesoscale convective complexes forming to the lee of the Rocky Mountains.

2.0 OBSERVATIONAL REQUIREMENTS FOR PREDICTING CONVECTIVE STORM DEVELOPMENT INTENSITY AND MOVEMENT AS SUGGESTED BY RECENT NUMERICAL EXPERIMENTS

During the course of this grant we have conducted five case studies of convective storms in 1) a South Florida environment, 2) a hurricane environment, 3) another South Florida environment, 4) the environment of a high altitude plateau, and 5) the environment of the Illinois plains. Unlike investigations such as Klemp and Wilhelmson (1978a,b) Schlesinger (1975); Miller and Thorpe (1978); Miller and Pearce (1974) our studies have dealt with environments of relatively weak shear. As a result we find in general a greater dependence of storm properties on the details of the immediate mesoscale environment before and during the

storm in question. Such mesoscale forced storms usually produce less wind than the highly sheared storms, but may produce similar or higher rainfall amounts. Because these storms are such a strong function of the local environment the thrust of our research over the past four years has dealt with understanding the initialization of these storms.

For the purposes of this grant we have also attempted to make some general conclusions, based on our studies, on what environmental factors must be observed in order to accurately predict storm development and movement. The ultimate goal beyond the scope of this grant would then be to observe the proper variables by satellite with current or future technology and make accurate predictions of storm occurrences.

The first study which we will discuss is our investigation of cumulus initiation in the South Florida environment. This study (Tripoli and Cotton, 1980) demonstrated that cumulonimbus intensity was strongly dependent on mean environmental low level convergence. However it was concluded the structure and movement seemed to be more closely linked to the intensity of the local initiating mechanism. This conclusion is important because it shows that definition of mean convergence and the thermodynamic and wind profiles on the scale of 30-50 km will tell us something about the ultimate intensity of a storm in that environment but the structure and movement is dependent on initial motions on the scale of 1-10 km. We feel such motions are usually the result of previous or concurrent convection near the region in question. Therefore to accurately forecast an individual convective storm in the South Florida sea breeze environment, detailed cumulus scale motions, especially in the boundary layer, must be observed and forecasted.

The second study which we will discuss is our simulation of a cumulonimbus cloud in a hurricane environment. A description of this simulation was presented at the 13th Technical Conference on Hurricane and Tropical Meteorology 1-5 December, 1980, held in Miami Beach, Florida. We were motivated to perform this study by recent research of McBride (1979) which implied the importance of deep convection to the overall momentum budget of a hurricane. We attempted to simulate a cumulonimbus cloud in the composite environment of different hurricane sectors to find if any differences in vertical momentum redistribution might occur. Our initialization techniques were those used in the Florida study by Tripoli and Cotton (1980) where a storm is perturbed by both a mean and focused convergence. Because we lacked any observational data on convergence we first decided to use the convergence profile used in our previous study in Florida. Such an initialization was unsuccessful in producing deep convection using composite enviroments in several storm sectors. We concluded that this was due to the fact that such composites were averaged over hurricane sectors which included cloudy and noncloudy regions. These environments were therefore not moist enough or unstable enough to be characteristic of the environment in a rainband. We therefore next searched for a sounding obviously taken within a rainband. Initiating the storm in this environment again failed to produce deep convection but instead produced a stratus-like cloud. Our conclusion was that the convergence profile we assumed was not deep enough. We there acquired a very deep and strong convergence profile typical of peak rainband convergence found in the Hack and Schubert (personal communication) hurricane model. This profile was then used for the mean and a focused convergence. Our results

were again dissapointing. We found such convergence only led to deep tropospheric stable lifting and uniform rainfall in the absence of any cumulonimbus activity. In a "last ditch" effort to initiate convection we again used the hurricane model derived convergence field, but limited the initial focusing to lower levels so that moisture would be drawn primarily from the very moist levels. This initialization led to the development of a cumulonimbus cloud which was weak below 400 mb, but became very strong aloft.

The results of this study have again demonstrated a strong sensitivity of cloud growth to magnitudes and distribution of initial convergence on the scale of the cloud. We find the hurricane environment in general is very stable and strong forcing is necessary to produce unstable moist convection. In order to predict the location and intensity of convection within rainbands, not only is the mean rainband convergence important, but so is the nature of the localized forcing which initiates the cumulonimbus cloud.

Another major case study undertaken by our group was the weather modification study of a cumulus over South Florida. A preliminary report of this case study is given by Nehrkorn (1981). We chose to simulate a highly observed cloud line of 25 August, 1975 south of Lake Okeechobee. Based on surface mesonet data we estimated initial convergence assuming a vertical profile similar to the Tropoli and Cotton (1980) study. A symmetric focused component was also assumed and adjusted through a number of test cases to obtain the weakest cloud growth while still having convection possible. This was done so we could find the strongest response to seeding we could. Because this experiment was our first experience with the ice phase we discovered oversights in the formulation and implementation of the code that led to an unrealistically

vigorous response to our seeding. After correcting these problems we found very little dynamic response to seeding.

After further analysis of the data and discussions with John Cunning of NOAA we decided to improve the initialization technique we used. Instead of using a mean initial convergence spread evenly across the domain, we approximated the closely linear convergence observed by the mesonet stations by a line. The focused convergence was then applied along the line. Instead of using the same abritrary convergence profile again, we attempted to infer the vertical profile from wind shifts in the pibal observations taken northwest of the convergence line. The initial field was then constructed in order to reproduce the observed winds northwest of the simulated line as observed. We also assumed a conceptual model of the flow southeast of the line based on the existence of a sea breeze front. This simulation led to a much more realistic cloud growth pattern than before. The cloud was so intense, however, that there was little that seeding such a cloud could have done to enhance its growth.

Later discussions with John Cunning revealed that the observed cloud had no rain at the ground until cloud top reached above 10-12 km MSL and experienced a marked surface pressure drop prior to the rainfall. Our cloud began raining when cloud tops reached only 5 km MSL and surface pressure responded by rising. We concluded the warm process was too intense. As a result, adjustments in our conversion and accretion formulas of raindrop growth were made and we were then successful in delaying rain slightly. We found, however, that even this slight delay led to much lowered pressure beneath the cloud as observed. However, when rain began the pressure rose quickly near the surface. Also the onset of rain led to deep growth of the cloud and the natural initiation of the ice phase.

Further comparisons with John Cunning's observations showed we also formed large ice particles much more quickly than observed. As a result we made some improvements to our graupel parameterization by making the number of assumed graupel particles a function of the total mass of graupel computed. This adjustment led to a delay of the ice phase. However, more vigorous explosive growth occurred later when the ice phase commenced.

Finally, we concluded that rain should be delayed even more if the simulated onset of rain was to properly match observations. Because the rain was responsible for the rapid glaciation once the ice phase began, we felt its onset was of high importance. Also, our examination of foil impactor data revealed that very little rain actually existed within the cloud even as it grew to 10 km. At this point, we decided to consider the findings of Sax et al. (1981). Contrary to popular belief he showed that the CCN (cloud condensation nuclei) number concentrations vary considerably across South Florida, becomming very continental near the interior, where our simulated cloud was found. He found average concentrations to range from 500 to 2000 cm^{-3}. We have been assuming a mild continental concentration of 300 cm^{-3}. So our next experiment was to try again with a CCN concentration of 1000 cm^{-3}. The result was no rain at all while the cloud grew lethargically to 10-12 km. This cloud compares favorably with observations prior to seeding. At this time our experiments on this case study are continuing.

Our conclusions appropriate to this contract are there is large and unexpected sensitivity of cloud and cloud system growth to details of the

microphysics in addition to the detailed three dimensional configuration of the initial convergence. Because of the high variability of CCN across the Florida peninsula, a cumulus may develop explosively in one region and not rain at all in another. This can occur even with the same initial convergence and thermodynamic profile simply because of differences in CCN which Sax et al. (1981) found to occur. As a result we conclude that observations of CCN are important in predicting individual cloud growth and intensity in South Florida.

The next case study we completed recently was the case of a large quasi-steady cumulus which developed over South Park, Colorado on 19 July 1977. South Park is a high mountain plateau of 3.1 km MSL where we conducted the South Park Area Cumulus Experiment (SPACE). The storm we chose to simulate was analyzed by Cotton et al. (1982) and Knupp and Cotton (1982a,b) using triple doppler radar, radiosonde, and a PAM network. The qausi-steady storm which we simulated, was unique among other storms in the same vicinity because 1) it moved northwest while other storms moved north or northeast, and 2) its lifetime was greater than any of the other storms. As shown by Cotton et al. (1982) initial development of the storm took place along a north-south convergence line where thermally driven south-easterly valley winds met the well-mixed south westerlies to the west. During the storm development, a meso-cold front passed from the north shifting the surface winds to a uniform northerly direction. At the time of frontal passage, the storm grew much larger and began its relative movement toward the west. So we ask what was it that made that cell change direction and become steady whereas other cells along the line did not? We also ask was the steady storm structured after the initial environment, the post frontal environment or both.

In our first simulation we initialized the storm using a modified form of the gust front initialization technique developed by Miller & Thorpe (1981). Since there was no apparent mean surface convergence in the PAM stations after the passage of the meso-front, we felt the storm must be forced by a local convergence. The result of this circulation was a line of cells whose structure in the meridional direction resembled the cell of interest, but which differed greatly in the zonal direction. We next considered the possibility that the forced westward movement may have resulted from the interaction of the outflow of the simulated cell with other storms along the previous convergence line. The direction of preferred development in regions of intersecting gust fronts has been extensively discussed by Purdom and Marcus (1982) based on studies of satellite movie loops. Our next experiment was therefore an attempt to find if a westward moving cell would be favored if a point of intersection between outflow from the convective line to the north and the simulated cell moved westward. We found no enhanced vertical motion at the intersection point and no tendency for a westward moving cell to be favored.

Next we attempted to simulate the storm in the pre-meso front environment, which was characterized by the convergence line. We simulated a weaker short lived northward moving storm similar to the prefrontal storms observed. However, the type of cell we observed after the front passed was not formed.

Finally we initiated the storm as before in the prefrontal environment and introduced a cold front from the north to pass underneath our developing cell at the same point in its lifetime as was observed in South Park. The result was that we were successful in reproducing the relative westward movement of the observed cell off of the convergence line and in obtaining a relatively steady circulation that matched

observations well. We also found that the movement and development were sensitive to details in the wind profile specified initially on either side of the convergence line. We found it was necessary to specify a well-mixed westerly component to the west and a low level circulation to the east in order to obtain a storm circulation similar to observations.

From this case study we again support evidence that storm structure is strongly forced by details of initial conditions. We also find that storm structure, movement and intensity may be strongly influenced by changes in the environment while the storm is developing. Therefore, a forecast of this particular storm's behavior would have to be based on both the initial environment and the correctly forecasted evolution of the environment.

The last simulation case study is that of the Heymsfield May 1978 cell analyzed by Heymsfield (1981). Our simulation of the observed cell A-5, supported under this grant, is described extensively in section 5 of this report. The results of that study as with our other studies, demonstrate a strong dependence of the storm structure and evolution on the detailed description of the initialization fields. Most notably we concluded that the updraft/downdraft structure of cell A-8 must be obtained by the forcing of a previous cell's outflow.

In summary, we conclude that the accurate prediction of the evolution of a convective storm depends upon accurate observations of 1) mean environmental convergence, 2) initial convergence on the cloud-scale and related temperature perturbations found in outflow convergence, and 3) microphysical properties of the air mass, i.e., CCN. We also find that a detailed description of the evolution of the environment in the vicinity of the storm during the storm's development may also strongly influence the structure, movement and intensity.

3.0 INTERPRETATION OF 3D EXPERIMENTS WITH REGARD TO RELATIONSHIP BETWEEN OVERSHOOTING TOPS AND SURFACE WIND GUSTS

As part of this grant, we have also studied the communication between upper tropospheric convection behavior and lower tropospheric convective phenomena. An objective of this study was to further examine the relationships between "explosively" rising convective towers (or overshooting tops into the stratosphere) and severe wind gusts and/or tornadoes. Fujita and Byers (1977) reported on the analysis of a cumulonimbus which produced a severe surface wind gust or downburst and exhibited an overshooting top behavior on satellite imagery. Fujita and Byers (F & B) hypothesized a cell model to explain the dynamic linkage between overshooting tops and downbursts. The model involves tops overshooting the anvil, then collapsing into a strong downdraft (located at approximately 10 km) and a trail of precipitation. It is hypothesized that entrainment at the top transports dry air and large horizontal momentum downward. Ice crystals are hypothesized to rapidly sublime in the subsaturated entrained air, thereby taking up heat from the air resulting in a cold, negatively buoyant downdraft. The collapsing top and entrained air accelerate the train of precipitation and import fast horizontal momentum from the stratosphere. A successive rise and fall of the top are hypothesized to create a family of downburst cells that moves away from the parent thunderstorm. A major weakness in the F & B theory is that the magnitude of θ_e of tropopause-level air is so large that very large forcing or ice-phase diabatic processes are required for air to descend to the surface.

In recent years, we have obtained two significant cases of overshooting tops in our simulation of cumulus clouds with the CSU three-

dimensional (3-D) cloud model (Tripoli and Cotton, 1980). In both cases, the simulation of an overshooting top was fortuitous.

In the first case, which has been reported in the first-year report to NASA under Grant No. NSG 5341, an overshooting top was fortuitously obtained in a simulation of the dynamic response of a cloud to massive seeding. Being our first exercise of the model with the ice-phase model activated, artificially large ice-phase growth tendencies were generated when seeded crystal concentrations were introduced. As a consequence of not checking the tendencies to determine if more ice was being generated than available water, an artificially large ice mass was produced and an excess latent heat release was generated. This initiated a vigorous explosively growing tower which penetrated well into the stratosphere. Consistent with Fujita and Byer's (F & B) model, the tower plunged back into the troposphere and initiated a 10 m s^{-1} downdraft near the tropopause (see Fig. 1). However, the mechanism of communication between the overshooting top and the surface as envisaged by F & B was not evident in the simulation. Instead, as the tower began to explosively rise, low-valued θ_e air existing in the lower mid-troposphere was entrained into the wake of the vigorously rising bubble, forming a vigorous downdraft. The downdraft penetrated to the surface and formed an intense wind gust. Thus, we concluded that the basic mechanism linking overshooting tops and surface wind gusts is the dynamic entrainment associated with vertical mass flux divergence due to "explosive growth". The question remains, however, can intense downbursts be generated under conditions of a more realistically created mass flux divergence?

Further support for this hypothesis was obtained in our second overshooting top simulation. A description of this simulation was presented at the 13th Technical Conference on Hurricanes and Tropical Meteorology 1-5 December, 1980, held in Miami Beach, Florida. In this case, a cumulo-

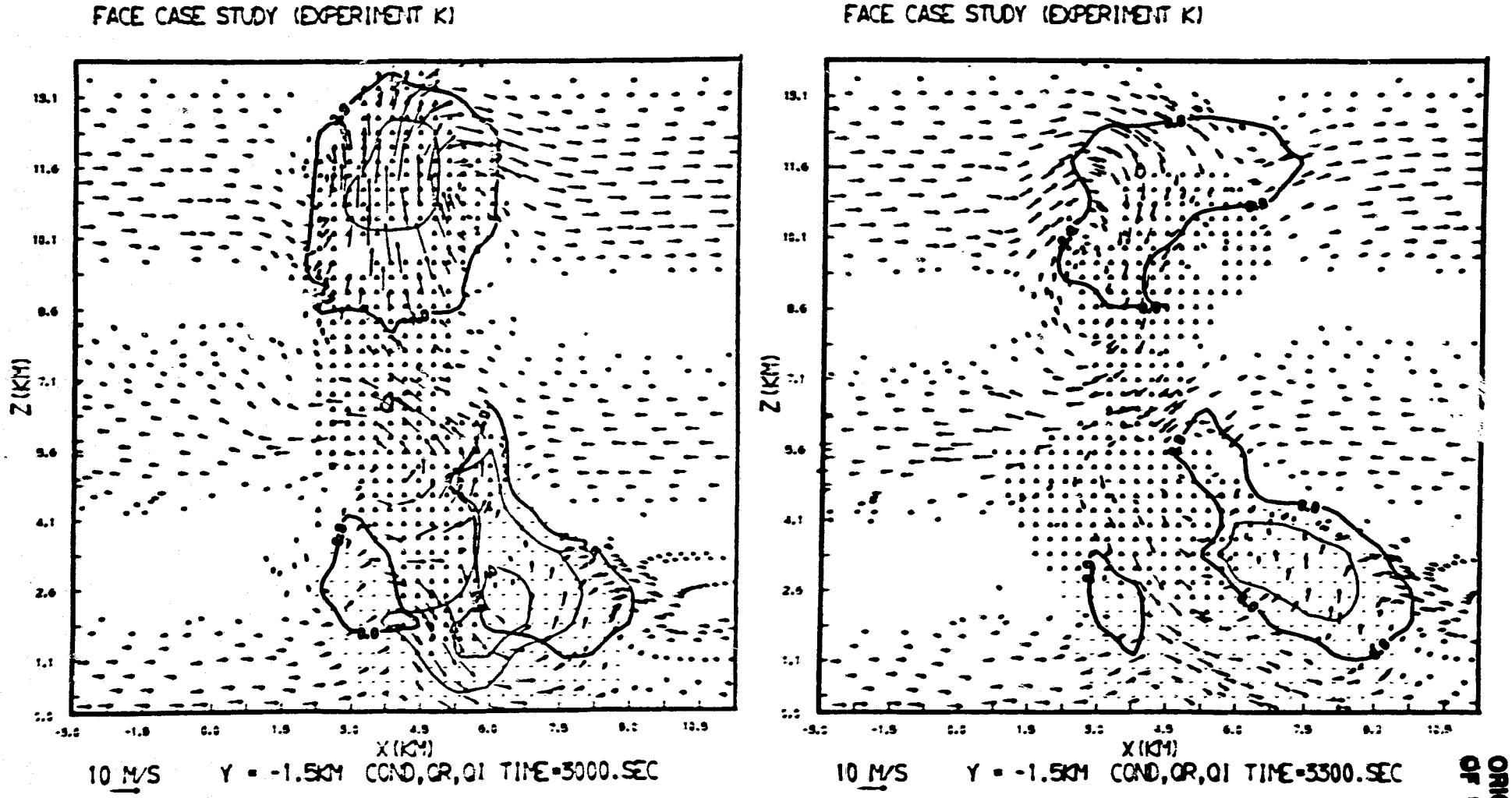

Figure 1. Vertical cross section through seeded cloud with excessive ice production. Figure 1a is 3000 s and Figure 1b is 300 s later. (From Nehrkorn, 1981).

nimbus circulation started in the characteristically stable lower troposphere environment of a hurricane were met by failure. In a frustrated attempt to generate a deep convective cloud before the conference presentation, the initially-imposed cloud-scale vertical motion was greatly enhanced over prior simulations, such as reported in Tripoli and Cotton (1980). The result was a convective tower which rose through the stable environment of the lower troposphere and grew explosively once it encountered the lesser stability in the upper troposphere. Again, the explosively rising tower overshot the tropopause, plunged back into the troposphere and generated downdrafts of the order of 10 m s^{-1} just below the tropopause. In this case, however, the air entrained into the storm in the wake of the explosively rising tower did not have a pronounced minimum value of θ_e. As a consequence, a lower tropospheric downdraft was primarily driven by water loading and damped in intensity as the air warmed while descending to the surface. No significant surface wind gust was detected in the simulation. This further supports our contention that surface wind gusts and/or downdrafts have their origin in the entrainment of low-valued θ_e air in the lower mid-troposphere. The association of surface wind gusts with overshooting tops does not appear to be a cause and effect relationship.

Clearly, what we need is a well-documented (i.e., multiple Doppler radar, surface mesonets, etc.) case in which an explosively rising convective tower penetrates the tropopause and a surface downburst or microburst is observed. Simulations with the 3-D model of such events should better establish a causal/effect relationship between upper tropospheric convective behavior and surface phenomena. It should be noted that in the simulation of the

cumulonimbi in a tropical cyclone, associated with the explosively growing tower was a low-level meso-vortex having tornado-like characteristics, similar to observed updraft mesocyclones in tornadic storms (Brandes, 1978). Thus another mode of low-level convective phenomena associated with upper tropospheric convection can be investigated with the model.

4.0 THE DEVELOPMENT OF SOFTWARE FOR EMULATING SATELLITE-INFERRED CLOUD PROPERTIES USING 3D CLOUD MODEL-PREDICTED DATA

Before leaving our group and joining G.E. MATSCO to work with NASA, Mr. Mark Stephens began the development of algorithms to emulate the analysis of satellite-derived cloud top isotherms using data predicted with the 3D cloud model. The algorithm involves a search for cloud top and mapping of a satellite plane of data (i.e., cloud top temperature). Using data predicted by the model in its non-icephase version, he then computed the rate of expansion of isotherm area $\left(\frac{d \ln A}{dt}\right)$.

Stephens then compared the predicted $\frac{d \ln A}{dt}$ to the predicted horizontal velocity divergence D. The divergence was computed at the height having an average horizontal temperature corresponding to the isotherm used in calculating $\frac{d \ln A}{dt}$. Also, the D was evaluated over the area of the isotherm projected onto the plane on which D is to be computed.

The rate of isotherm expansion was also compared with predicted total eddy kinetic energy and the location and amplitude of maximum updraft speed as well as precipitation intensity.

In the test case, Stephens found generally poor correspondence between $\frac{d \ln A}{dt}$ and D. The best correlation occurred at the time that the storm was at its peak kinetic energy early in the cloud's life history (30 to 40 min). After this time, other factors affecting isotherm expansion became more influential. Some of these factors were model dependent,

especially for the stage of model development at that time. Factors affecting isotherm expansion other than velocity divergence include:

1) The anvil not only expands outward from a central point, but also extends its area by cloud water condensing or moving upward through a region. This effect can be expected to be of greater importance when the ice-phase is included in the model predictions.
2) Since the anvil is composed of cloud water, it is more influenced by evaporation than a similar anvil composed of ice particles.
3) The above-mentioned evaporation of the anvil also leads to a disorganized anvil structure which contributes to a noisy estimate of $\frac{d \ln A}{dt}$.

The calculation of $\frac{d \ln A}{dt}$ must also be terminated when the anvil reaches the lateral boundary of the model.

5.0 SIMULATION OF HEYMSFIELD'S NIMROD CASE

As part of this grant, we attempted to numerically simulate the observed structure of cell A-5 which was observed as part of the NIMROD (Northern Illinois Meteorological Research on Downbursts) experiment near Chicago in Spring 1978 (Fugita, 1979). An extensive analysis of the triple doppler data of cell A-5 was presented by Heymsfield (1982). Based on the results of that study, Heymsfield calculated updraft and downdraft trajectories in a coordinate relative to the updraft maximum. These trajectories are shown in Fig. 2. It is interesting that the updraft trajectory points primarily downshear while the downdraft trajectories are in a relatively upshear direction. Presumably the updraft moves upshear in the lowest 2 km where horizontal cross sections show inflow from the northeast. Based on these trajectories, Heymsfield drew a conceptual model of the structure of cell A-5 given in Fig. 3.

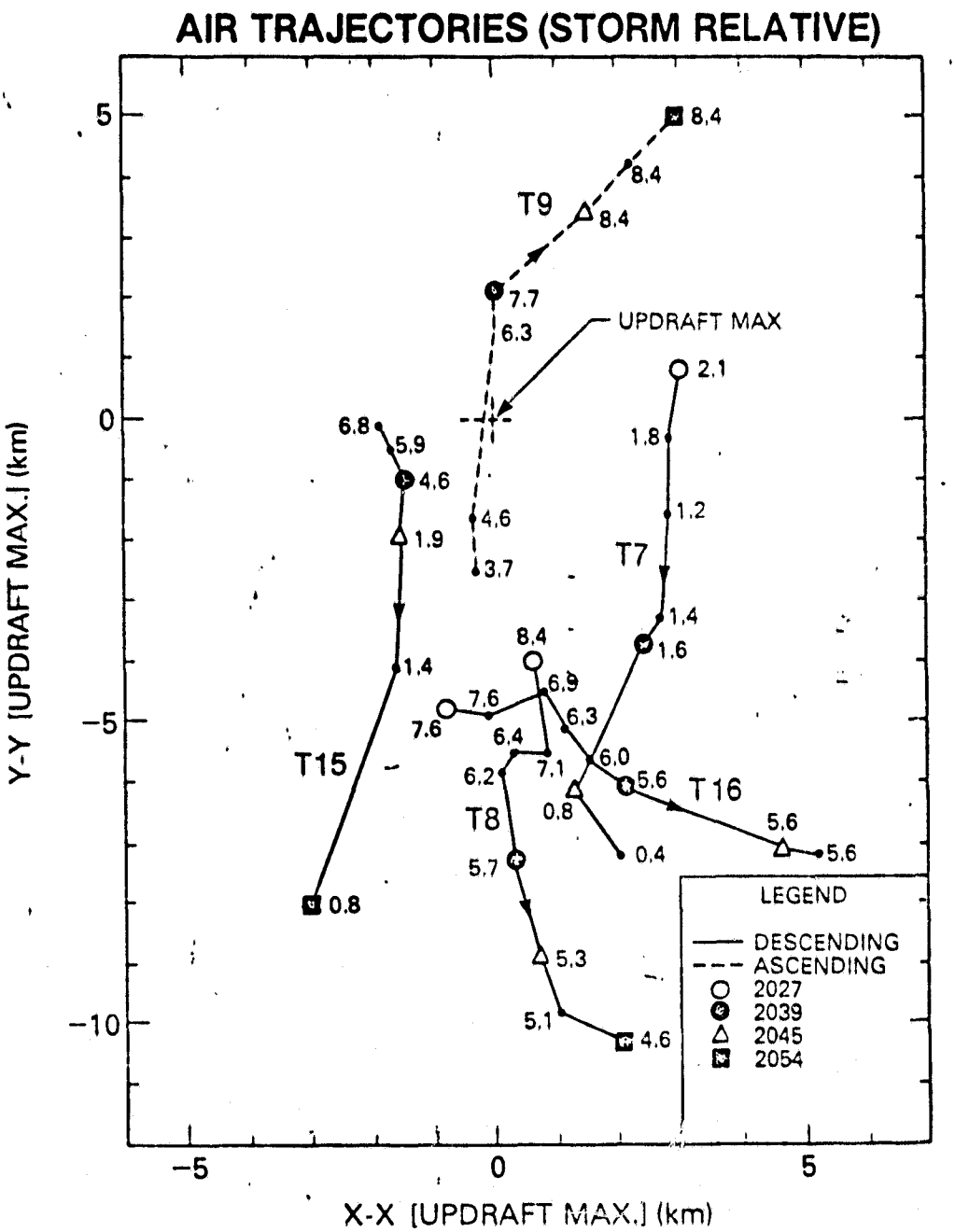

Figure 2: Air trajectories. Positions are given relative to updraft of cell A_5 located at (0 km, 0 km). Numbers give height in kilometers; arrow heads show direction of air parcel trajectory. (From Heymsfield, 1981)

The downdrafts labeled L, R, and DV were forced by flow convergence at midlevels upshear of the updraft. Downdraft R was weak at midlevels such that no trajectiories from 7-8 km MSL penetrated below 4.6 km MSL. However a low level downdraft from 2.1 km (shown in Fig. 3) did reach the ground. The upshear downdraft to the left did appear to be stronger and penetrated to the ground. Although Heymsfield showed no trajectories indicating where the air in downdraft DD finally ended up, the downshear downdraft was consistently observed with radar and inferred to be weak.

In order to help explain the principal dynamic mechanisms which led to the observed structure we attempted to simulate the lifecycle of A-5 with the CSU 3 dimensional cloud model. After obtaining all radiosonde and mesonet observations made on the storm day we next needed to construct an initial field representative of the storm initiation environment. Based on the advice of Dr. Heymsfield we first decided to use radiosonde observations at 1800 LST. At that time the mesonet stations seemed to show a convergence line running southwest to northeast at about 210^{o}. The vertical convergence profile was not shown so we had to guess on its variation with height. To do so, we subtracted the mean vector of 13.1 ms^{-1} wind at 210^{o} from the observed wind profile and viewed the cross convergence line component observed to the left of the line. We found a noticable windshift at 2.8 km AGL below which the cross line wind blew toward the convergence line and above which the cross line wind blew out from the convergence line. We then assumed that the cross convergence line wind to the right of the convergence line below 4.1 km would blow opposite to that observed to left. Hence an associated vertical motion is implied.

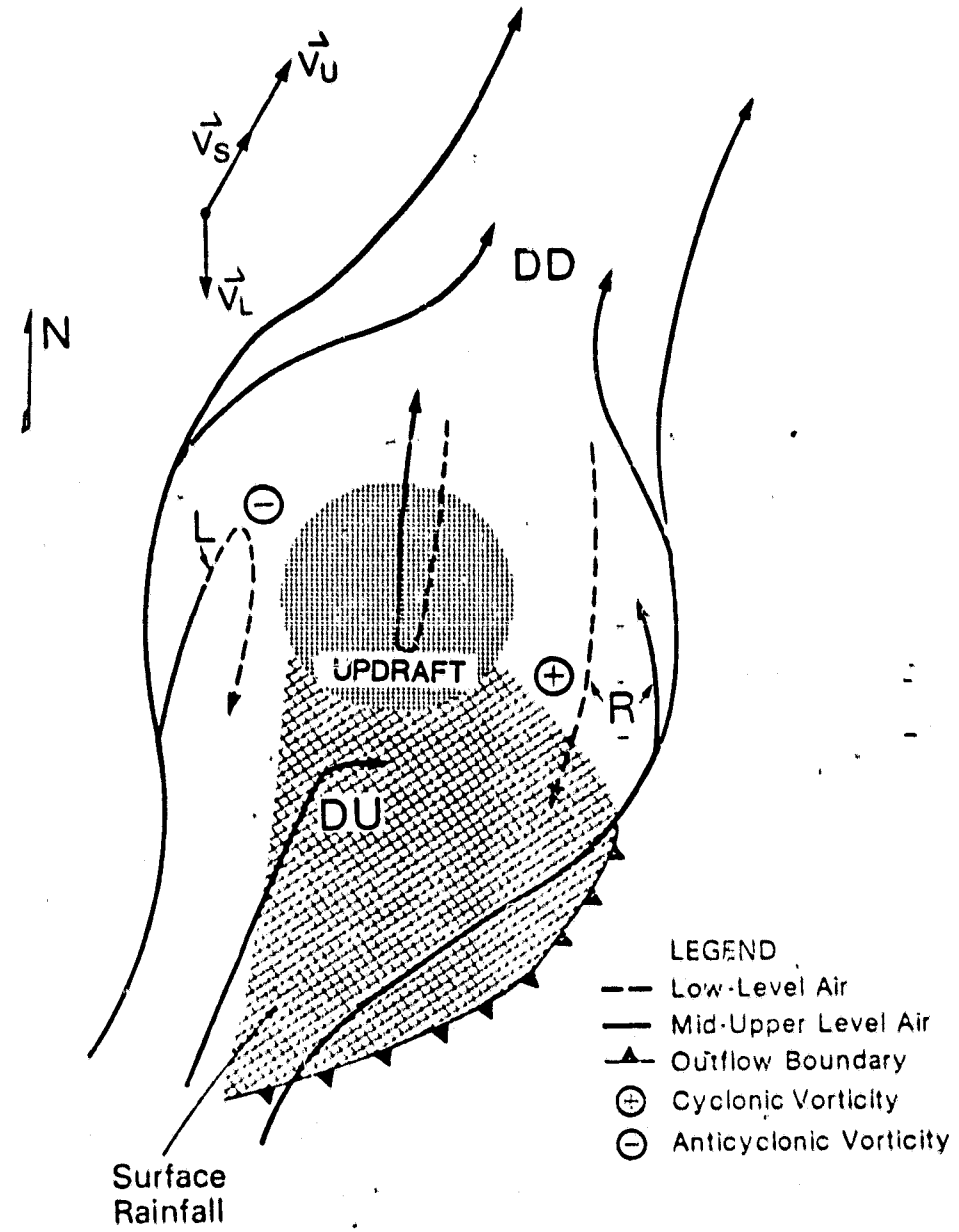

Figure 3: Schematic of updraft and downdrafts in mature period (2030-2039) of cell A_5. Outflow boundary is indicated by barbed front. Downdraft trajectories are indicated by DU, DD, L, and R. See text for details.

In order to perturb an unstable updraft we had to initially move surface moisture and potential temperature up to cloud base in addition to supplying a focused (see Tripoli and Cotton, 1980) vertical motion. The disadvantage of such a perturbation is that until a downdraft is established the base of the updraft will advect downwind of the source air thus initially tilting it upshear with height. When precipitation or entrainment initiates downward motion it then must always be downshear. If the cloud, however, was initiated with surface convergence forced by outflow from the upshear direction, the translation of the downshear updraft base would be opposed giving low level upshear updraft tilt. This may lead to the downshear downdraft more effectively. Unfortunately when initiation is performed with initial outflow other problems occur. First any updraft tilt is forced to occur only downshear and therefore other possibilities are eliminated. Hence, we force a structure we are trying to determine. Second, the outflow tends to form an arc of cloud cells where in nature a single cell would be preferred with more complex terrain and cell interaction. Third, it is difficult to determine how fast to move, how long to perturbate, and how intense to make the initial outflow source region without extensive trial and error simulations in three dimensions.

We therefore elected to first try the focused convergence initial perturbation and hope that a secondary updraft will form downshear resulting from precipitation. A cross section taken along the convergence line at 1000 s simulation time is shown in Fig. 4. As expected a strong updraft of 14-17 ms^{-1} developed and moved upshear with very little tilt downshear. After 1500 s (Fig. 5) precipitation commences downshear of the updraft initiating a strong downdraft from 4 km to the

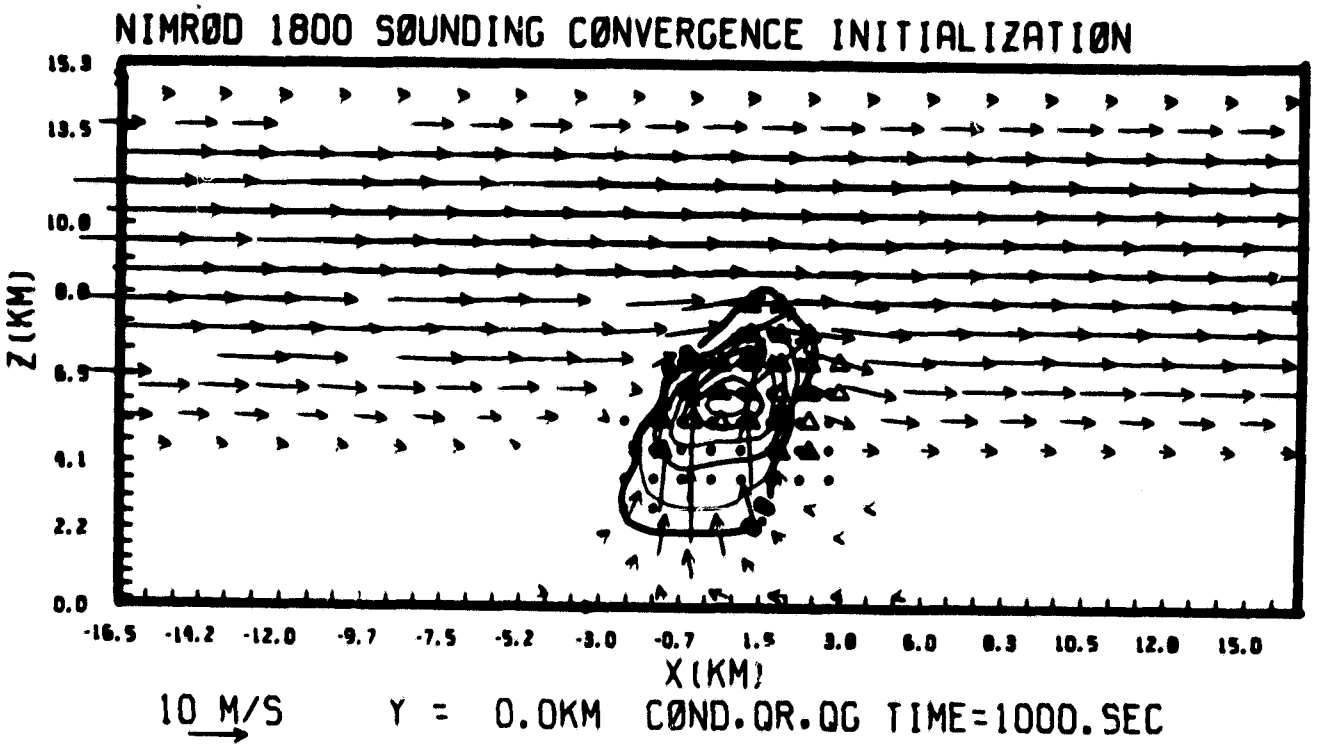

Figure 4: Flow and condensation field for x-z (northwest to southeast) cross-section through 3D numerical simulation of cloud at 1000s simulation time in environment observed by 1800 CST sounding. Wind vectors are scaled as shown. Heavy dark contour surrounds region of saturation and contours are of total condensate beginning with 1g kg^{-1} and intervals 1g kg^{-1}. Small circles indicate presence of rain water and triangles indicate the presence of graupel water.

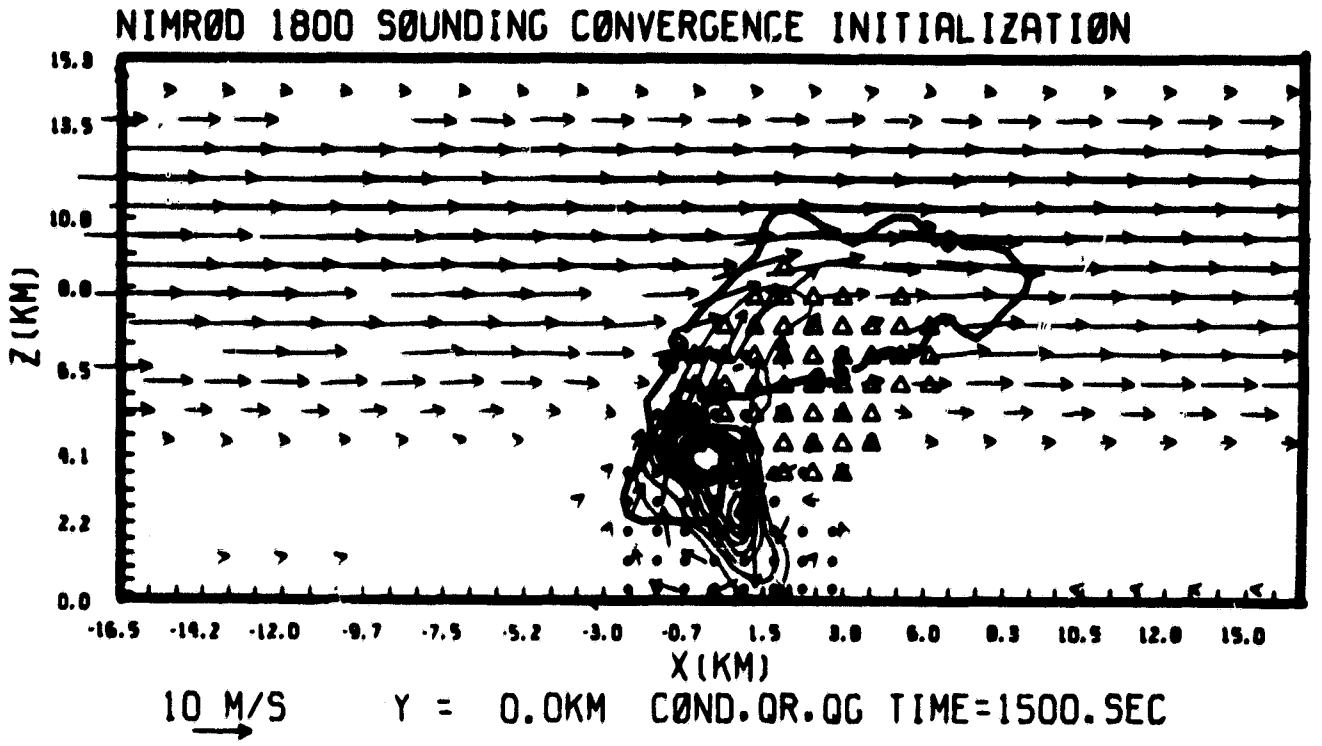

Figure 5: Same as Fig. 4 except at 1500s simulation time.

ground. The downdraft intensity reached nearly 17 ms^{-1}, originating up to 3.2 km AGL. However, at 2000 s simulation time (Fig. 6) surface outflow is evident, but necessary updraft development downshear is not taking place. The horizontal cross-sections at 1000, 1500, 2000 and 2500 s also demonstrate this (see Figs. 7 - 10).

The observations of cell A-5 were made between 2000 and 2100 LST. However, our first simulation was based on a sounding observed at 1800 LST. Further study of the 2000 LST data showed a substantiallly greater shear in the lowest 6 km in the vicinity of the convergence line, than was found in the 1800 LST sounding. We concluded that the weak secondary downshear updraft development was likely due to the weak shear at low levels in the earlier sounding. We therefore took the 2000 LST sounding and derived another convergence profile. The newer convergence field was considerably weaker than that derived from the 1800 LST data. The convergence line was less visible on the mesonetwork as well. Using the 2000 LST data we then initialized the model and performed a simulation. The result was no direct development at all. We attributed this to much increased stability near the surface in the 2000 LST sounding as nightfall arrived. After studying the mesonet data more carefully we found that near the sounding site surface temperatures were substantially cooler and drier than those along the line where cell A-5 developed. In the vicinity of cell A-5 surface temperatures and dew points were much more like the earlier 1800 LST observations. Perhaps clear skies away from the convergence line allowed increased radiational cooling and drying subsidence from the convective line helped produce the clear skies.

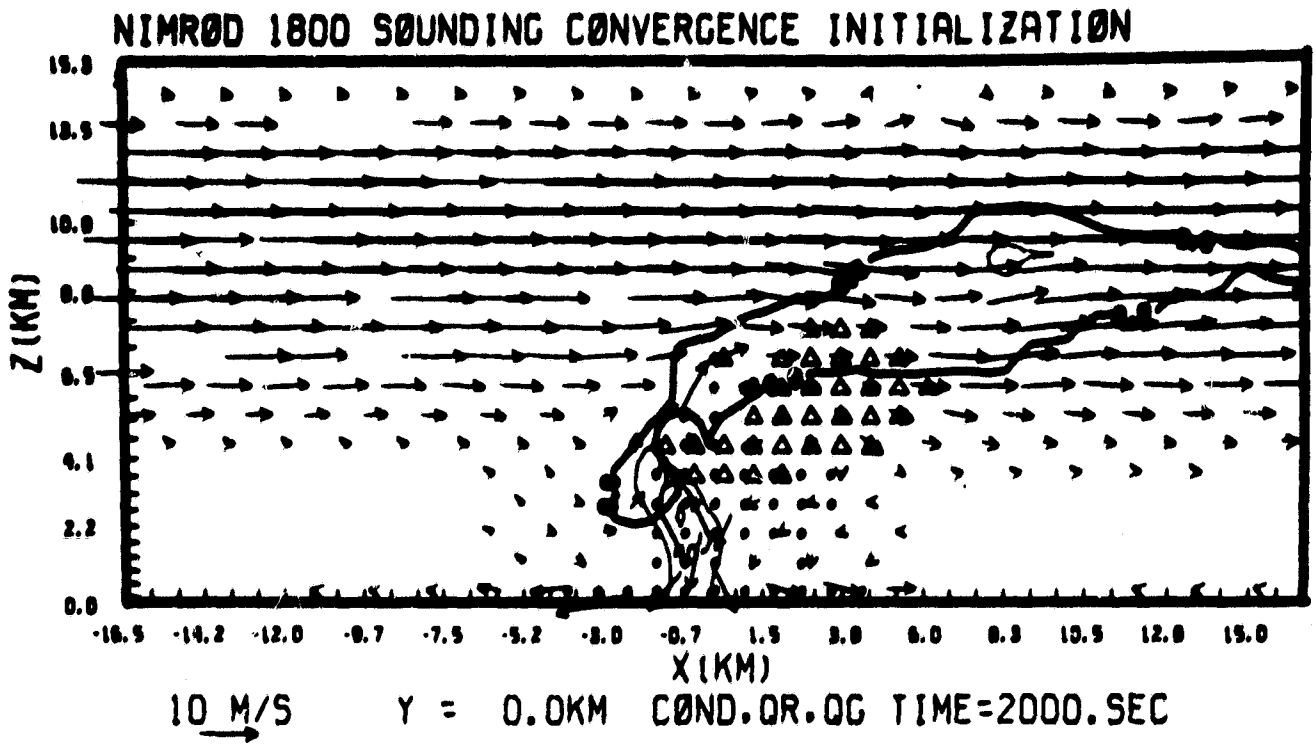

Figure 6: Same as Fig. 4 except at 2000s simulation time.

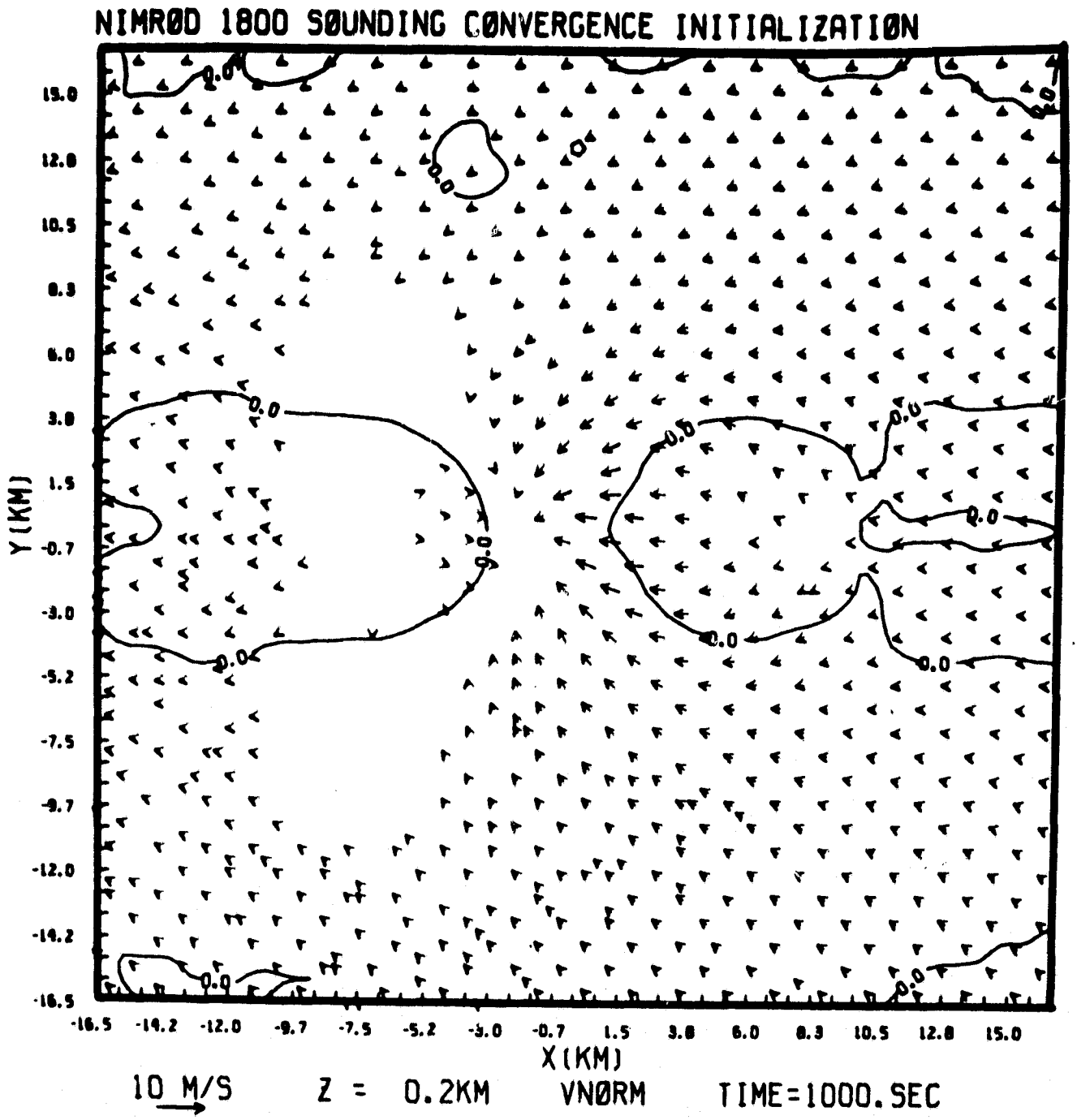

Figure 7: Flow and condensation field for x-y (horizontal) cross-section through 3D numerical simulation of cloud at 1000s simulation time in environment observed by 1800 CST sounding. Wind vectors are scaled as shown. Heavy dark contour will surround any region of saturation and light contours are of vertical motion in intervals of 1 ms^{-1}. Negative values are shown by dashed contours.

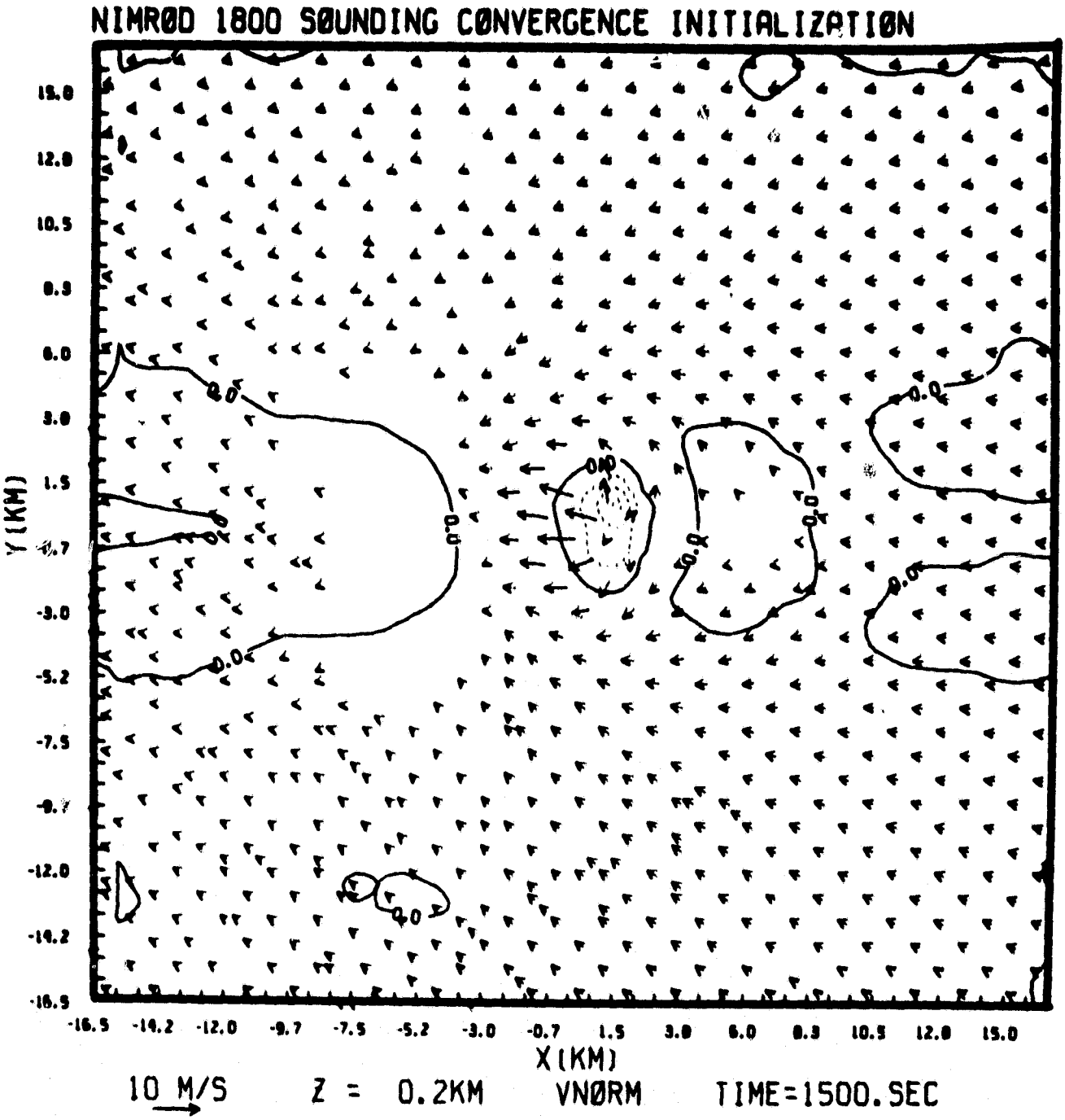

Figure 8: Same as Fig. 7 except at 1500s simulation time.

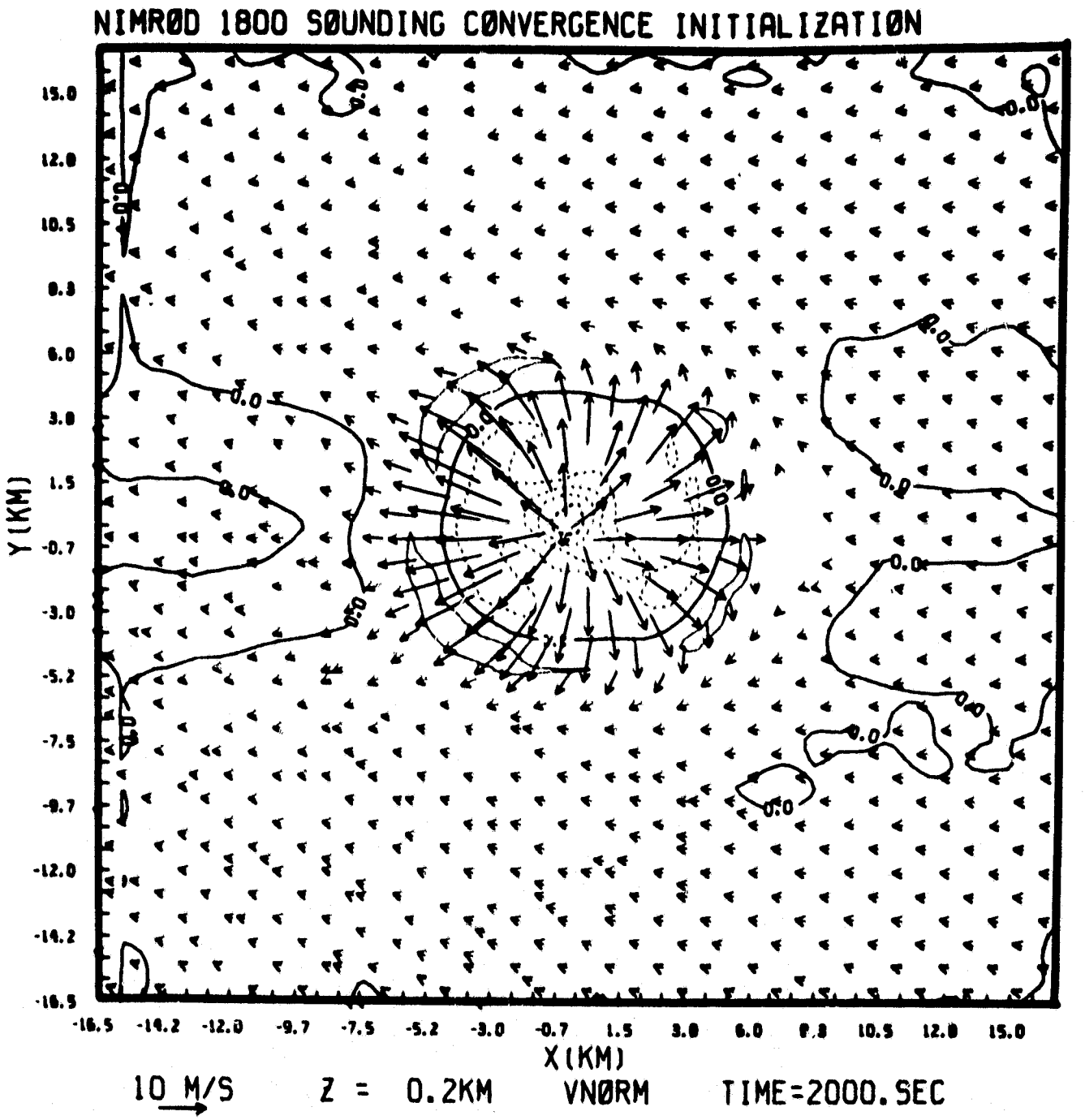

Figure 9: Same as Fig. 7 except at 2000s simulation time.

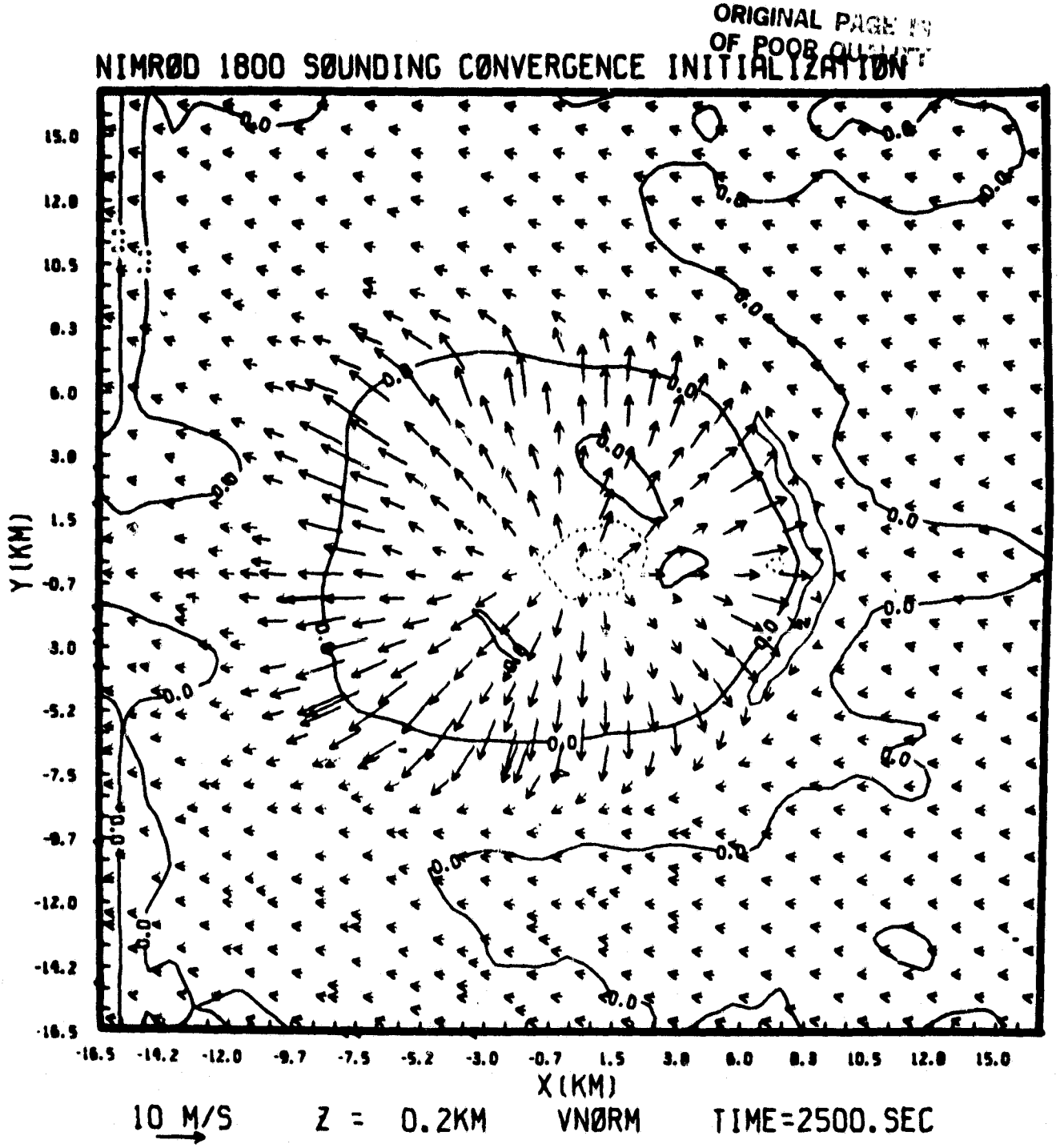

Figure 10: Same as Fig. 7 except at 2500s simulation time.

Therefore we elected to again try to simulate cell A-8 in the 2000 LST environment except for using the warmer temperatures and dew points of the 1800 LST observations in the lowest 1 km. This simulation did produce a convective cloud of a somewhat different nature than the first simulation. A cross section of the simulation taken along the convergence line at 1000 s is given in Fig. 11. The updraft tilts downshear with height as in the first experiment, however the increased northeasterly momentum near the surface increases the tilt and forces precipitation further northeast of the updraft core. By 1500 s (Fig. 12) intense precipitation cuts off the updraft inflow as in the first experiment. The low level flow at this time (Fig. 13) shows the surface outflow pattern and the remaining split updraft core upshear. By 2500 s the continued surface outflow led to the demise of the original cell and the formation of a small new cell downshear (see Fig. 14). The new cell continues to develop and grows to the size shown in Fig. 15 by 3500 s. The secondary cell, however was too weak to develop enough precipitation and associated downdraft to maintain its surface convergence. Therefore as the effects of the original cell's outflow diminished, the secondary cell slowed its movement downshear, assumed no tilt and precipitation fell on the updraft. This structure finally led to the dissipation of the cell. There are a number of possible explanations why the secondary cell failed to obtain sufficient intensity to force its own existance. First, the forcing from the first cell may have been too weak to kick off a cell of sufficient magnitude to encourage further growth. Second, the outflow from the first cell may have been too dry because of improperly modeled characteristics of the first cell. For instance, the forcing cell for A-5 may have had an upshear tilt with

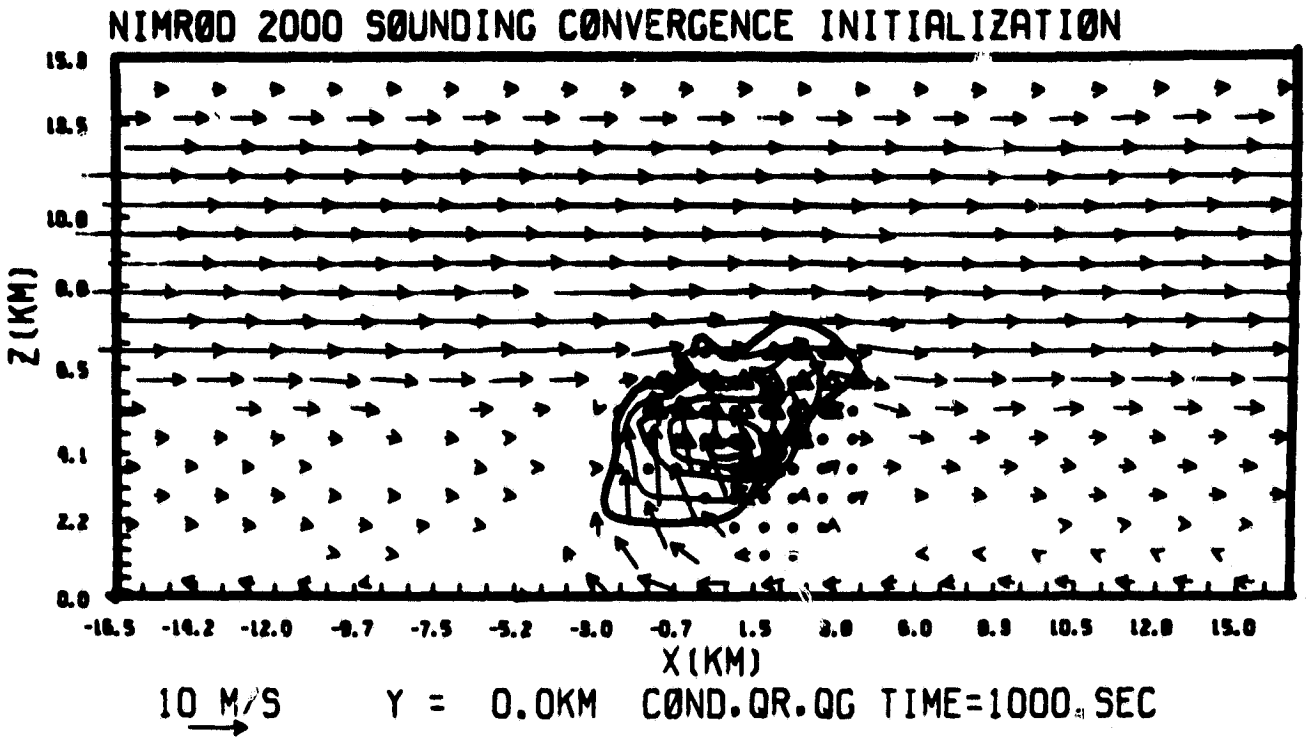

Figure 11: Same as Fig. 4 except for simulation based on sounding observed at 2000 CST.

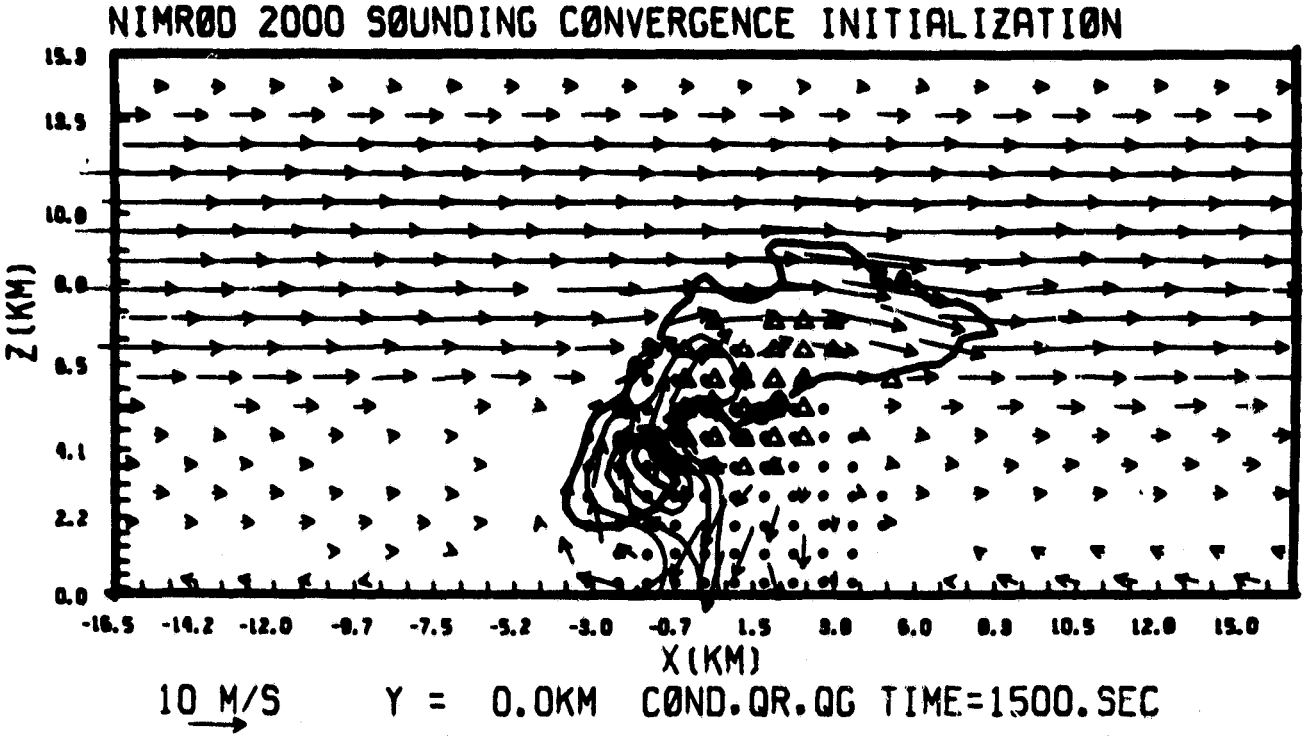

Figure 12: Same as Fig. 5 except for simulation based on sounding observed at 2000 CST.

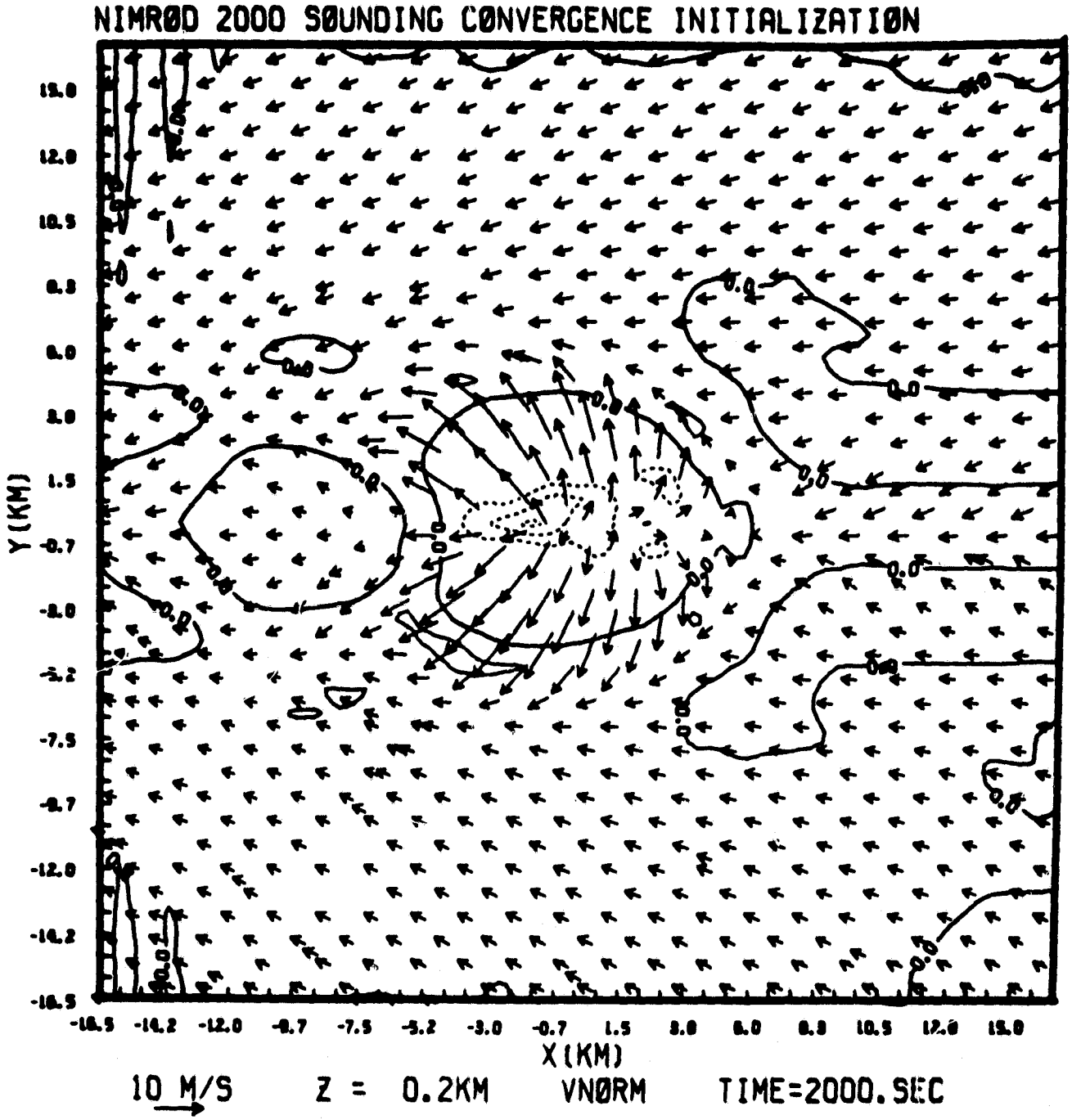

Figure 13: Same as Fig. 8 except for simulation based on sounding observed at 2000 CST.

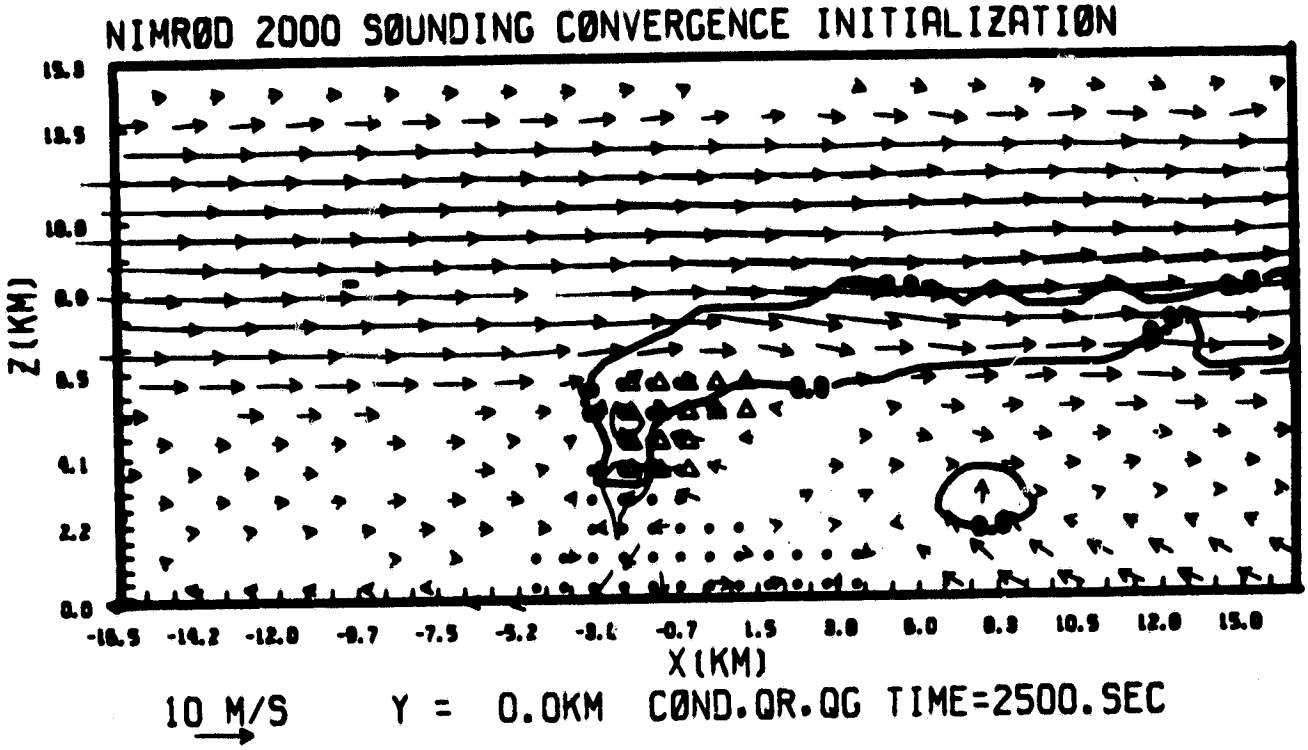

Figure 14: Same as Fig. 4 except for simulation based on sounding observed at 2000 CST and at simulation time of 2000s.

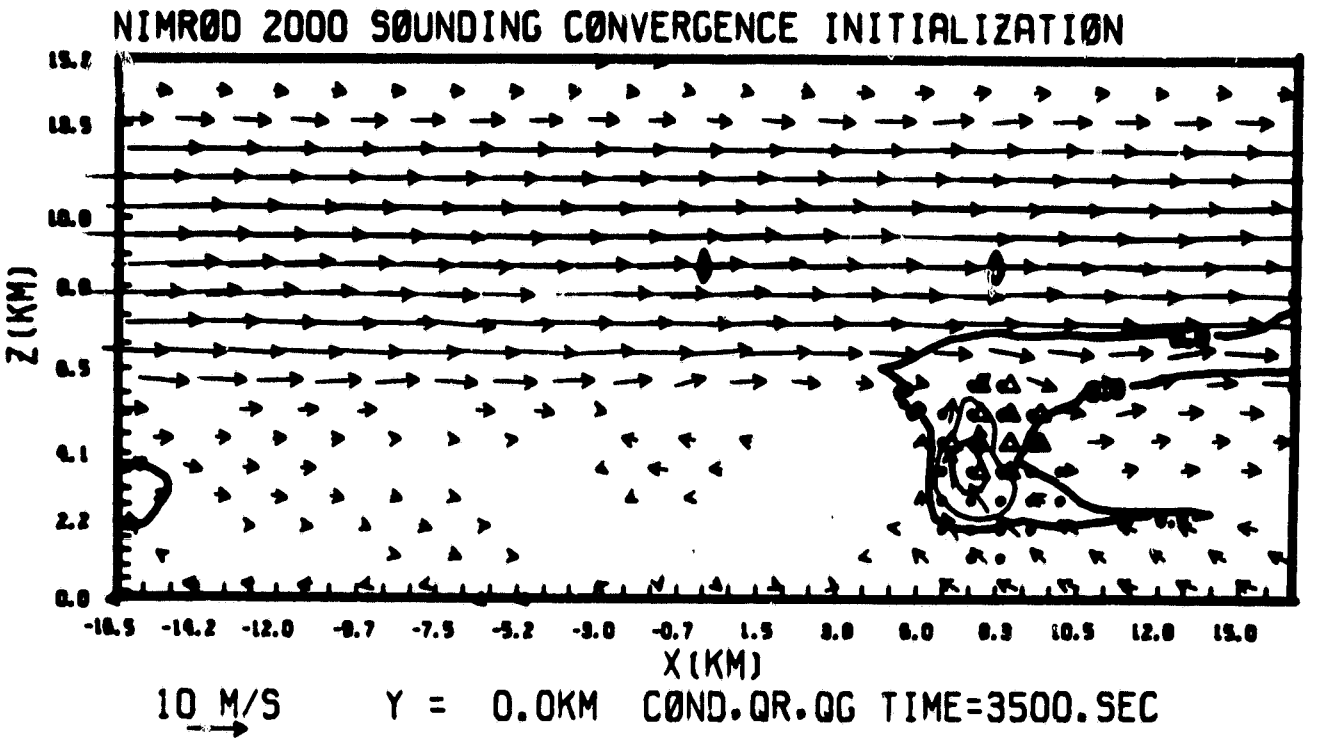

Figure 15: Same as Fig. 4 except for simulation based on sounding observed at 2000 CST and at simulation time of 3500s.

height and a greater volume of saturated air at low levels downshear of the downdraft. This may have led to a downdraft which was supported more by the rapid evaporation of cloud water rather than just rain as in our simulation. Obviously, an improper simulation of the microphysical growth of rain will affect the timing and intensity of the simulated downdraft adversely as well. Finally, the environment of the secondary cell may have been altered so that it was unsuitable for more intense convective development.

We attempted one additional simulation of cell A-5 under this contract. In that experiment a convergence field within the 2000 LST observed environment was set up initially. Next, a cooling was imposed at levels below 2.5 km and within a radius of 4 km at the domain center. Such cooling was hoped to initiate a surface outflow which would force a cell downshear. However, the cooling was insufficient to force the initial cell and the experiment was terminated at one-half hour of simulation. At this point we terminated our work under this contract due to lack of funding.

Many transient features of the first 2000 LST simulation compared well with the analysis of Heymsfield. For instance during the growth of the simulated cell through mid-levels the structure shown in Fig. 16 was obtained. This can be compared to Heymsfield's Doppler radar depiction of cell A-5 shown in Fig. 17. The flow structure compares well at this level. Most notably the model has reproduced the downshear vortex couplet and the downshear downdraft DD. The anticyclonic vortex does seem to be more powerful than observed, however. The downshear downdraft resembles convergence of flow downstream of an obstacle and the drag and melting of graupel falling from the downshear tilting updraft above. Lower down (See Fig. 18) the downdraft intensifies

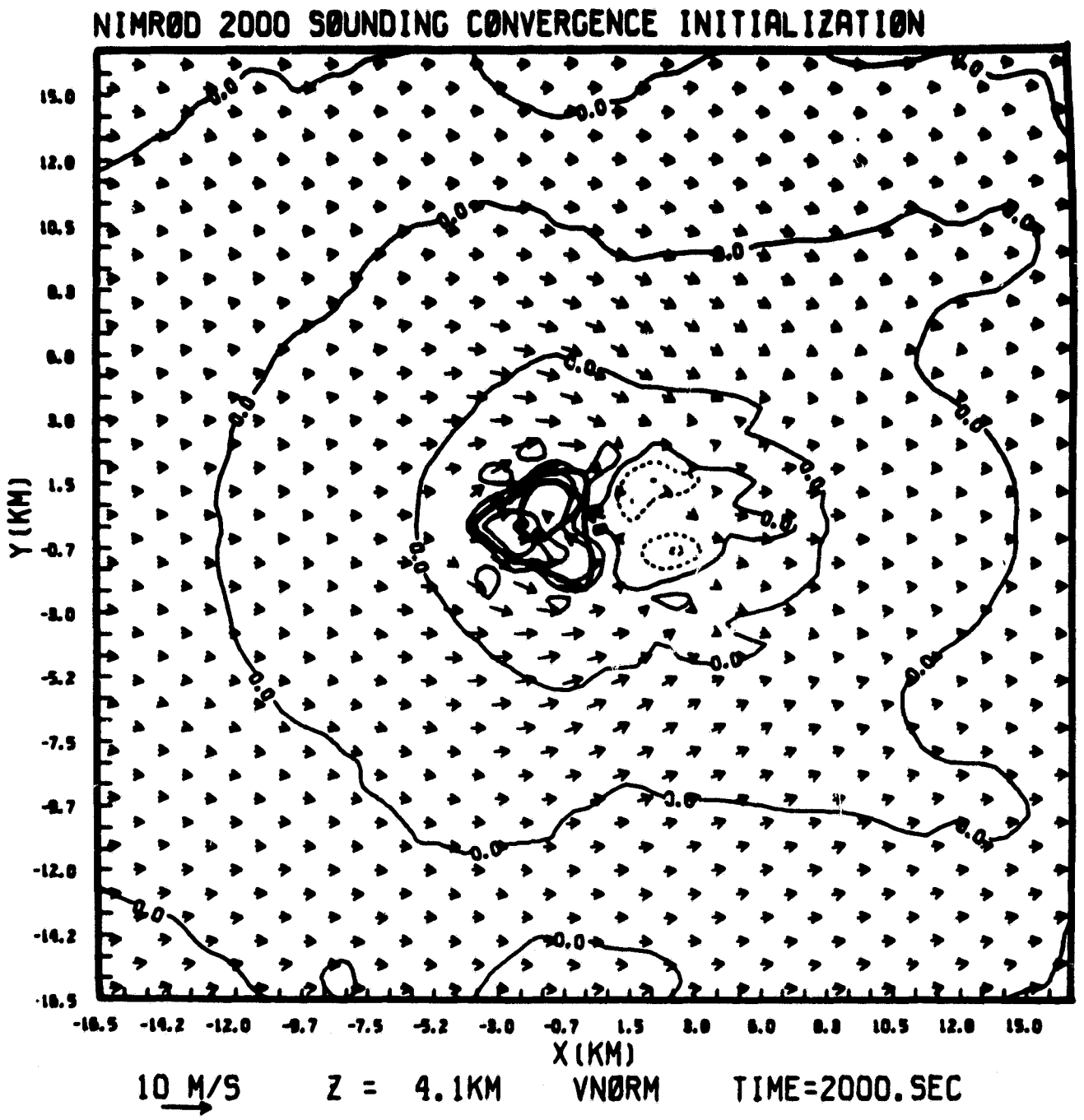

Figure 16: Same as Fig. 7 except for simulation based on sounding observed at 2000 CST and at simulation time of 2000s and at height of 4.1 km AGL.

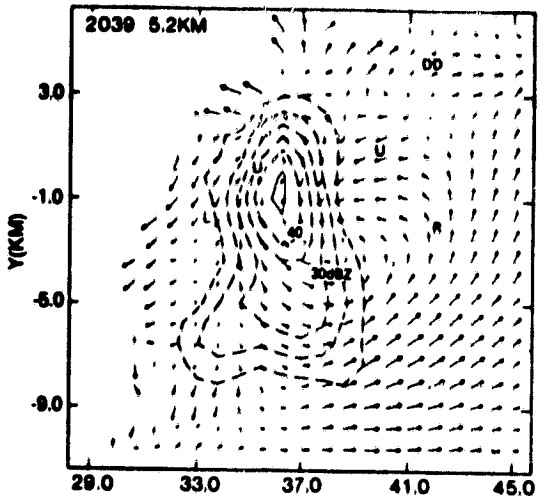

Figure 17: Flow field ground cell C-8 observed by Doppler radar at 2039 CST. (from Heymsfield, 1981)

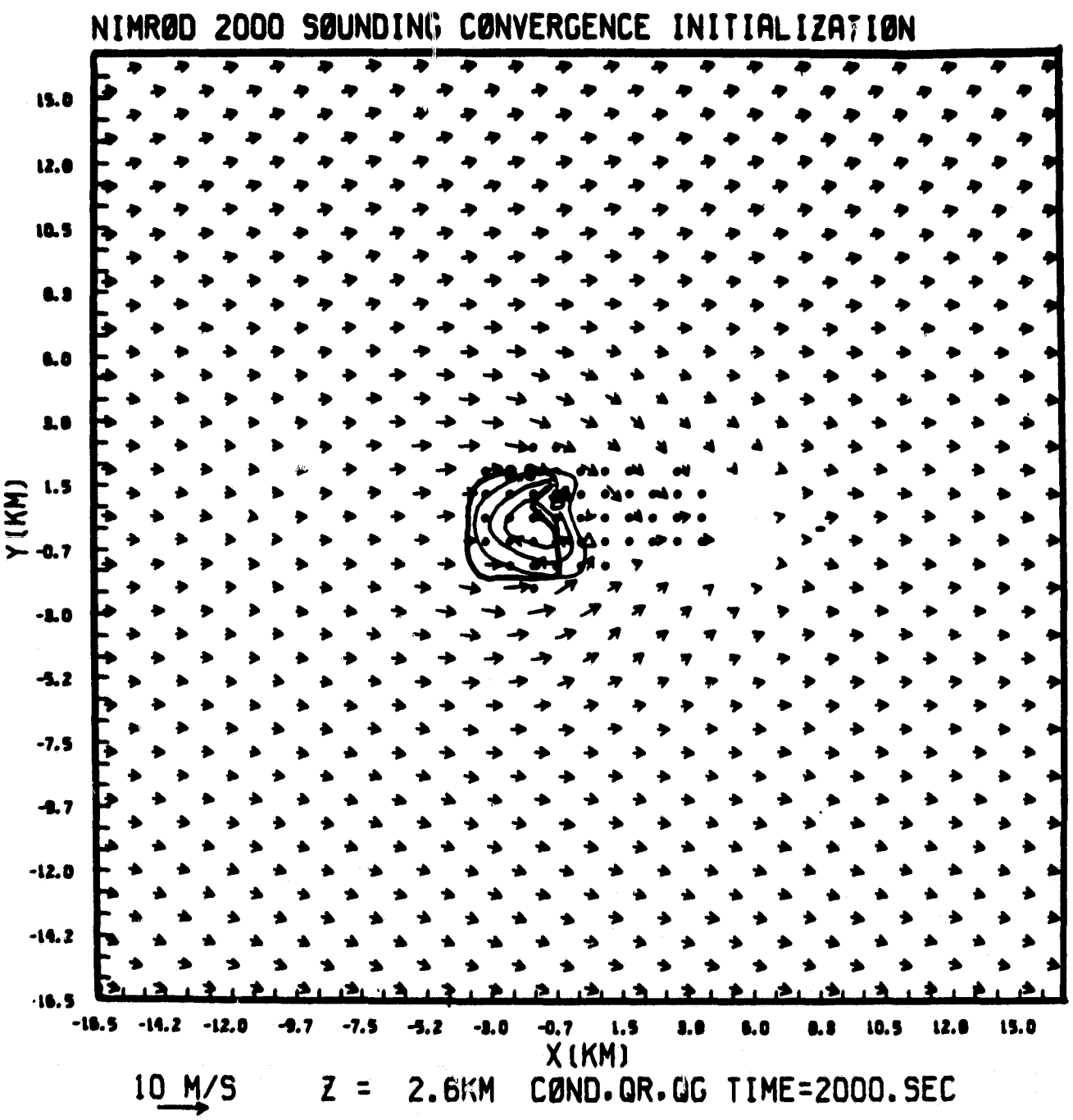

Figure 18: Same as Fig. 16 except at 2.6 km AGL.

and is shifted upshear. This downshear tilt with height was shown on the trajectories of Heymsfield shown earlier. The downdraft near the surface is shown in Fig. 13 at 1500 s and Fig. 19 at 2500 s. The downdraft core is moving upshear with time. We would expect trajectories of the time variant model predictions to be very similar to Heymsfield although the cloud circulation itself never becomes as steady as the observations indicated.

The results of these experiments again suggest a strong dependence of storm structure on the initial environment of the storm and perhaps the evolving environment during the life of the storm. Our shortcomings can be directly linked to an insufficient description of the environment at the time of the storm. Because we had to make assumptions pertaining to the environment (to which we demonstrated a high sensitivity in our simulations), it is not suprising that we were unsuccessful in producing a storm exactly like A-5. It is our experience that the individual cumulus cloud is much like synoptic scale disturbances in its requirement for specification of initial conditions. We would not expect to accurately simulate an occluding front and low pressure trough approaching Detroit based on a single sounding taken in Omaha the previous evening. Likewise the accurate simulation of an observed cumulonimbus storm requires perhaps tens or hundreds of points around the disturbance at which the atmosphere is sampled through its entire depth. If such data were available, we would then need to study more advanced dynamic initialization techniques in order to incorporate the detailed analysis into the model. We believe this is where small scale modeling must go if the individual cell structure of clouds such as A-5 are to be accurately simulated.

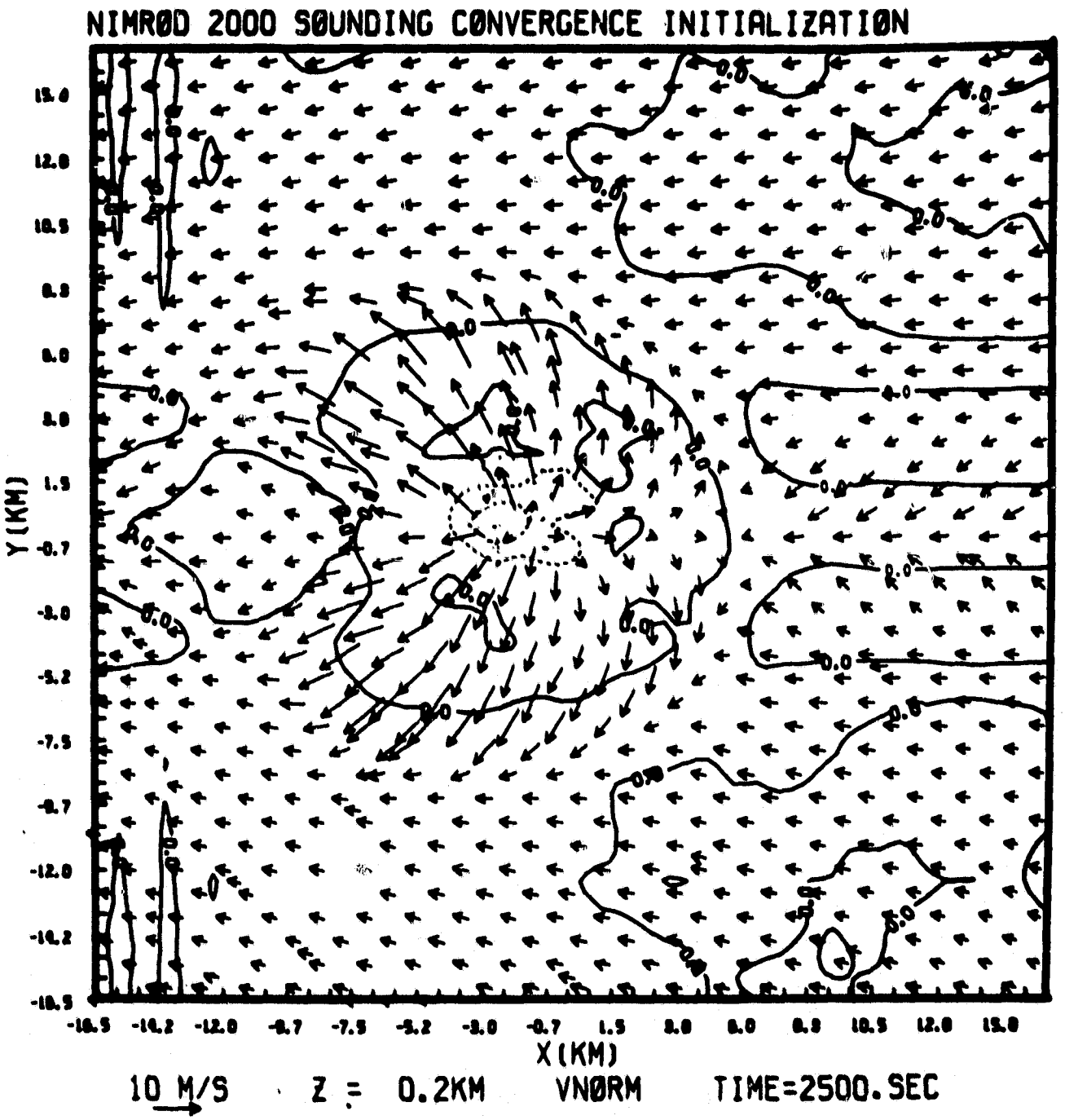

Figure 19: Same as Fig. 13 except at 2500s simulation time and at height .2 km AGL.

6.0 DEVELOPMENT OF A CONCEPTUAL/SEMI-QUANTITATIVE MODEL OF EASTWARD PROPAGATING, MESOSCALE CONVECTIVE COMPLEXES FORMING TO THE LEE OF THE ROCKY MOUNTAINS

The development of a conceptual/semi-quantitative model of eastward propagating, mesoscale convective complexes has been concentrated on the analysis of convective complexes forming during the period 3 August to 10 August, 1977. A two-part paper has been submitted and revised for publication in the Monthly Weather Review entitled: A Long-Lived Mesoscale Convective Complex, Part I - The Mountain Generated Component, and Part II - Morphology of the Mature Complex (see Appendices 1 and 2). A condensed version of Part II was presented in a paper at the 12th Conference on Severe Local Storms in San Antonio, Jan 1982 (see Appendix 3).

Part I is basically a synthesis of George's (1979) thesis. The paper follows a scenario of convective evolution from the early morning micro-meteorological scale, to the mid-day ridge/valley circulation and mountain cumuli/cumulonimbus, to mid-afternoon plains cumulonimubs and squall lines, to the formation of a mesoscale convective complex (MCC).

In Part II, the pre-MCC synoptic field is re-analyzed and the morphology of the mature MCC is described including:

i) the interaction of the MCC with the remains of the previous day's MCC

ii) the intrusion of dry, high momentum air into the back of the storm at 500 mb

iii) a broad region of high momentum outflow from the storm just below the tropopause

iv) a significant meso-anticyclone at 200 mb which was not present prior to the formation of the MCC

v) lack of direct interaction with the polar front jet well to the north

vi) divergence profiles similar to tropical clusters

vii) virtually no evidence of poleward meridional heat transport associated with the MCC as one would expect in a baroclinic system.

It is concluded that the MCC's studied are basically tropical in nature and their dynamics are dominated by buoyant accelerations. Associated weak baroclinic features, such as a surface stationary front, serve to trigger and direct the release of convective instability. It is suggested from this analysis that a certain amount of baroclinicity may be compatible with an MCC, but as the baroclinicity increases the convection either tends to organize itself into the linear structure of a squall line or the system as a whole undergoes a transformation into a rapidly occulding cyclonic wave.

The two-part MCC paper stresses mesoscale processes for the pre-MCC developmental stage and shifts emphasis to the synoptic scale for the mature MCC stage. This synoptic analysis for two specific mature MCCs complements well the composite MCC studies by Maddox (1981, 1982) and the MCC modelling results of Fritsch and Maddox (1981). Relying primarily on synoptic rawinsonde data, these studies have not extended into the meso-β scale (~20-200 km) sub-structure of the meso-α (~200-2000 km) parent system. Under support of this contract, we have attempted to refine the conceptual MCC model to include these smaller scales by continuing the investigation of the 3-10 Aug 1977 MCC episode, focusing on the MCCs meso-β scale sub-structure.

In papers presented at the IAMAP Third Scientific Assembly (Hamburg, Aug 1981) and the Fourth Conference on Hydrometeorology (Reno, Oct 1981) [see Appendices 4 and 5], we showed that the MCC displays and internal radar echo structure more complex than the near-circular cloud-top shield and synoptic studies would imply. This meso-β scale complexity is manifested spatially and temporally within a given MCC, as well as in the great variability displayed from one MCC to another. Despite this complexity, consistent meso-β scale characteristics were identified for several of the MCCs. For example, the component meso-β scale centers of convective activity were located consistently along meso-α to synoptic scale features (such as fronts, the previous day's MCC outflow boundary, or a lee-side line of orogenic convection). The core of the MCC characteristically developed from a meso-β scale convective cluster that intensified near the intersection of two such meso-α scale features. A much more restricted area of low-level radar echo and precipitation was consistently observed than what the conceptual meso-α scale vertical circulation might imply (suggesting that the extensive cold cloud shield is more a result of diverging convective cloud debris than organized meso-α scale ascent, and/or that there is significant sub-anvil evaporation of the meso-α scale precipitation).

Furthermore, significant differences were observed between those MCCs in the episode that formed to the immediate lee of the Rockies and those that formed another 500-800 km to the east. The western systems all involved the orogenic line of convection induced by a meso-α scale mountain/plains diurnal circulation, while the eastern systems formed without the benefit of this particular forcing mechanism.

Also, the eastern systems generally displayed less meso-β scale complexity and better fit the conceptual model of a single-cellular, meso-α scale MCC.

This meso-β scale analysis of the 3-10 Aug 1977 MCC episode is continuing on a more quantitative basis, utilizing hourly precipitation, radar, and enhanced IR satellite data. We believe that the improved conceptual/semi-quantitative model, extending into the meso-β scale, will contribute significantly to the current understanding of the MCC life cycle. A paper on this topic is currently in preparation for submission to the Monthly Weather Review.

ACKNOWLEDGEMENTS

The authors wish to thank Mr. Mark Stephens for his contribution to our studies of model anvil outflow versus updraft intensity. We also would like to thank Mr. Thomas Nehrkorn for his contribution to our studied of linkage between overshooting tops and downdrafts. Mr. Gad Levy provided valuable assistance in the Nimrod case study and associated analysis. We also acknowledge the work of Dr. Peter Wetzel, Mr. Ray McAnelly, and Mr. Ray George toward the analysis of Mesoscale Convective Complexes. Thanks are especially due Brenda Thompson for typing the manuscript.

Numerical model simulations and analysis were performed on the NCAR (National Center for Atmospheric Research) CRAY 1 computer. NCAR is sponsored by the National Science Foundation. All data pertaining to the South Park Area Cumulus Experiment (SPACE) was collected as part of NSF Grant ATM 7908297. Simulations studies of SPACE data were sponsored by NSF Grant ATM 8113082. Simulations of Florida Area Cumulus Experiment (FACE) data were sponsored both by NSF Grant

ATM 7908297 and National Oceanic and Atmospheric Administration (NOAA) Grant NA81RAH00001 Amend. #4 Item #6.

Simulations and analysis reported in this paper were supported under NASA Grant NSG 5341.

7.0 REFERENCES

Cotton, W.R., R.L. George, P.J. Wetzel and R.L. McAnelly, 1982: A long-lived mesoscale convective complex. Part I - The mountain generated component. Submitted to Mon. Wea. Rev., Dec. 1981.

Fritsch, J.M., and R.A. Maddox, 1981: Convectively driven mesoscale weather systems aloft. J. Appl. Meteor., 20, 9-26.

Fujita, T. and H. Byers, 1977: Spearhead echo and downdraft in the crash of an airliner. Mon. Wea. Rev., 105, 129-146.

Heymsfield, Gerald M., 1981: Evolution of downdrafts and rotation in an Illinois thunderstorm. Mon. Wea. Rev., 109, 1969-1988.

Klemp, J.B. and R.B. Wilhelmson, 1978a: The simulation of three-dimensional convective storm dynamics. J. Atmos. Sci., 35, 1070-1096.

_____ and _____, 1978b: Simulations of right- and left-moving storms produced through storm splitting. J. Atmos. Sci., 35, 1097-1110.

Knupp, K.R. and W.R. Cotton, 1981a: An intense, quasi-steady thunderstorm over mountainous terrain. Part II: Doppler radar observations of the storm morphological structure. To be published in J. Atmos. Sci.

_____ and _____, 1982b: An intense, quasi-steady thunderstorm over mountainous terrain. Part III: Doppler radar observations of the turbulent structure. To be published in J. Atmos. Sci.

Maddox, R.A., 1981: The structure and life-cycle of midlatutide mesoscale convective complexes. Atmos. Sci. Paper No. 336, Dept. of Atmos. Sci., Colorado State Univ., Ft. Collins, CO 80523, 311 pp.

Maddox, R.A., 1982: Large scale meteorological conditions associated with midlatitude mesoscale convective complexes. Submitted to Mon. Wea. Rev.

McBride, J.L., 1979: Observational analysis of tropical cyclone formation. Dept. of Atmos. Sci., Paper No. 308, Colorado State University, Fort Collins, CO, 230 pp.

Miller, M.J. and R.P. Pearce, 1974: A three-dimensional primitive equation model of cumulonimbus convective. Quart. J. Roy. Meteor. Soc., 100, 133-154.

Miller, M.J. and A. J. Thorpe, 1981: Radiation conditions for the lateral boundaries of limited-area numberical models. Quart. J. Roy. Meteor. Soc., 107, 615-628.

Nehrkorn, T., 1981: A three-dimensional simulation of the dynamic response of a Florida cumulus to seeding. M.S. Thesis, Colorado State University, Fort Collins, CO, 99 pp.

Purdom, J.F.W. and K. Marcus, 1981: Thunderstorm triggered mechanisms over the Southeast United States. Preprints: 12th Conf. on Severe Local Storms, Jan. 12-15, 1982, San Antonio, AMS, pp. 487-488.

Sax, Robert I. and James G. Hudson, 1981: Continentality of South Florida summertime CCN aerosol. J. Atmos. Sci., 38, 1467-1469.

Schlesinger, R.E., 1974: A three-dimensional numerical model of an isolated deep convective cloud: Preliminary results. J. Atmos. Sci., 32, 934.

Thorpe, A.J. and M.J. Miller, 1978: Numerical simulations showing the role of downdraft in cumulonimbus motion and splitting. Quart. J. Roy. Meteor. Soc., 104, 873-893.

Tripoli, G.J. and W.R. Cotton, 1980: A numerical investigation of several factors contributing to the observed variable intensity of deep convection over S. Florida. J. Appl. Meteor., 19, 1037-1063.

8.0 APPENDICES

Wetzel, P.J., W.R. Cotton and R.L. McAnelly, 1982b: The dynamic structure of the mesoscale convective complex -- some case studies. Preprints, 12th Conf. on Severe Local Storms (San Antonio), Amer. Meteor. Soc., Boston, 265-268.

McAnelly, R.L., and W.R. Cotton, 1981a: The meso-β scale structure and evolution of middle-latitude meso-α scale convective complexes. Presented at IAMAP Third Scientific Assembly (Hamburg, Federal Republic of Germany) (Available from Dept. of Atmospheric Science, Colorado State Univ., Ft. Collins, CO 80523), 34 pp.

_____, and _____, 1981b: The meso-β scale structure and precipitation characteristics of middle-latitude meso-α scale convective complexes. Preprints, Fourth Conf. on Hydrometeorology (Reno), Amer. Meteor. Soc., Boston, 81-87.

APPENDIX 1

THE DYNAMIC STRUCTURE OF THE MESOSCALE CONVECTIVE COMPLEX--SOME CASE STUDIES

Peter J. Wetzel[1], William R. Cotton[2], and Ray L. McAnelly[2]

[1]Goddard Laboratory for Atmospheric Sciences, NASA/Goddard Space Flight Center, Greenbelt, MD 20771

[2]Department of Atmospheric Science, Colorado State University, Fort Collins, CO 80523

During the summer months, a nocturnal precipitation maximum occurs over a broad region of the central High Plains. More than 60% of all precipitation during the months of June, July, and August falls between the hours of 2000 and 0800 local time within an area covering all of Nebraska, Kansas, Iowa, and northern Missouri. Evidence suggests that this precipitation frequently comes from mesoscale systems which originate as afternoon convection over, or immediately leeward of the Rocky Mountains and move eastward, growing in response to the high moisture content of the air over the Great Plains.

During the period from 3 to 10 August 1977, mesoscale convective complexes (MCC's) were observed to develop daily near the Colorado Rockies and move generally eastward along a surface stationary front, sometimes maintaining their identity for several days. Figure 1 shows the tracks of these systems as well as a number of others which developed further east in Missouri and Iowa. During this episode, an excessive amount of precipitation fell in a 100-200 km wide band just south of the stationary front and extending from Colorado to the Atlantic coast. In the seven day period from 1200 GMT 4 August to 1200 GMT 11 August 1977, a total of 102 mm of precipitation was measured at Goodland, Kansas, 100 mm at Kansas City, 124 mm at Chicago, and 129 mm at Buffalo, New York. Minor flooding occurred in a number of locations along this band; for example, on 6 August, Parke County in west central Indiana received 175-225 mm of precipitation in six hours and a total of 250-325 mm in 24 hours.

Figure 2 is representative of the synoptic pattern which produced this episode. The episode began when a strong blocking ridge developed off the west coast of the United States and extended northward across eastern Alaska. This development initiated a slow steady flow of cool Canadian air southward to meet tropical air from the Gulf of Mexico and form the stationary front mentioned above. Weak shortwaves were observed circulating around the stationary 50 kPa low center over Hudson Bay. These were occasionally associated with particular convective systems during part of their lifetime. In Figure 2, the outline of the -52°C isotherm associated with MCC no. 1 (Figure 1) is seen associated with a short wave in the central United States. The two shortwaves entering the northwestern part of the county contribute to the development of system no. 2. Some aspects of the dynamic structure of MCC's 1 and 2 near the time of their mature stage are discussed below.

At 12Z 4 August 1977, system no. 1 was just past its mature, or most intense phase. It has been shown by Maddox et al. (1981) that upper tropospheric flow patterns are drastically modified by MCC's, primarily in the form of a broad anticyclonic pattern of wind anomalies near the tropopause. Such a pattern is evident in the vicinity of system no. 1 (see Figure 3); however, as shown by the representative wind profiles of Figure 4, the region of anvil outflow which produces the anticyclonic pattern, although having broad horizontal dimensions, is very shallow in the vertical. The wind profile within the MCC produced "jet" apparent in Figure 3 is very different from a typical synoptic scale jet in which the vertical wind shear is spread uniformly throughout the troposphere. Because the MCC outflow is so shallow, 12 hour forecast errors in the wind field when convection is omitted are limited to a narrow band near the tropopause. 300 mb wind forecasts, for example, are found to be much more correct. The shallowness of the outflow also accounts for the fact that at all levels the observed wind field shows very little effect of the MCC after 24 hours.

The anticyclonic flow pattern is also apparent near system no. 2, both in the wind pattern and the 200 mb height contours. Figure 5 shows a distinct storm scale anticyclone at a time shortly after the mature stage of this system. This feature was not apparent 12 hours earlier and it disappears 12 hours later; however, during the most intense phase of the system it is clear that significant upper tropospheric warming is produced. This is also apparent in the 500-200 mb thickness change from 0000 to 1200 GMT 5 August (Fig. 6). The maximum thickness increase of over 60 m, corresponding to a mean warming in this layer of over 3 K, was centered over the MCC and was focused to the length scale of the system.

Divergence in the vicinity of both MCC nos. 1 and 2 was calculated at two levels using the method of Bellamy (1949), which employs the rawinsonde data directly and requires no preanalysis or interpretation of the reported winds. Divergence maps are presented in Figure 7. At

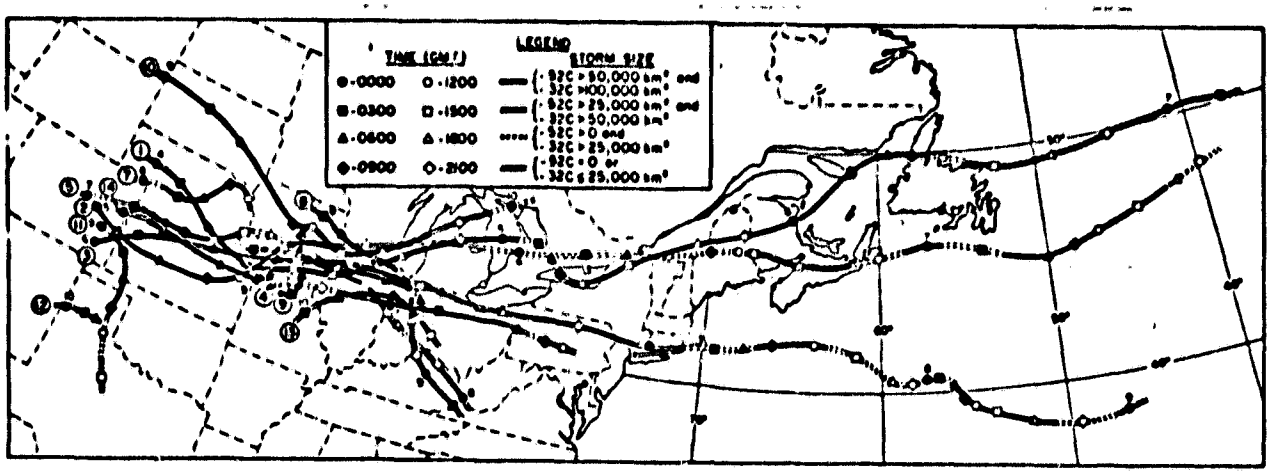

Figure 1. Tracks of the centroid of the fourteen MCC's which developed during the episode of 3-10 August 1977. Circled number is the system number. The date is given near the 0000 GMT symbol.

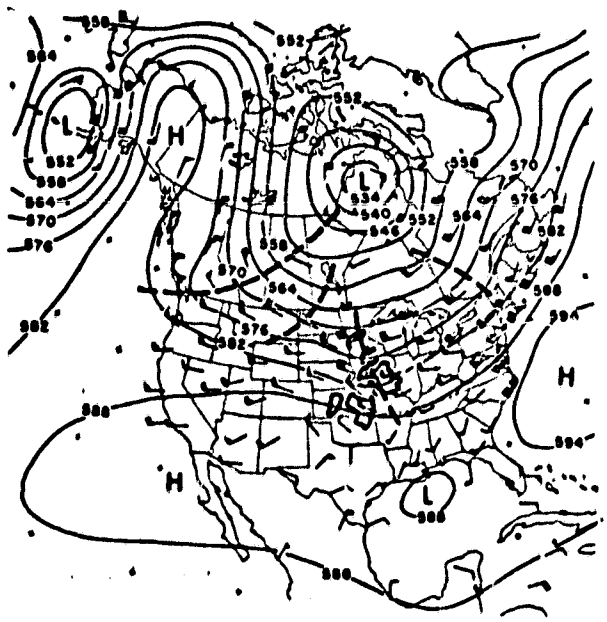

Figure 2. 500 mb analysis for 1200 GMT 4 August 1977. Dashed lines mark positions of shortwave troughs. Also outlined in the central U.S. is the -52°C infrared isotherm of the MCC in that area.

200 mb (Figures 7b, d), the expected broad region of divergence is seen in the vicinity of both systems. Surrounding each system was a ring of presumably compensating convergence. In both cases, the strongest horizontal gradient of divergence occurred on the southeastern flank of the system. A more surprising result is the divergence pattern at 500 mb--supposedly near the level of non-divergence in baroclinically driven storms. In Figures 7a, c we see a distinct divergence-convergence couplet associated with each storm and imbedded within a field of near zero divergence values. This feature may be reflective of the process of entrainment of middle level air into the rear flank of the storms.

Figure 4. Wind velocity profiles at 1200 GMT 4 August 1977 for Peoria, Ill. (solid), Salem, Ill. (dashed) and Little Rock, Ark. (dotted).

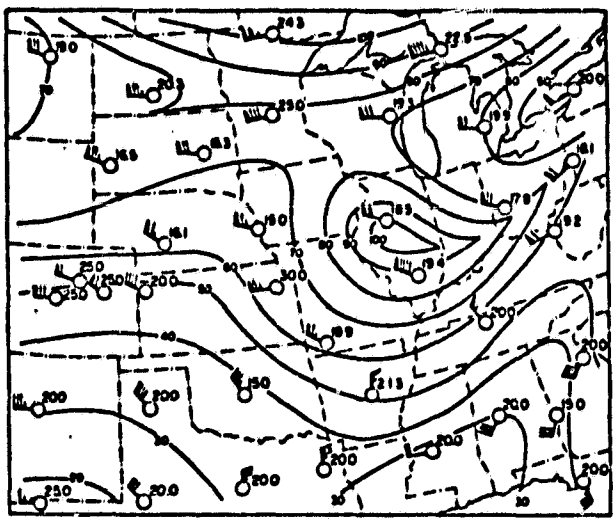

Figure 3. Upper tropospheric maximum wind at 1200 GMT 4 August 1977, plotted and analyzed in knots, with pressure level of corresponding wind vector in kPa.

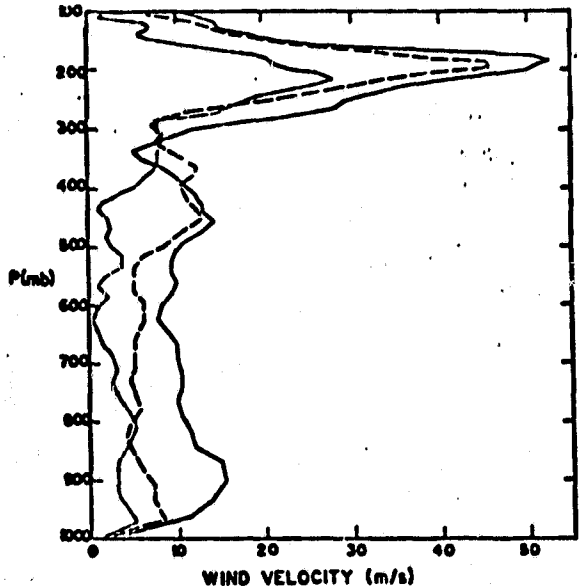

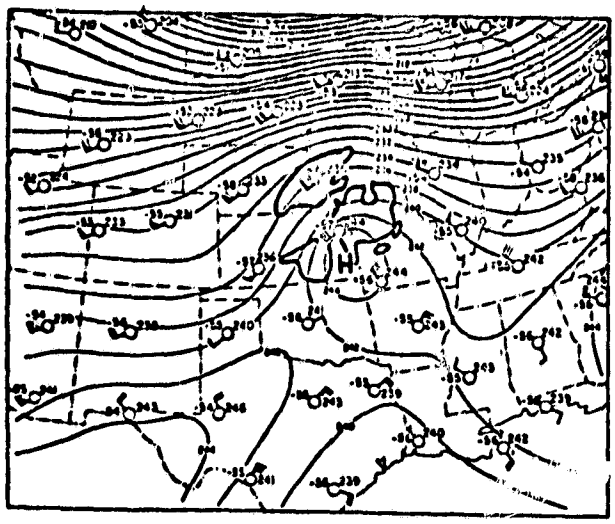

Figure 5. 20 kPa height analysis for 1200 GMT 5 August 1977, with the area of satellite observed apparent black body temperature less than -52°C shaded and outlined by a heavy solid line.

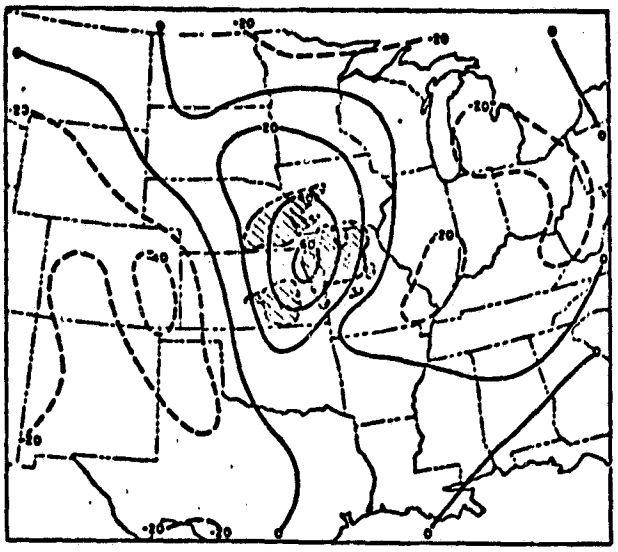

Figure 6. 12-h change in 50-25 kPa thickness (in meters) from 0000 GMT to 1200 GMT 5 August 1977. Negative-valued contours are dashed. Area with satellite observed apparent black body temperature less than -52°C at 1200 GMT 5 August is shaded.

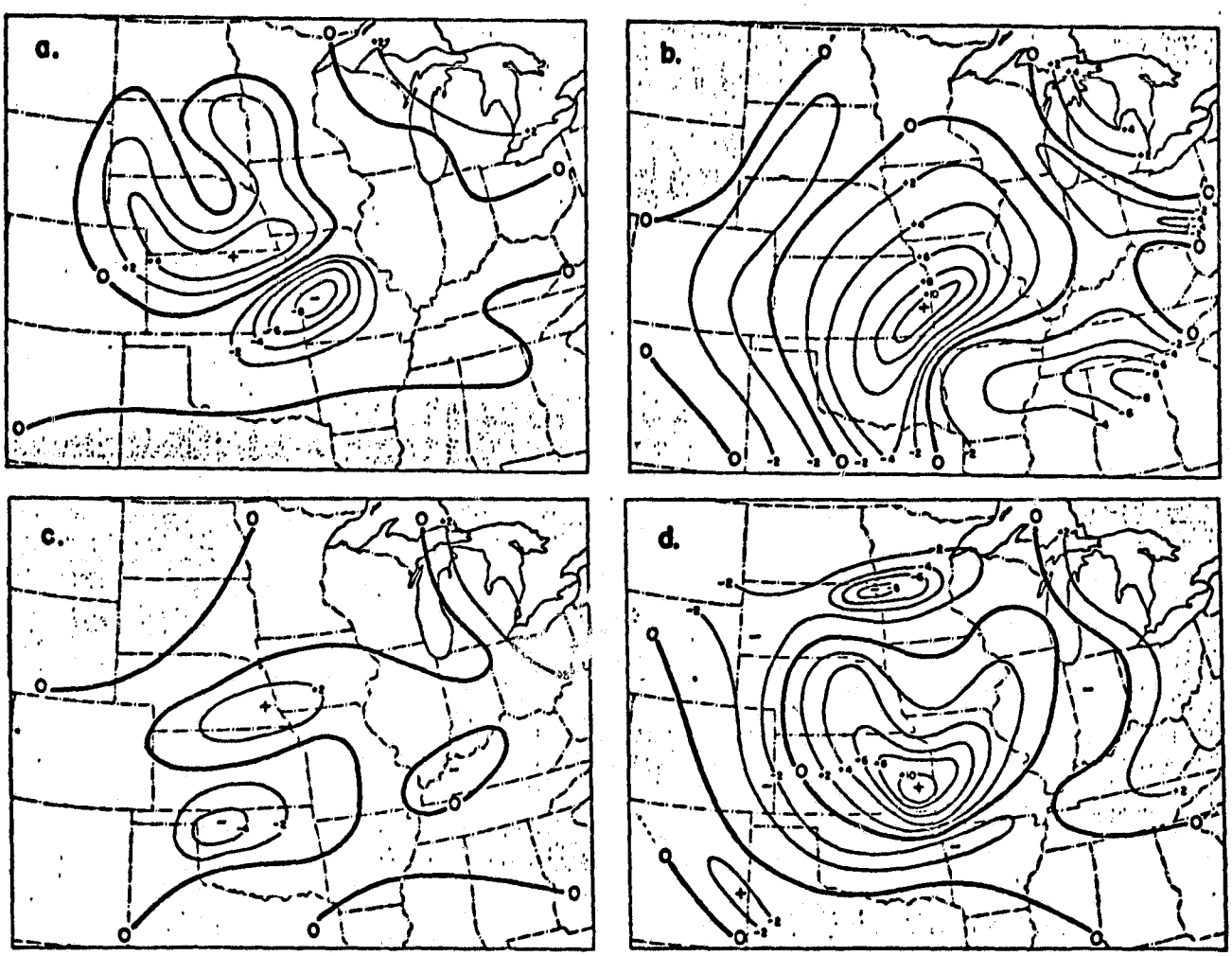

Figure 7. Maps of divergence (convergence negative) calculated using the method of Bellamy (1949) for (a) 50 kPa at 1200 GMT 4 August 1977; (b) same as (a) for 20 kPa; (c) 50 kPa at 1200 GMT 5 August 1977; (d) same as (c) for 20 kPa. Contours analyzed at intervals of 2×10^{-5} sec^{-1}.

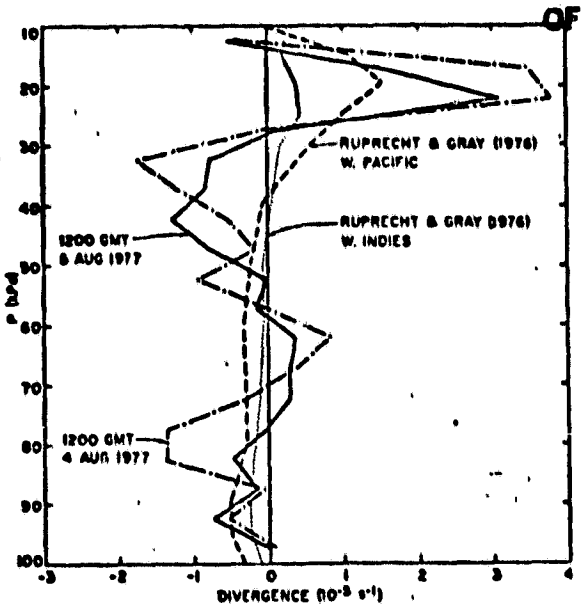

Figure 8. Vertical profiles of divergence as reported by Ruprecht and Gray (1976) for tropical cloud clusters, and as calculated using the method of Bellamy (1949) within polygons surrounding the MCC's studied here. For 1200 GMT 4 August 1977, the polygon used has an area of 512,000 km² and has at its boundary the following stations: Oklahoma City; Monett, Missouri; Salem, Illinois; Peoria, Illinois; Omaha, Nebraska; North Platte, Nebraska, and Amarillo, Texas. For 1200 GMT 5 August 1977, the polygon used has an area of 523,000 km² and has at its boundary the following stations: Oklahoma City; Monett; Peoria; Huron, South Dakota; North Platte, Nebraska; and Dodge City, Kansas.

Vertical profiles of mean divergence in 50 mb layers in the vicinity of the two MCC's were also calculated and appear in Figure 8. These profiles were constructed using data obtained from stations arranged in a polygon surrounding each MCC, again using the technique discussed by Bellamy (1949). The area within the polygon selected for 1200 GMT 4 August was 512,000 km^2, and 523,000 km^2 for the following day's MCC. Also shown on Figure 8 for comparison are composite calculations of divergence profiles in tropical cloud clusters as presented by Ruprecht and Gray (1976). The area within which Ruprecht and Gray calculated divergence is only about 40% of that used for the MCC's, so direct quantitative comparison of these curves is not possible. The smoother, less detailed nature of the cloud cluster profiles can be attributed to the large number of soundings and storms combined into these composite profiles; nevertheless, the similarities between MCC and cloud cluster divergence structures stand out clearly. Both have a general convergence throughout the lower and middle troposphere with a narrow layer of relatively strong divergence centered at 20 kPa associated with the storm outflow. The magnitude of the divergence values presented in Figure 8 is comparable to that produced by a typical baroclinically driven mid-latitude cyclone; and since the polygonal area used in the divergence calculation (equivalent to a square 700 km on a side) would also encompass the circulation of such a cyclone, one may conclude that the magnitude of mass displaced by an MCC is similar to that of a conventional cyclone.

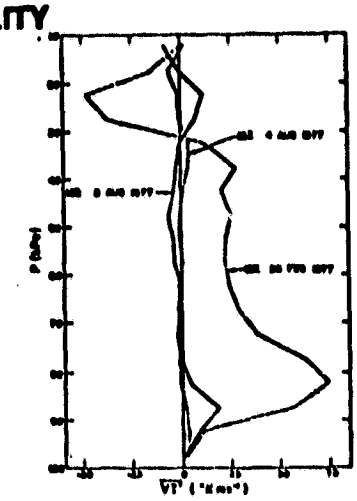

Figure 9. Vertical profiles of nine stations average meridional heat transport for the two MCC's and for a mature winter cyclone centered at the same point. The nine stations used for each profile are the following: North Platte, Nebraska; Omaha, Nebraska; Peoria, Illinois; Topeka, Kansas; Dodge City, Kansas; Salem, Illinois; Oklahoma City; Monett, Missouri; and Little Rock, Arkansas.

As a further comparison between baroclinically driven systems and MCC's, the vertical profiles of average meridional sensible heat transport by the two storms are plotted in Figure 9 along with the profile from a mature winter cyclone centered at the same location. Each profile was constructed by calculating a nine station, 50 mb layer mean temperature for each layer from the surface to 100 mb. Each individual station's deviation from that mean, T', was then multiplied by the meridional wind component V (equivalent to V' since the mean value of V is assumed to be zero), and the nine values of VT' were averaged arithmetically. The results show that the winter cyclone generated a strong northward transport of heat through the troposphere while little northward heat transport was produced by the MCC's. In fact, throughout much of the troposphere, except near the tropopause and the surface, there was a slight southward transport of heat by these systems. The low-level transport can probably be attributed to the effects of the low-level jet. From Figures 8 and 9, one is led to the conclusion that a weather system which displaces as much mass as a baroclinic system without transporting significant sensible heat poleward must be operating in a predominantly barotropic environment and must be basically driven by convective instability in a manner similar to tropical cloud clusters.

REFERENCES

Bellamy, J. C., 1949: Objective calculations of divergence, vertical velocity and vorticity. Bull. Amer. Meteor. Soc., 30, 45-49.

Maddox, R. A., D. J. Perkey, and J. M. Fritsch, 1981: Evolution of upper tropospheric features during the development of a mesoscale convective complex. J. Atmos. Sci., (in press).

Ruprecht, E. and W. M. Gray, 1976: Analysis of satellite-observed tropical cloud clusters. I. Wind and dynamics fields. Tellus, 28, 391-413.

APPENDIX 2

Presented at IAMAP Third Scientific Assembly (Hamburg, Federal Republic of Germany), Aug. 1981. (Avail. from Colorado State University, Dept. of Atmospheric Science, Ft. Collins, CO 80523).

The Meso-β Scale Structure and Evolution of Middle-Latitude Meso-α Scale Convective Complexes

Ray L. McAnelly and William R. Cotton

Department of Atmospheric Science
Colorado State University
Fort Collins, Colorado 80523

1. INTRODUCTION

The mid-latitude Mesoscale Convective Complex (MCC) has been identified and described by Maddox (1980) as a unique class of convection, organized on the meso-α[1] scale (250-2500 km; see Orlanski (1975) for a detailed discussion of scale terminology), which accounts for much of the convective season precipitation over a large portion of the United States (US) mid-section. The predominantly nocturnal occurrence of thunderstorms in this area has been long established (Means, 1944; Wallace, 1975), and previous attempts to describe their mesoscale organizational characteristics have generally invoked the squall line conceptual model (Porter et al., 1955; Miller, 1967). However, based on the relatively new geostationary satellite vantage, Maddox (1981) demonstrated that the MCC has distinctly different structural and dynamical characteristics from the squall line. Among its distinctive features are a long-lived, near circular cold cloud shield, large areas of light precipitation (with embedded, locally heavy precipitation), a mesoscale mid-to-upper tropospheric warm core, and a large-amplitude anticyclonic outflow in the upper troposphere that strongly perturbs the larger-scale environment. Fritsch and Maddox (1981) have further described the upper-level structure of the MCC and, with numerical model support, have inferred that a mesoscale region of mean ascent in the mid-to-upper

[1] Hereafter, α and β will be referred to as a and b, respectively.

troposphere is a fundamental aspect of the MCC that explains many of the observed features.

The previously cited MCC studies concentrated on their gross satellite-based characteristics, synoptic-network data, and a rather coarse mesoscale numerical model, and were therefore focused and somewhat limited to the meso-a structure and the macroscale (>2500 km) environment of the MCC. While Maddox (1980) recognized the role of intense meso-b scale (25-250 km) convective systems in initiating the MCC and in continuing to produce locally heavy rains within the larger, mature complex, no systematic study of the meso-b structure of the MCC has been made. A more detailed description of the meso-b substructure of the MCC would lead to a better understanding of the processes by which the mature meso-a system evolves from its incipient meso-b components, persists for several hours, and then fragments and loses its organized characteristics. Given the consistent meso-a features of the MCC on one hand and the more capricious nature of convective scale processes on the other, this paper describes intermediate meso-b characteristics of the MCC that are observed to be somewhat consistent from case to case.

2. CASES STUDIED AND DATA UTILIZED

As evidenced by Maddox's (1981) two-season MCC climatology, successive MCCs often develop daily over a several day period when a slowly evolving large-scale circulation pattern becomes favorable for their formation. The MCCs studied here composed such an eight-day episode, 3-10 Aug 1977, in which afternoon and evening convection developed upscale each day into one or more MCCs that persisted well into the night. The quasi-stationary synoptic pattern at 50 kPa during this episode consisted of a strong low centered in the Hudson Bay region, a ridge off the west coast extending well into eastern

Alaska, and a polar jet running southward in western Canada and turning zonal along the US-Canadian border. A low-level deformation field and weak cool surges maintained a quasi-stationary surface front extending from the Nebraska region to the Great Lakes and New England, with a low-level southerly flow of maritime tropical air to the south of the front on the west side of the Atlantic subtropical high.

The tracks of 14 MCCs in this episode are shown in Fig. 1, based on GOES infrared (IR) satellite-defined centroids of convection associated with each MCC. (The darkened tracked indicate periods when the convection met Maddox's [1980] areal and thermal criteria for a mature MCC.) There are two general genesis regions evident, one along the eastern slopes of the Rockies and High Plains, and the other further east in the Missouri and Mississippi River basins. Other notable features in Fig. 1 are that the MCCs tended to occur in the vicinity of, and track along, the quasi-stationary surface front, and that the remnants of decayed complexes persisted as identifiable regions of loosely organized convection for long periods (up to 3 days) that occasionally reintensified into mature complexes. Cotton et al. (198) analyzed the mountain generation and High Plains evolution of a north-south meso-b squall line of 4 Aug 1977, and Wetzel et al. (1981) further documented its role in the formation of MCC number 2 in Fig. 1. Wetzel et al. examined the three-dimensional structure of systems 1 and 2 in as much detail as could be inferred from the synoptic data at 1200 GMT on 4 and 5 Aug, respectively (when both systems were several hours past this maximum intensity). In this paper we examine the meso-b structure and evolution and precipitation characteristics of systems 1, 2, and 3, generated on the High Plains, and systems 6 and 8, which were generated in the eastern region.

Radar data sources include PPI radar film from six National Weather Service (NWS) sites, observation logs, summary charts, manually digitized radar (MDR) plots, and multi-tilt digital PPIs from the High Plains Experiment (HIPLEX) site in western Kansas. GOES IR imagery, hourly precipitation data, and conventional surface and upper-air data are also utilized.

3. THE MESO-B SUBSTRUCTURE AND EVOLUTION OF THE MCCs

In this section, summaries of the evolution of five of the more well-defined MCCs of the episode are presented in order to emphasize certain features that are common to many of these systems and which therefore help to generalize their lifecycles. Figures 2-4 illustrate several important evolutionary features of systems 1, 2, and 3, which were successively generated on the High Plains in the first three days of the episode, reaching their maximum extent in the Kansas/Nebraska region. Included in these figures are GOES-east IR apparent blackbody isotherms of -40 and $-62^{o}C$, meso-b clusters and lines of relatively strong convection, and approximate displacements of those features since the previous map time or over the previous 3 h (if in existence for that long). The identification of meso-b features was subjectively based primarily on NWS radar film which was generally of a poor quality as far as quantitative intensity resolution was concerned. However, the temporal resolution of the PPI data was generally excellent, so an amalgamation of intensity inferences, using all data sources, allowed the reliable identification of relatively strong meso-b scale echo entities that persisted for well over an hour. Each meso-b feature depicted may represent near-solid echo coverage, or alternately, simply a cluster or line of discrete echoes that maintains a meso-b cohesiveness. Some areas of weak echo, isolated echoes, and

meso-b echo features that apparently had little effect on the MCC development are omitted for the sake of clarity.

Figure 2a shows some of the synoptic features at the time when the pre-MCC convection was beginning to organize, 0000 GMT 4 Aug. A weak 70 kPa shortwave extended from western Nebraska to the Texas panhandle, with the low-level jet in the same region. A surface trough was located along the lee side of the Rockies, with another trough dipping into southeastern Nebraska. An area of mid-level moisture and weak residual convection from the previous day extended from southeastern Missouri northwestward through eastern Kansas.

The satellite and radar map for 0300 GMT (Fig. 2b) depicts three meso-b convective clusters (labeled A, B, and C) in a north-south line in western Nebraska and Kansas. These had formed in the Wyoming and Colorado foothills along the trough shown in Fig. 2a and are typical of the orogenic convection induced by difference in the mountain plateau and plains diurnal heating cycle (Cotton et al., 1981). Cluster A formed earliest and was most intense, producing the bulk of the cold cloud shield which met MCC criteria by 0200 GMT. Storms in this cluster produced strong winds and large hail in western Nebraska. Another group of meso-b features (D, E, F) formed in a northwest-southeast orientation along the residual moisture axis in Fig. 2a. These were newer and less intense than the orogenic clusters, but were beginning to intensify rapidly as the faster eastward propagating orogenic line approached.

By 0500 GMT (Fig. 2c), clusters A and B had moved eastward and assumed meso-b squall-line characteristics. This was likely due to their propagating into the low-level jet region, thereby increasing the low-to-mid-tropospheric shear (50 kPa winds were fairly uniform, ~15 m s^{-1}

and northwesterly). The motion of clusters A and B over the previous 5 h (Fig. 2b, c) was confluent, perhaps steered by the confluent 70 kPa winds displayed in Fig. 2a for LIC, LBF, and DDC. This confluence of meso-b convective features may be instrumental in forcing the development of the MCC. As the meso-a line (composed of meso-b clusters A, B and C) in Fig. 2b moved east and formed a triple intersection with the E-F meso-a line and the surface trough shown in Fig. 2a, the meso-b features nearest the region of intersection (A and F) intensified. The western portion of F merged into the northeast end of A, while the southeastern portion of F split into a right-moving severe storm that produced a 50 km hailswath and merged with the meso-b band E.

Over the next 2 h, lines A and B continued their confluence, merged, and overtook F, creating a single large meso-b (or small meso-a) band of intense convection by 0700 GMT (Fig. 2d). A tornado occurrence and a 200 km track of severe surface winds accompanied the merging of these lines (these and other severe weather events are extracted from Storm Data, published by the National Climatic Center). Cluster D lost its discrete identity as it became lost in an expanding echo of uniform intensity that merged into the A-B-F band.

The maximum intensity of the MCC, as judged by the largest areal extent of the coldest enhanced IR contour (not shown), occurred at 0800 GMT. Despite the large cold cloud shield and weaker cells and patches of echo both ahead of and behind the intense meso-b echo depicted in Fig. 2d, nearly all of the hourly precipitation reports are confined to the depicted meso-b region.

By 1000 GMT (Fig. 2e), the single intense meso-b cluster had fragmented into several smaller meso-b clusters. Whereas up until the time

of maximum MCC intensity the meso-b convective features displayed a confluent tendency, in the weakening stage they became difluent, with the northern bands propagating easterly, the southern ones more southeasterly. This difluent propagation may be due to further growth being forced at the boundary of the expanding surface meso-high, which intensified most rapidly during the period of concentrated meso-b convection at MCC maximum intensity. Another mechanism that might explain the difluent propagation is a difluent low-to-mid tropospheric shear, where enhanced moist layer inflow relative to the moving storms would favor growth in the difluent direction. The vector difference between the 50 kPa wind and the centroid of the surface, 85 kPa and 70 kPa wind vectors (which crudely estimates a mean moist-layer wind) at 1200 GMT is displayed at several sites in Fig. 2e. The difluence displayed by these shear vectors is somewhat consistent with the observed meso-b cluster motions. This differential motion led to a commonly observed feature in dissipating MCCs, whereby the cloud shield lost its circularity and lengthened in a northeast-southwest orientation and assumed more of a meso-a comma cloud configuration that is more typical of a short-wave disturbance.

The next day's MCC, system 2 in Fig. 1, displayed similarities to, but also some significant differences from, MCC number 1. At the pre-MCC stage at 0000 GMT 5 August (Fig. 3a), the 70 kPa height field displayed only a very weak trough extending from northwest Colorado to Oklahoma. The low-level jet was again established in the Texas panhandle, and surface features consisted of a cold front advancing into Wyoming and South Dakota, stationary fronts through southern Nebraska and across southern Kansas into Illinois (the latter was the outflow boundary from the previous

day's MCC as it tracked on eastward), and a strong meso-high on the Colorado and New Mexico High Plains, produced by the afternoon orogenic convective line. This meso-a north-south line of storms was similar to, but farther south than, the previous day's orogenic line.

By 0300 GMT (Fig. 3b), the orogenic line, consisting of three meso-b clusters (A, B, C), had moved eastward, with B producing severe surface winds and hail in southeast Colorado. New meso-b lines (D, E), oriented east-west, developed in Kansas, the southern one (D) occurring along the stationary front separating the cooler, moister wake of the previous day's MCC from the unmodified maritime tropical air to the south. This was one hour prior to MCC initiation, as determined by IR cloud shield area.

As the eastward moving meso-a orogenic line (A, B, C) intersected the western end of the newer meso-a east-west line (D, E), the meso-b entities at the region of intersection (B, D) intensified rapidly, as was the case the day before. By 0600 GMT (Fig. 3c), the MCC was well established and centered on cluster B, which merged with the western end of D, developed rapidly towards line E to the east, and produced local hourly rainfalls of 60 mm. A new meso-b line, F, developed in central Nebraska along the east-west stationary front shown in Fig. 3a.

The MCC had achieved maximum intensity and was beginning to weaken by 0900 GMT (Fig. 3d). A and B had merged and expanded into a large precipitation region, but not too intense. Line D split off of B and, as with the southernmost echoes in the previous day's weakening system, displayed a southeastward propagation. Bands E and E, both originating as east-west lines, remained essentially stationary in the westerly steering flow as individual cells propagated eastward along the complexes. E

developed in areal extent as the A-B cluster approached it.

The squall-line characteristics displayed by the intense meso-b line during the mature phase of the first MCC (see Fig. 2d) did not occur in MCC 2, probably because the low-to-mid tropospheric shear was not as strong (west-northwesterly 50 kPa wind of only 5-10 m s^{-1}). In the dissipation stage (1200 GMT, Fig. 3e), the A-B cluster split, with B merging into E and A merging into F to give two weak meso-b bands with a squall-like configuration. The A-F band propagated east-northeastward while the E-B band moved southeasterly, again consistent with the difluent moist layer to 50 kPa shear.

The third MCC in Fig. 1 had similarities with and differences from the previous two. The Wyoming-South Dakota cold front in Fig. 3a had advanced into northern Kansas and eastern Colorado by 0000 GMT 6 August. Two north-south waves of orogenic convection developed from the upslope conditions north of the front and were separated by about 4 h and 200 km. A mesoscale band of weak convection developed in a northeast-southwest orientation along the front in southern Nebraska and northern Kansas. By 0300 GMT (Fig. 4), the most intense meso-b cluster of the first orogenic wave (A) had approached the weak frontal band (C) and intensified, followed shortly by the rapid intensification of meso-b cluster B in the second orogenic wave, together producing the MCC. A and C merged into a meso-a band from southeast Nebraska to southwest Kansas and remained the most significant feature of the MCC as cluster B weakened rapidly by 0600 GMT. The front apparently had a strong controlling influence on the organization of this MCC, as evidenced by the A-C band remaining strongly tied to the frontal position, by less complex meso-b substructure and by little difluent propagation of meso-b features occurring with MCC dissipation.

The High Plains MCCs, described above, were all characterized by their upscale intensification being centered on a meso-b component in a north-south meso-a orogenic line that intersected another meso-a feature to the east. While this quite regularly observed orogenic component is instrumental in many of the western plains MCCs, the eastern genesis region does not have the strong topographic forcing to help generate its MCCs. We now briefly summarize the evolution of systems 6 and 8 in order to point out similarities and differences to the western plains systems.

Figure 5a shows some synoptic features at and around 0000 GMT 7 Aug that help explain all three of the MCCs formed on this day (systems 4, 5, and 6). The 70 kPa height field has a shortwave trough through the eastern Dakotas, with a weaker, shorter wave through Colorado into the Texas panhandle. At 0300 GMT, when the initial convection of system 6 appeared, surface features consisted of a warm front extending from Colorado through central Iowa and a trough from South Dakota to northeast Colorado. The western MCC (system 5) developed at the triple intersection of an orogenic meso-a line and the surface front and trough in northeastern Colorado. 9 hours earlier, at 1800 GMT 6 Aug, the position of the surface warm front (broken warm front symbol) was across northern Missouri, where it was intersected by a north-south band of residual moisture from the dissipated system 3 (line of circles). MCC number 4 initiated at this intersection at that time. At 0300 GMT 7 Aug, system 4 was a mature MCC centered over Indiana and had left a wake boundary trailing to the northwest where it intersected the warm front in western Iowa. This feature was barely evident in high resolution visible satellite imagery, but it was also supported by surface observations. Warm moist air to the west

of the outflow boundary and to the south of the warm front was being advected northward toward the intersection.

The initial convection leading to the MCC appeared after 0300 GMT in extreme northwest Missouri within the warm moist surface air. By 0600 GMT (Fig. 5b), this cluster (labeled A) had gradually produced a large meso-b cloud shield centered over southeastern Iowa. Another meso-b echo feature, line B, had first appeared about an hour earlier. Line B developed within a broad weak band of convection that was apparently triggered by the weak outflow boundary in Fig. 5a and advecting northeast, as evidenced by an advancing northwest-southeast cloud band that had just reached enhanced levels in the IR imagery (-32°C in Figs. 5 and 6) and appeared as an eastward extension to the meso-b cluster A cloud shield.

About this time, meso-b scale interaction apparently developed between cluster A and line B and rapid development into an MCC ensued in the region of the intersecting outflow boundary and the warm front. By 0800 GMT (Fig. 5c), line B had transformed into an intense meso-b cluster and the eastward extending cloud shield had broadened considerably, continuing to develop toward the east. Figure 5d (1000 GMT) shows that cluster B propagated rapidly eastward (out of our radar data coverage), with the overshooting IR tops showing it to persist as the core of the MCC. Cluster A remained anchored to the west side of the MCC as an intense meso-b entity, fed by a strong southwesterly low-level flow into the storm.

Maximum intensity of the MCC occurred about 1100 GMT. By 1200 GMT (Fig. 5e), an east-west meso-b convective line (C) had developed and separated from the parent cluster A. The beginning of this line development was evident 2 h earlier in Fig. 5d. It developed southwestward along

a meso-b scale band of mid-level moisture (source unknown) that was apparent in IR images. The propagation of line C away from its parent cluster, as the MCC weakened and assumed more of an east-west line or structure, was a difluent motion between meso-b entities, also observed in the western MCCs as they began to decay.

The thermal discontinuity along the mesohigh outflow boundary in Fig. 5a, which helped to trigger MCC 6 early on 7 Aug. was strengthened and maintained by the convection associated with MCC 6 in eastern Iowa, northeast Missouri, and Illinois. Through the mid-day hours of 7 Aug, mostly sunny skies to the southwest of this boundary in Missouri and overcast to the northeast permitted a differential PBL heating that further reinforced the boundary. A meso-b remnant of the decayed, western MCC 5 was triggered as it crossed eastward over this boundary in northwest Missouri, and it reintensified into a small mature MCC by 0000 GMT 8 Aug. This further maintained the boundary as much precipitation fell east of it. The position of this MCC is superimposed on the 0000 GMT 8 Aug synoptic map (Fig. 6a). The thermal boundary through Iowa and Missouri was very well defined at this time, and the synoptic front had become stationary from eastern Colorado across Wisconsin. As each day before, a 70 kPa short-wave trough was in Colorado. A northeast Colorado meso-b cluster, part of an orogenic meso-a string of clusters, interacted with the front to produce a western MCC, system 7, in western Nebraska by 0500 GMT. The warm tongue of southerly flow intruding into Iowa was wedged between the two surface thermal boundaries and was ripe for convective development.

By 0500 GMT (Fig. 6b), linearly organized meso-b convective features, A and B, had developed and were aligned westward, just to the south of the

warm front, and southward along the mesoscale thermal boundary, respectively, from the point of intersection of these features in east-central Iowa. Another meso-b cluster, C, was along the warm front in northeast Iowa. Confluent motion of cluster C towards the intersection of lines A and B resulted in a consolidation of intense convection that produced a mature MCC within an hour. The meso-b clusters merged into a single large meso-b cluster A-B-C, with an east-west axis that persisted for 3 h (see Fig. 6c at 0700 GMT) as it slowly propagated eastward into central Illinois (and out of radar data coverage) without major structural evolution. Difluent fragmentation of meso-b features did not develop as much in this case as in most of the decaying MCCs, which may explain its very gradual demise; 7 h elapsed from the time of maximum intensity at 1000 GMT until it fell from meeting MCC criteria, compared with a normal period of 5 h.

4. PRECIPITATION CHARACTERISTICS OF THE MCCs

Despite the large uniform cold cloud shield in an MCC, the rainfall rates at a given time are far from uniform. Virtually all of the measurable hourly precipitation reports for the three western MCCs studied occurred within the shaded meso-b region indicated in Figs. 2-4 (and for intermediate hours not shown). At the most, the combined meso-b areas were less than half of the area within the -40°C isotherm, and substantial portions of the -62°C area were also rain-free. Even within the meso-b structures, the hourly reports show much variability that is characteristic of convective rainfall in general. An isohyet analysis for MCC 2 over Kansas (Fig. 7) illustrates the total storm variability (in which much of the temporal variability of the traveling meso-b systems is smoothed out). Note that the three sites in central Kansas reporting less than 0.25 inches are within the -62°C area in Fig. 3d and are nearly in the center of the MCC. The most uniform and widespread hourly precipitation reports occurred in

east-central Kansas in conjunction with the quasi-stationary meso-b complex E in Fig. 3. Along with the controls on meso-b structure exerted by the active cold front on MCC 3, discussed in Section 3, the front also produced a more uniform precipitation distribution (relative to systems 1 and 2), both overall and for hourly periods, due to the reduced meso-b substructure complexity.

The mature eastern MCCs in Figs. 5 and 6 also had cold anvil tops with areas that exceeded the total meso-b echo regions areas (and areas of measurable precipitation by about a factor of two. The spatial and temporal coherence of the meso-b features and the associated precipitation reports was more evident, being more persistent and slower to evolve than in their western counterparts. This difference may be due to the nature of upscale intensification in the few cases studied. The western MCCs evolved from two or more well-defined, pre-existing meso-b scale clusters, such as discrete orogenic clusters that interacted with each other and with other discrete meso-b clusters along a discontinuity to the east. The eastern MCCs, however, developed more on a single meso-b cluster that originated on a frontal or other thermal boundary. Thus, the more complex meso-b structure of the western pre-MCC allowed more possibilities for centers of MCC development and more combinations of meso-b scale interactions that can lead to rapidly evolving patterns. In the eastern systems, the development of the initial meso-b features into MCCs with predominant east-west axes resulted into more steady-state systems, in which convective cell movement was oriented approximately along the meso-b axes and structural evolution was not as volatile.

To investigate the precipitation intensity of the MCCs, the hourly rainfall reports from three western complexes (MCCs 1, 2, and 3) were

combined into a composite western MCC, while reports from the three eastern systems (6, 8, and 9) were composited into an eastern MCC. Compositing of the precipitation reports was with respect to beginning hour of the MCC, ending hour, and the hour of maximum intensity, all based on enhanced IR criteria (Maddox, 1980). The resultant composite complexes were both nine hours long with the maximum intensity occurring at the sixth (0800 GMT) and fifth (0900 GMT) hours for the western and eastern systems, respectively. The measurable precipitation amounts were stratified into various classes, with the percent of reports exceeding those thresholds plotted as a function of composite MCC time.

The eastern MCC rainfall distribution is shown in Fig. 8. The plots are indicative of what fraction of the active rain areas are intense. The results suggest that the percent of active rain areas exceeding all hourly thresholds (0.1, 0.2, 0.5 and 1.0 inches) increased from the initial pre-MCC convection to about 2 h after MCC initiation, at which time the fractional coverage of heavy precipitation (0.5, 1.0 inches) fell off steadily. This implies that the most intense convection (and severe weather potential) is early in the mature MCC stage when the meso-a complex is still developing. The fractional coverage of precipitation exceeding the less intense thresholds (0.1, 0.2 inches) continues to increase through the time of maximum MCC intensity, suggesting the spread of more uniform, light to moderate rainfall as the meso-a system develops. After maximum intensity, all thresholds decrease, suggesting that the precipitation in the diminishing MCC is more residual in character, becoming weaker and/or more intermittent.

The western composite MCC trends (Fig. 9) are similar, except that the more intense thresholds remain stable or slightly increase until MCC

maximum intensity, just as the lower thresholds, suggesting that intense convection persists further into the life cycle for the western system. This is also consistent with the more complex and more volatile meso-b substructure of the western system. The fraction of light precipitation (<0.1 inches) is greater for the western MCC, perhaps due to a reduction of moderate intensities by evaporation in the sub-cloud layer.

Figure 10 is a similar type plot of manually digitized radar (MDR) intensity distribution associated with the western composite MCC. While the areal coverage of echoes increases until MCC termination (number of non-zero MDR blocks curve), the plots show that the fraction of intense echoes maximizes about the first hour or two after MCC initiation, and then drops off steadily. This suggests that the severe weather potential (per unit area) is greatest in the early stages, but is somewhat inconsistent with the heavy precipitation reports persisting until MCC maximum intensity (Fig. 9). This may be explained by increased precipitation efficiency as the system moves east towards a moister environment and as the MCC region becomes more saturated through precipitation evaporation. Early in the west plains systems, when radar may be detecting a relatively large fraction of intense reflectivities aloft (1-3 km AGL), much of the precipitation is lost to virga.

With a limited amount of 3-dimensional (3-D) digital radar data from northwest Kansas, the 3-D morphology of portions of MCCs 2 and 3 were examined. An immense anvil overhang was observed in system 3, to the north and west of meso-b cluster B shown in Fig. 4. The outlines of the 5 dBZ echo at 3, 5, 7, and 9 km AGL are shown in Fig. 11. The region to the west of the radar is characterized by a 100-km anvil overhang echo, the top of which is uniform at 12-13 km and contributes to the uniform

IR satellite appearance of the MCC cloud shield. A north-south cross section through this feature (Fig. 12) shows it to be similar in dimension and shape to the anvil cloud associated with tropical cloud clusters (Houze and Leary, 1979; Zipser, 1977), but quite different in that the MCC anvil is echo-free below it. Thus, while "anvil" rain may account for much of the precipitation in maritime mesoscale systems (Zipser, 1977), virga probably robs much of this precipitation in continental MCCs, especially in the semi-arid High Plains. The cold, uniform MCC cloud shield may be indicative of mid-to-upper tropospheric meso-a scale ascent and precipitation generation (MAddox, 1980), but radar and hourly precipitation records show that surface rainfall is largely restricted to convection on the meso-b scale.

5. DISCUSSION AND SUMMARY

From a detailed examination of five MCCs occurring in an episode of 14 total MCCs, the following conclusions are inferred:

1. MCCs originating on the High Plains often develop from the growth, interaction and merger of multiple discrete meso-b convective clusters. These meso-b features tend to originate along larger, meso-a scale features, such as the eastern slopes of the Rockies, surface troughs or fronts, or regions of residual convection and mid-level moisture. The orogenic line of meso-b clusters is the most important, probably participating in most MCCs forming in western Kansas and Nebraska.
2. In all the western MCC cases, more than one meso-a feature as described above was important. The region of most intense meso-b convective development and MCC rapid growth is near the point

where these meso-a features intersect. Purdom (1979) has inferred from satellite imagery that convective development is preferential along discontinuities, such as fronts, arc cloud mesohigh boundaries, and dry lines, especially at the intersection of one of these features with another boundary or a cumulus field, due to superimposed vertical motion fields in such regions. While his work has concentrated on convective scale development on meso-b boundaries (e.g., arc clouds, requiring high-resolution visible imagery), the same thing appears to be occurring on a larger scale with MCC development. Meso-b convective clusters are spawned on meso-a scale features, and the intersection of the meso-a features reinforces the convection and activates its upscale development into an MCC.

3. The MCCs generated in the Missouri and Mississippi River basins did not evolve from the interaction of pre-existing, active meso-b convective clusters. However, they did develop at the intersection of meso-a and/or meso-b features, such as fronts and outflow boundaries and bands of mid-level residual moisture and weak convection. In both eastern and western systems, generation of a cool wake, or the reinforcement of a pre-existing thermal discontinuity, by an MCC was important in triggering another MCC the following day.
4. The configuration and development of meso-b clusters were more chaotic and random in the west, unless there were strong environmental controls, such as an active cold front or strong vertical wind shear. The latter tends to produce meso-b squall lines oriented perpendicular to the shear and also maintains the severe weather potential longer into the MCC lifecycle. The

less chaotic nature of the eastern MCC meso-b substructure may have been due to the fewer number of intense meso-b clusters that were involved in their genesis, limiting the modes of possible meso-b scale interaction.

5. In the absence of strong controlling influences (such as fronts), the decay of the MCC is characterized by (or perhaps caused by) the difluent propagation directions of the meso-b elements.
6. The precipitation produced by an MCC is largely confined to the meso-β convective features. A meso-a scale pattern of "anvil" rain, on the scale of the cold cloud shield, does not reach the surface.
7. The potential for severe weather is greatest in the early MCC stage, while the fraction of light to moderate precipitation increases through MCC maximum intensity, dropping off sharply thereafter.

ACKNOWLEDGMENTS

Dr. Peter J. Wetzel performed much of the preliminary analysis incorporated into this study. This research was supported under National Science Foundation Grant ATM-7908297, National Aeronautics and Space Administration Grant NSG-5341, and Office of Naval Research Grant N0000-79-C-0793.

REFERENCES

Cotton, W.R., R.L. George, and P.J. Wetzel, 1981: A long-lived mesoscale complex, Part I: The mountain generated component. Submitted for publication in Mon. Wea. Rev.

Fritsch, J.M., and R.A. Maddox, 1981: Convectively driven mesoscale weather systems aloft, Part I: Observations, Part II: Numerical simulations. J. Appl. Meteor., 20, 9-26.

Leary, C.A., and R.A. Houze, Jr., 1979: The structure and evolution of convection in a tropical cloud cluster. J. Atmos. Sci., 36, 437-357.

Maddox, R.A., 1980: Mesoscale convective complexes. Bull. Amer. Meteor. Soc., 61, 1374-1387.

Maddox, R.A., 1981: The structure and lifecycle of midlatitude mesoscale convective complexes. Ph.D. thesis, Dept. of Atmos. Science, Colorado State Univ., Fort Collins, Colorado, 260 pp.

Means, L.L., 1944: The nocturnal maximum occurrence of thunderstorms in the midwestern states. Misc. Report No. 16, The Univ. of Chicago, 38 pp.

Miller, R.C., 1967: Notes on analysis and severe storm forecasting procedures of the Military Weather Warning Center. AWS Tech. Report 200 (available from Headquarters Air Weather SErivce, Scott AFB, Illinois), 94 pp.

Orlanski, I., 1975: A rational subdivision of scales for atmospheric processes. Bull. Amer. Meteor. Soc., 56, 527-530.

Porter, J.M., L.L. Means, J.E. Hovde, and R.B. Chappell, 1955: A synoptic study on the formation of squall lines in the north central United States. Bull. Amer. Meteor. Soc., 36, 390-396.

Purdom, J.F.W., 1979: The development and evolution of deep convection. Preprints, 11th Conf. on Severe Local Storms, Kansas City, Missouri, AMS, Boston.

Wallace, J.M., 1975: Diurnal variations in precipitation and thunderstorm frequency over the conterminous United States. Mon. Wea. Rev., 103, 406-419.

Wetzel, P.J., W.R. Cotton, and R.L. McAnelly, 1981: A long-lived mesoscale convective complex, Part II: Morphology of the mature complex. Submitted for publication in Mon. Wea. Rev.

Zipser, E.J., 1977: Mesoscale and convective-scale downdrafts as distinct components of squall-line circulation. Mon. Wea. Rev., 105, 1568-1589.

LIST OF FIGURES

at 0300 GMT, 0600 GMT, and 0900 GMT, respectively. (e) Same as Fig. 2c except for 1200 GMT 5 August.

4. Same as Fig. 2b except for 0300 GMT 6 August 1977.

5. (a) Same as Fig. 2a except for 0000 GMT 7 Aug 1977. Also included is the 6-h earlier position of the warmfront at 1800 GMT 6 Aug (broken warmfront symbol) and line of residual mid-level moisture (line of c.), and the 0300 GMT 7 Aug positions of an MCC over Indiana (scalloped -32°C IR contour) and the boundary of its wake to the west. (b) – (e) Same as Fig. 2b except for 0600, 0800, 1000, and 1200 GMT 7 August 1977, respectively.

6. (a) Same as Fig. 5a, except for 0000 GMT 8 Aug. A small active MCC is centered over western Illinois, and there are no off-time features shown. (b) and (c) Same as Fig. 5b except for 0500 and 0700 GMT 8 Aug, respectively.

7. Isohyet analysis over Kansas for MCC number 2. Contours of 0, ¼ and 1 inch are drawn. MCC total precipitation for hourly recording stations is plotted to the nearest tenths of inches.

8. Composite eastern MCC measurable precipitation intensity distribution. Systems 6, 8, and 9 from Fig. 1 were composited, with their times of beginning maximum, and ending maturity normalized with respect to an idealized, average system. The percentages of measurable precipitation reports equal to or exceeding 0.1, 0.2, 0.5 and 1.0 in/hr are plotted against the composite hour, with the total number of measurable reports plotted at the top.

9. Same as Fig. 8 except for composite western MCC, derived from systems 1, 2, and 3.

10. Composite western MCC manually digitized radar intensity distribution. Composting is the same as for Fig. 9, and included in the composite are all non-zero MDR blocks subjectively judged to be associated with the MCCs. Plotted are percentages of non-zero MDR blocks exceeding or equal to VIP levels 2, 3, 4, and 5, and the system-average number of non-zero blocks, as a function of composite time.

11. 5 dBZ echo boundary at 3 km (hatched line; hatches point toward higher reflectivities), 5 km (dot-dashed), 7 km (dashed), and 9 km (scalloped) above HIPLEX radar site at Goodland, Kansas for 0230 GMT 6 Aug. Shaded regions denote reflectivities above 40 dBZ from the 1^{o} PPI. The range blanking (inner circle radius) is 25 km, and the maximum range (outer circle) is 150 km. Line A-B locates the cross section in Fig. 12. The echo overhang west of the radar is located under the cold cloud shield at the northwest lobe of the MCC depicted in Fig. 4. The 40 dBZ area southwest of the radar is the core of meso-β cluster B in Fig. 4.

12. Vertical cross section throguh anvil overhang along line A-B in Fig. 11. The dashed contour is the minimum detectable signal or 0 dBZ. The solid contours are in increments of 10 dBZ beginning at 10 dBZ, with the 20 dBZ contour drawn heavir, and regions exceeding 40 dBZ shaded. The heavy dashed line is the upper limit of data collection (12^{o} elevation) at nearer ranges. Other analyses indicated that reflectivity surfaces above that line were essentially horizontal.

ORIGINAL PAGE IS
OF POOR QUALITY

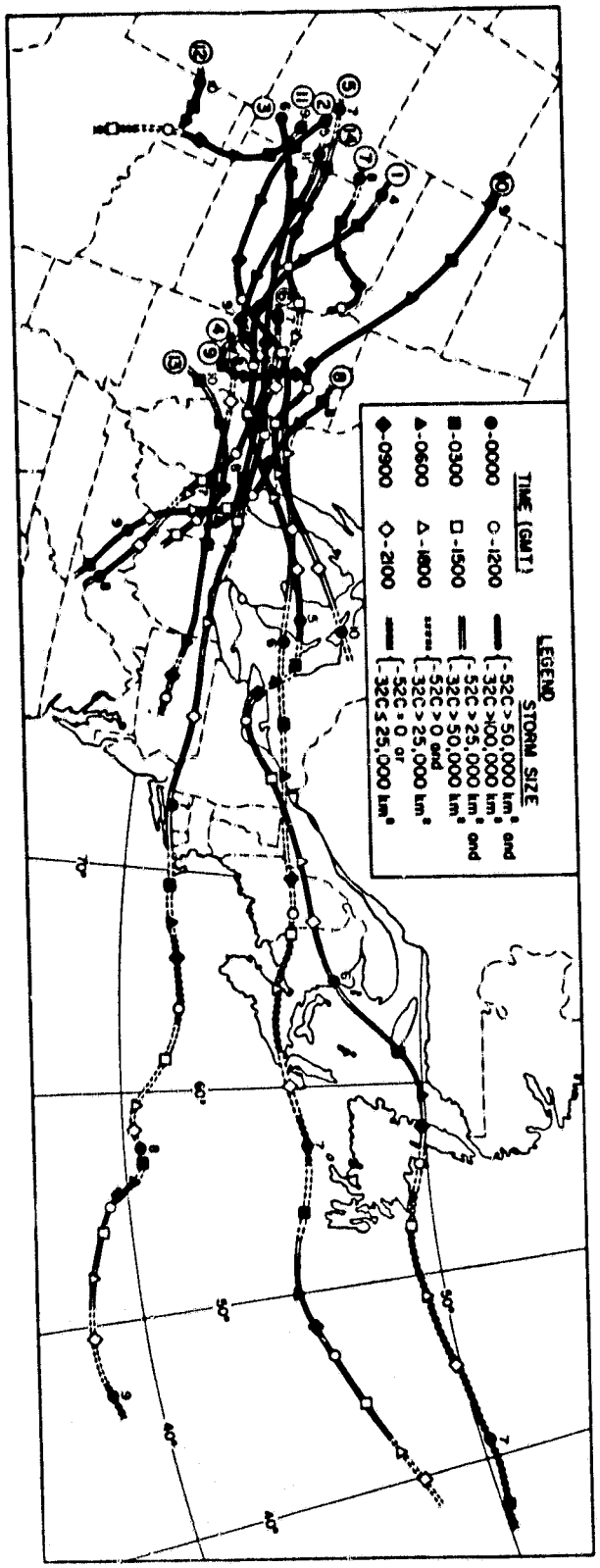

Fig. 1

Fig. 2

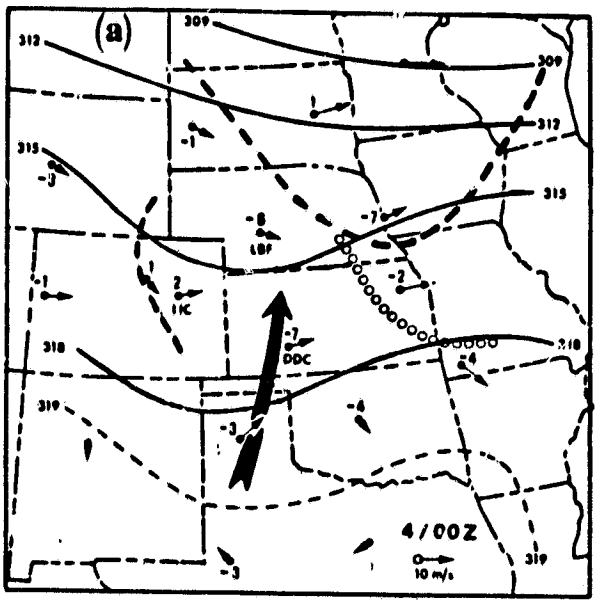

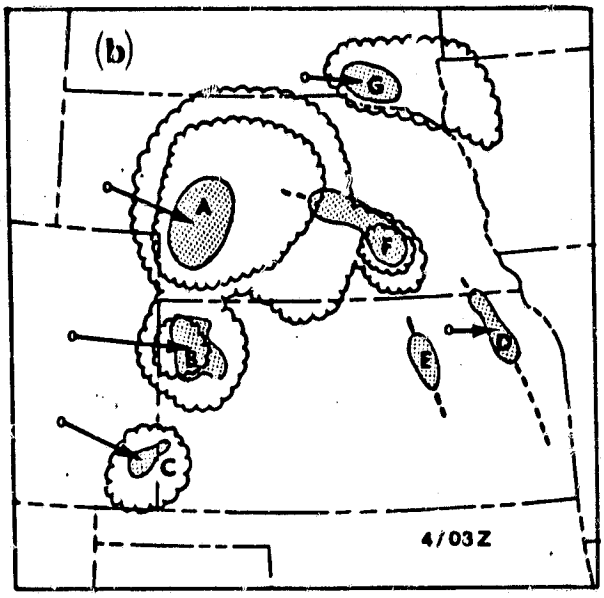

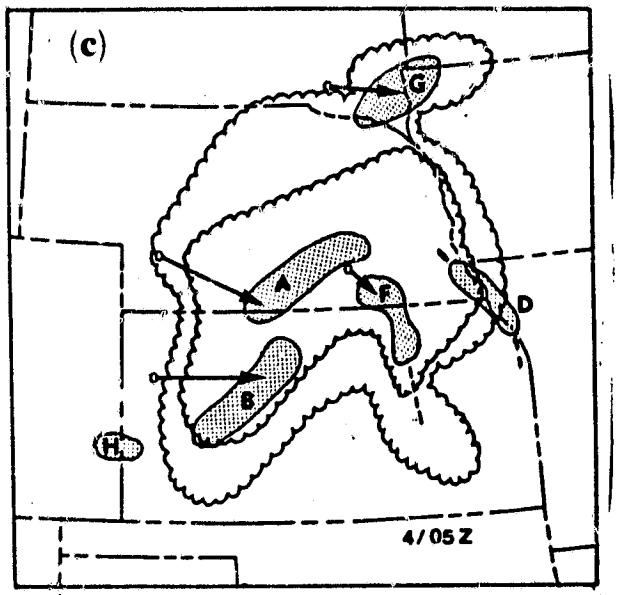

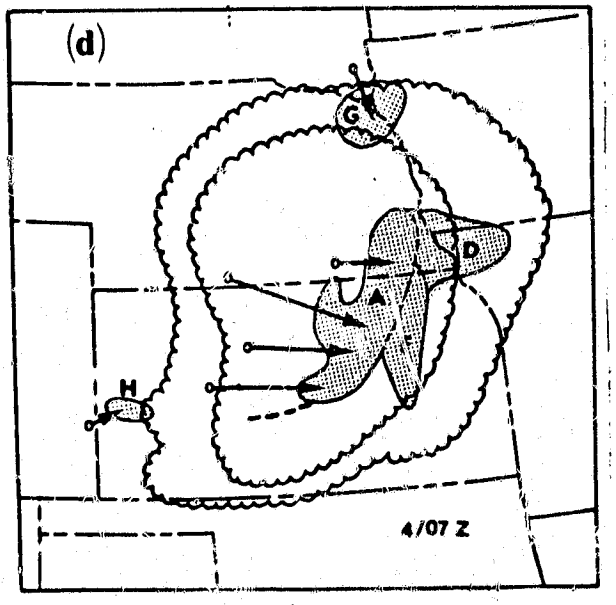

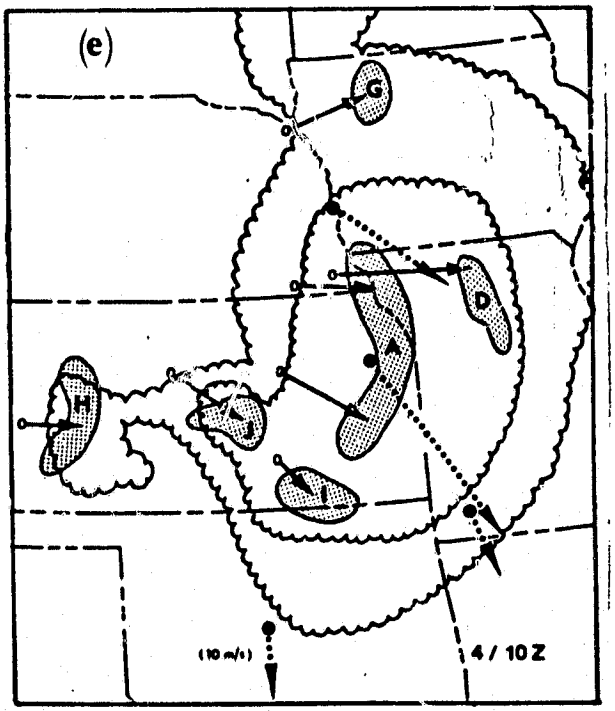

ORIGINAL PAGE IS
OF POOR QUALITY

Fig. 3

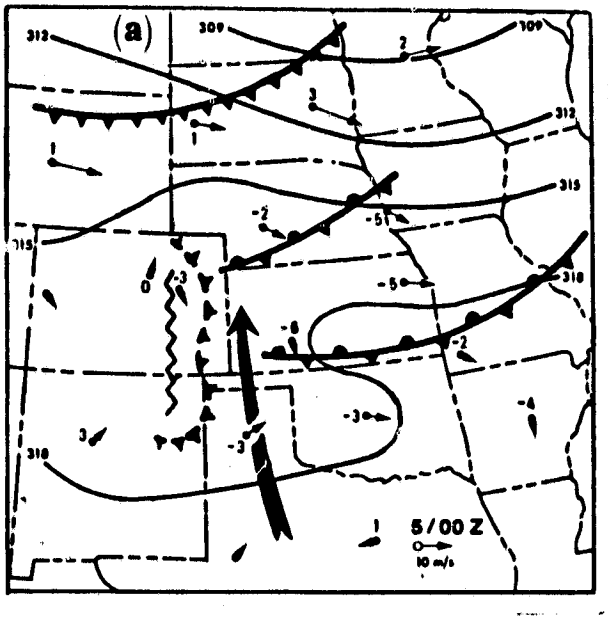

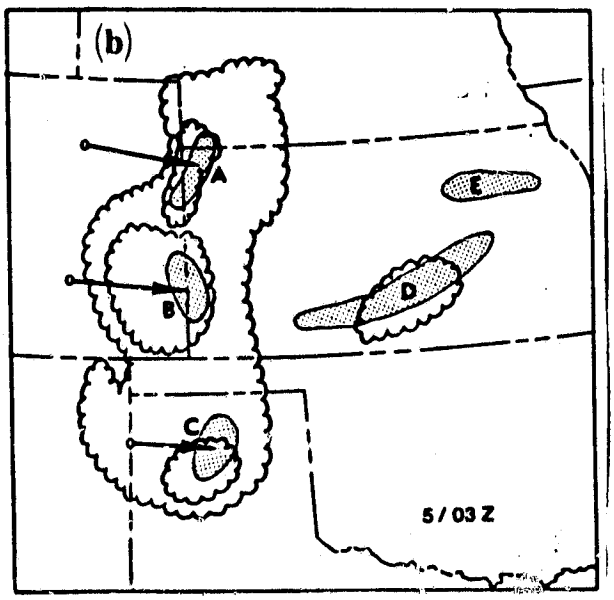

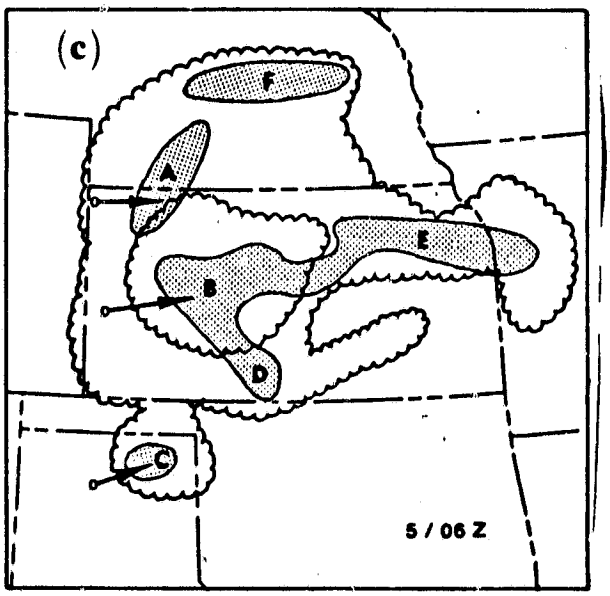

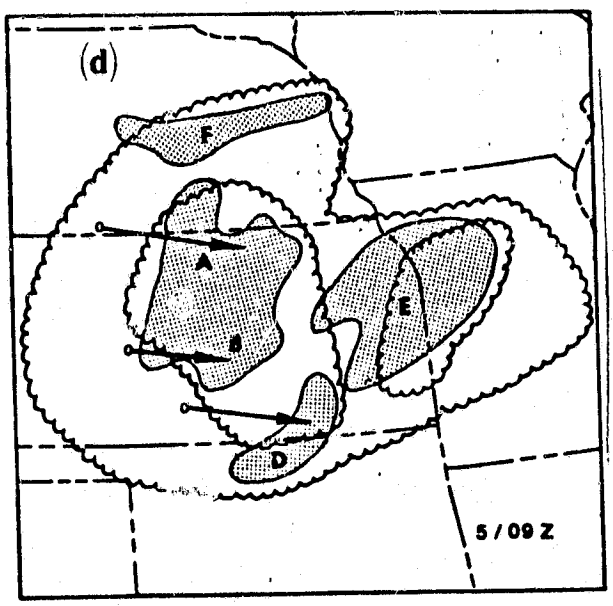

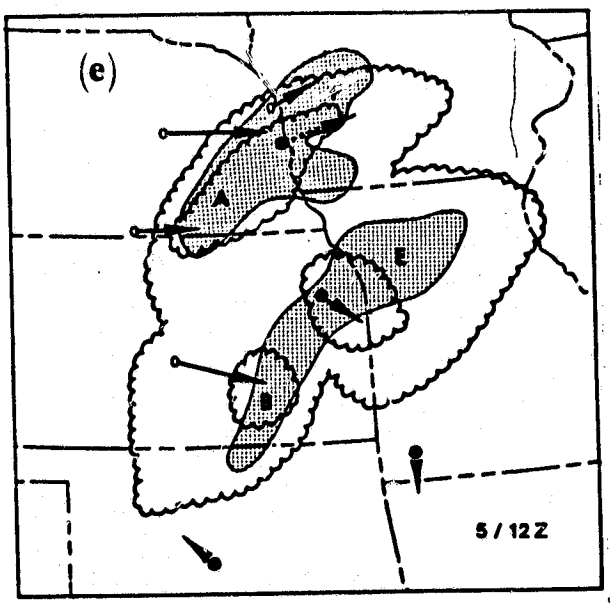

Fig. 4

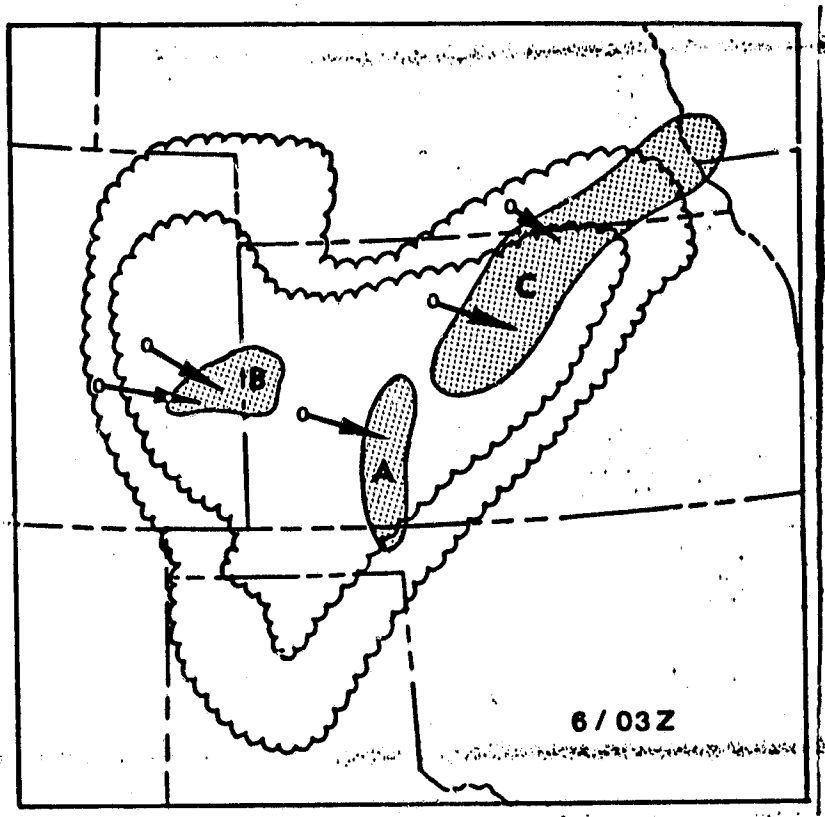

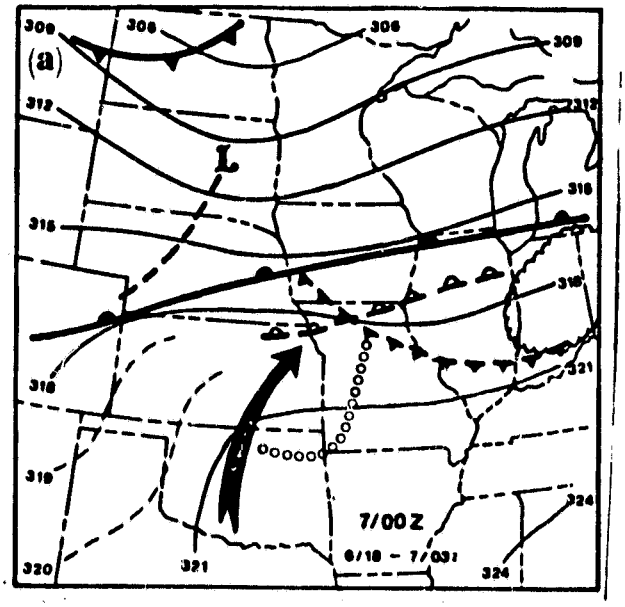

Fig. 5

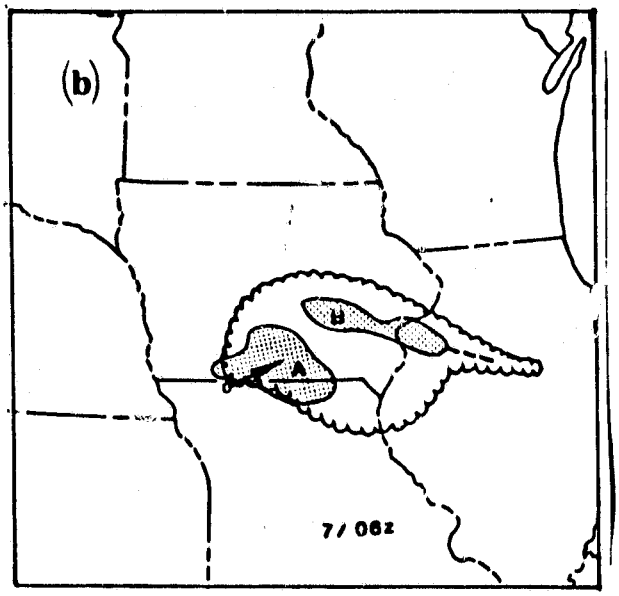

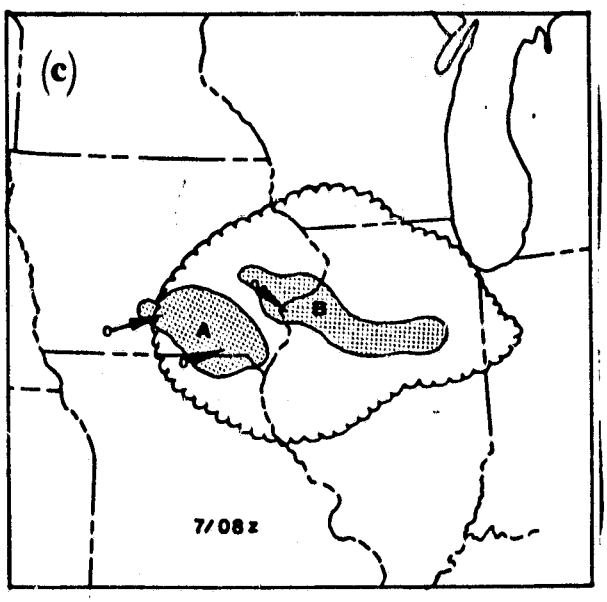

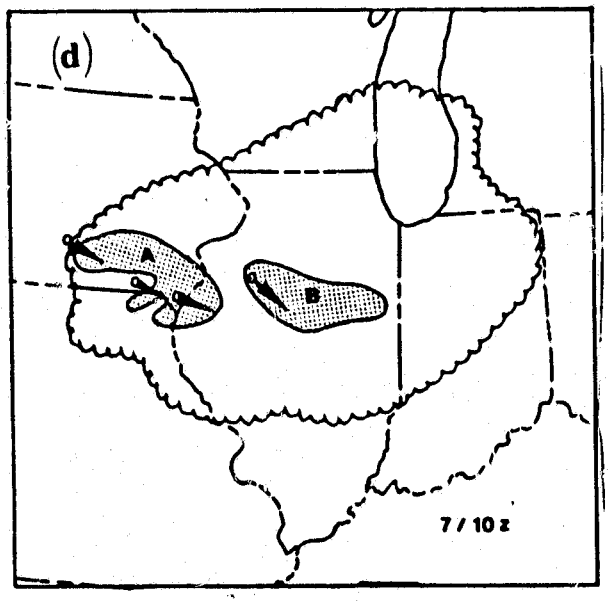

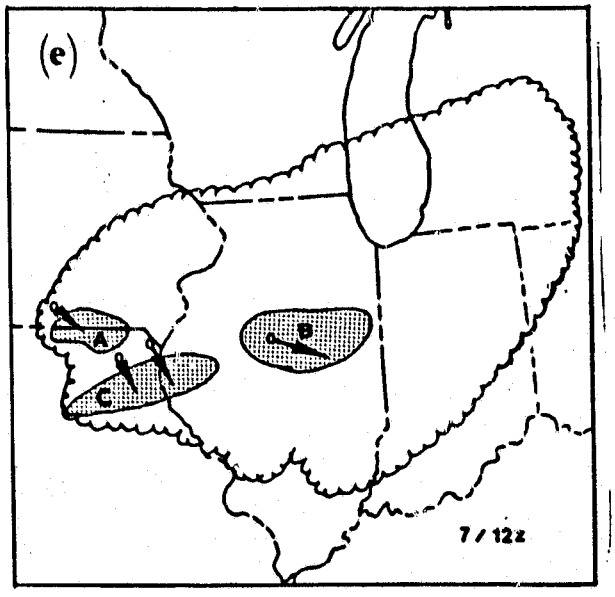

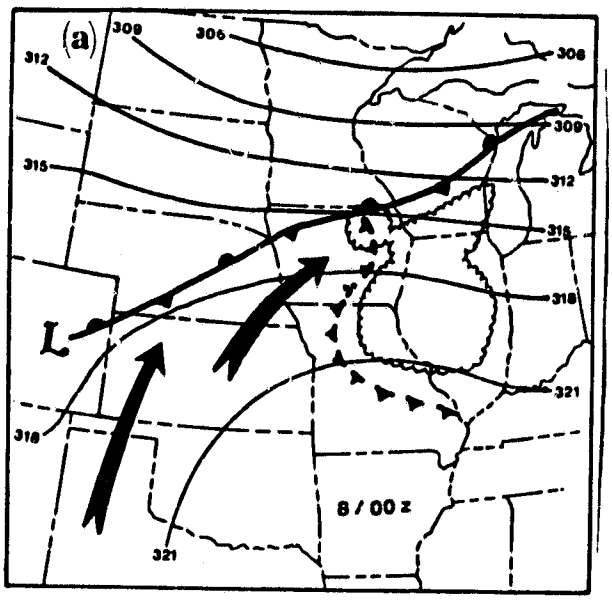

Fig. 6

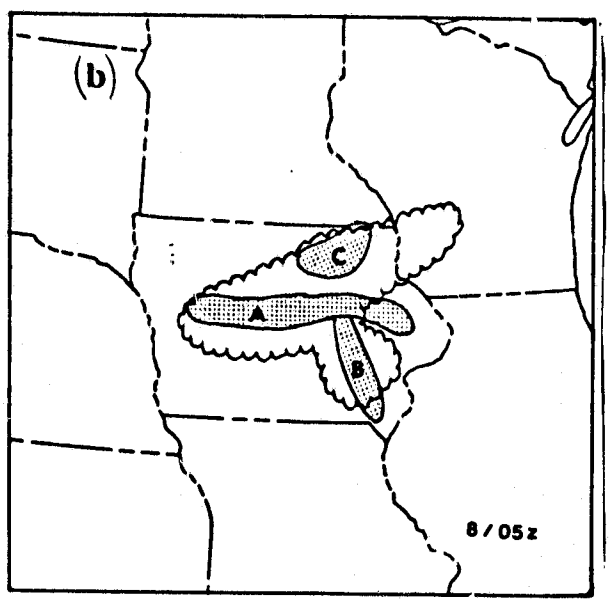

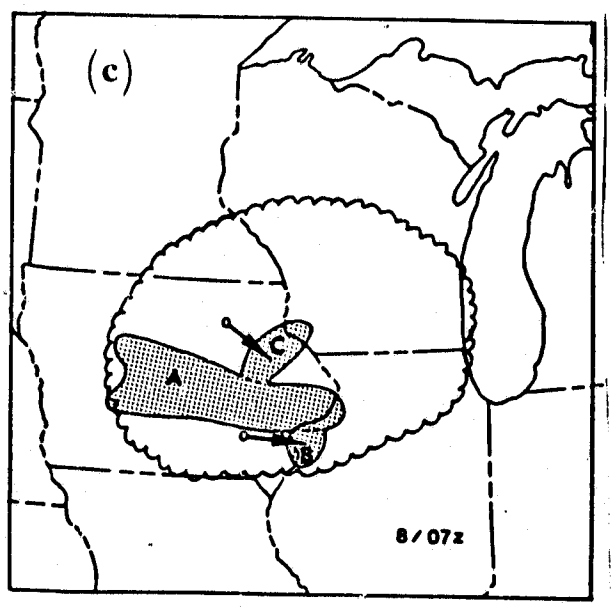

ORIGINAL PAGE IS
OF POOR QUALITY

Fig. 7

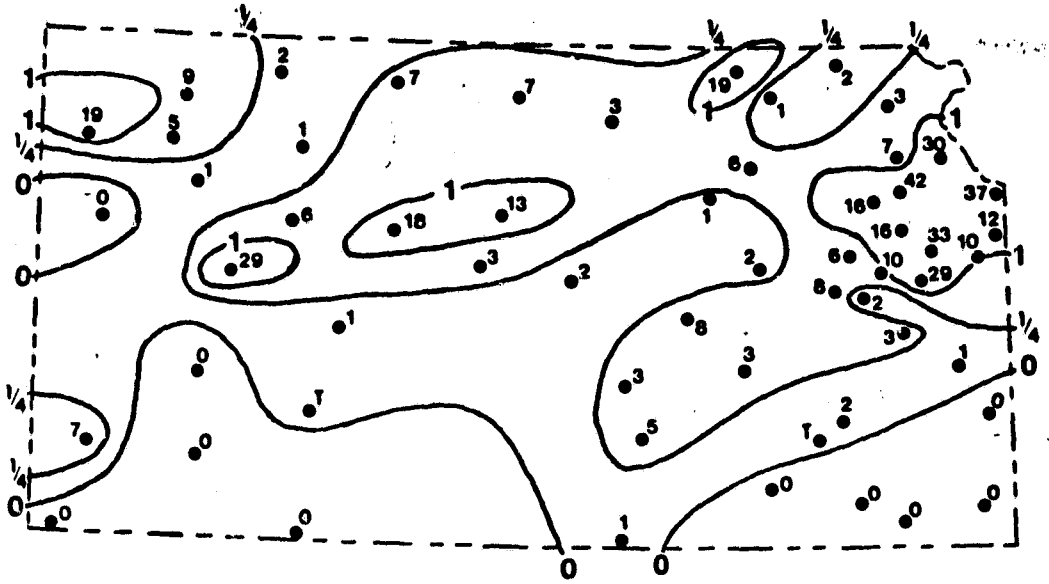

Fig. 8

EAST COMPOSITE

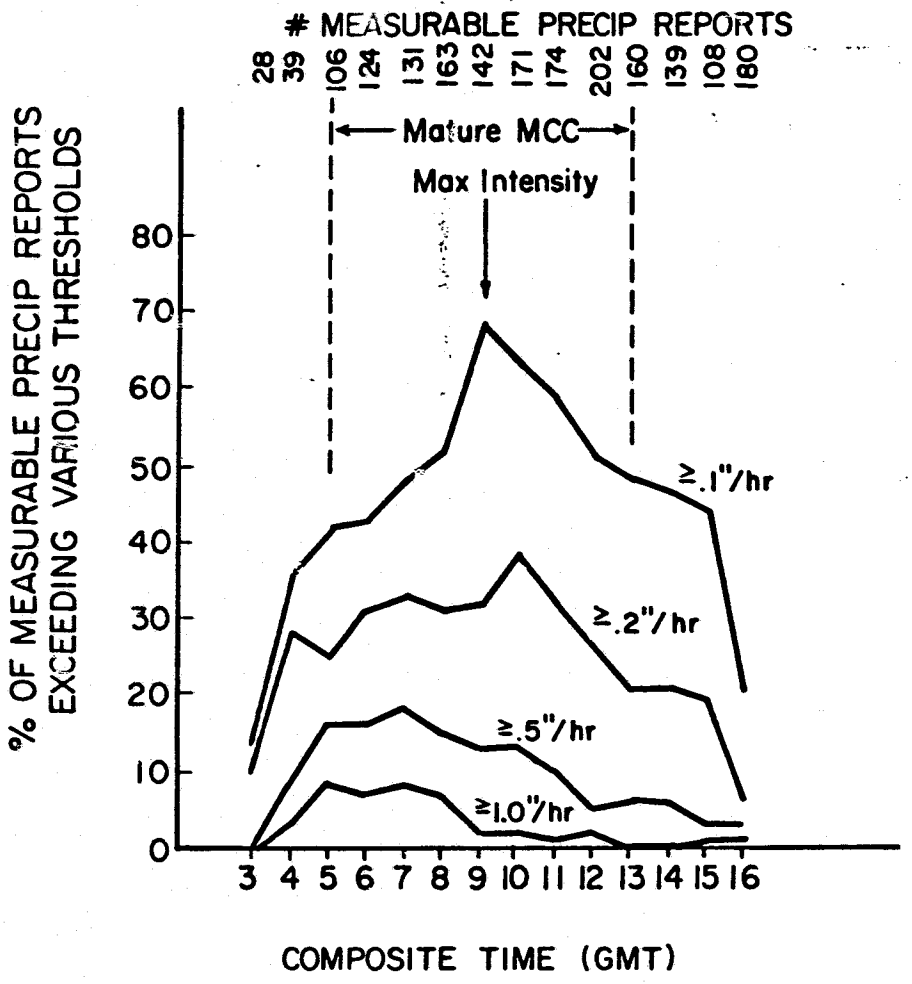

Fig. 9

WEST COMPOSITE

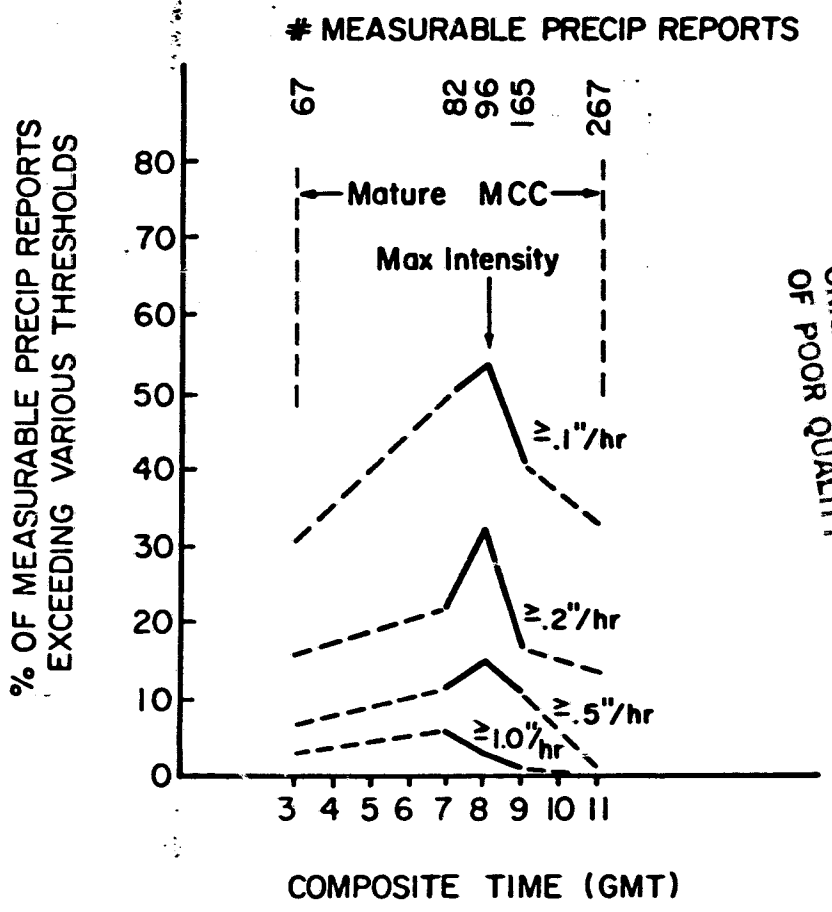

Fig. 10

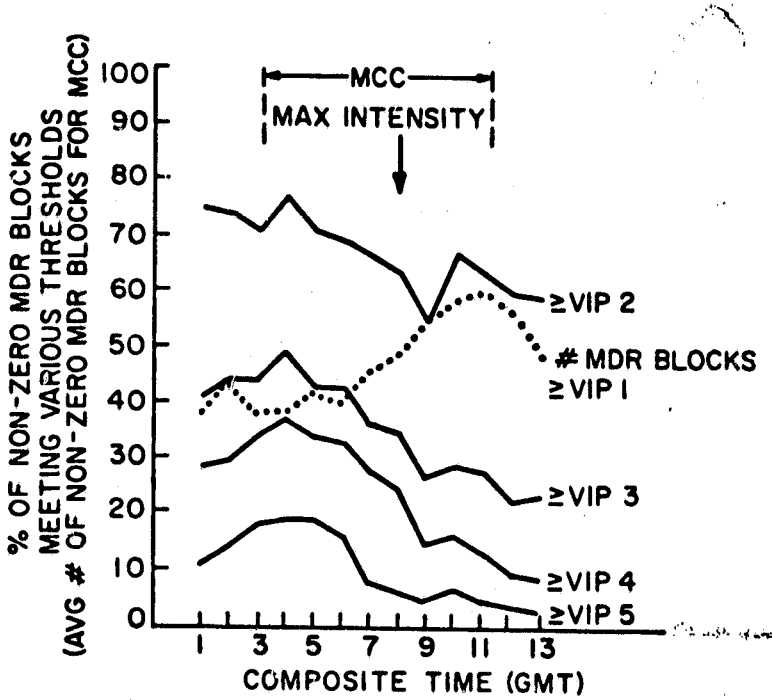

Fig. 11

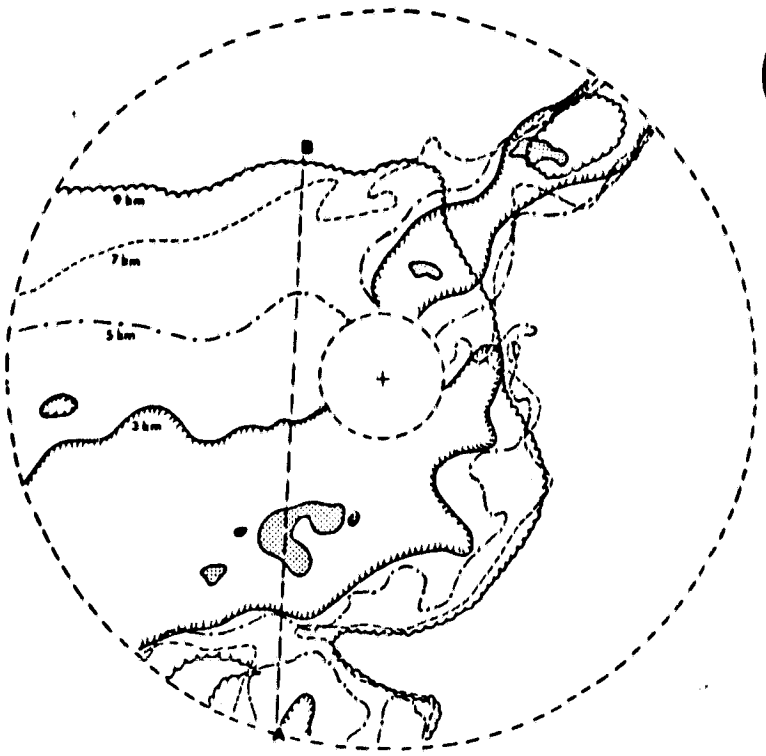

Fig. 12

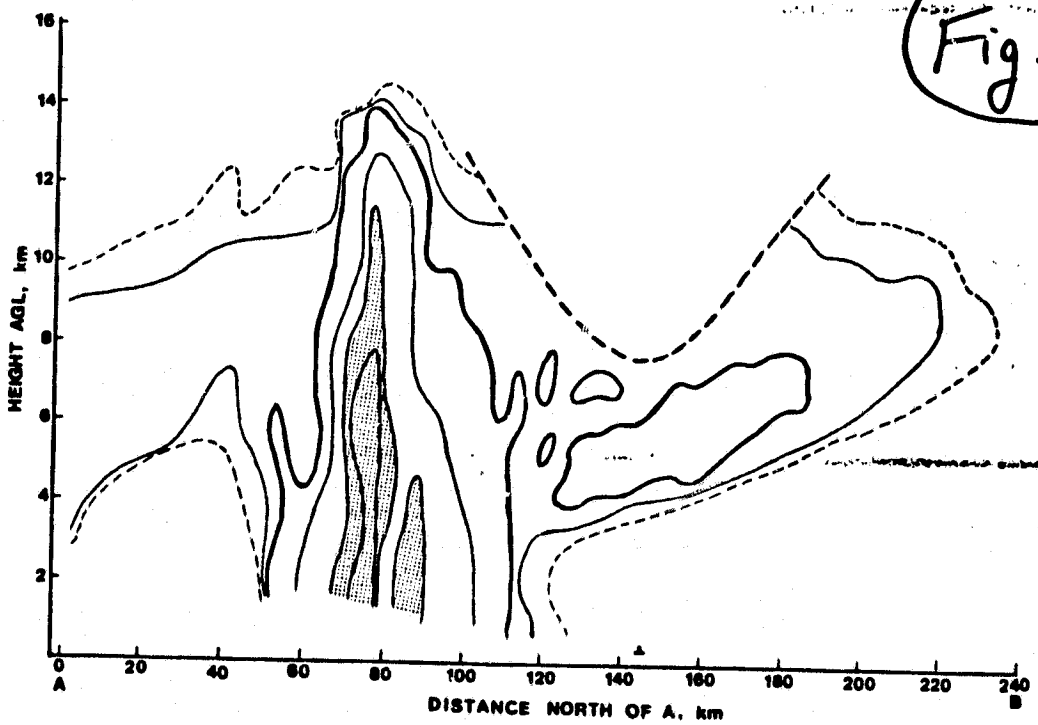

APPENDIX 3

Preprint Volume: Fourth Conference on Hydrometeorology, 7-9 October, 1981, Reno, Nevada, AMS.

THE MESO-β SCALE STRUCTURE AND PRECIPITATION CHARACTERISTICS OF MIDDLE-LATITUDE MESO-α SCALE CONVECTIVE COMPLEXES

Ray L. McAnelly and William R. Cotton

Department of Atmospheric Science
Colorado State University
Fort Collins, Colorado 80523

1. INTRODUCTION

Maddox (1980) indentified an important type of nocturnal convective system, the Mesoscale Convective Complex (MCC), that is organized on the meso-α scale[1] (250-2500 km) and which possibly accounts for much of the convective season precipitation over the central United States. The predominance of the nocturnal thunderstorm in this area has long been recognized (Means, 1944; Wallace, 1975) and most studies of its mesoscale organizational characteristics have generally attempted to describe them in relation to a squall line conceptual model (Porter et al., 1955; Miller, 1967). However, the relatively new satellite vantage has allowed the identification of the MCC as a unique system with structural and dynamic properties quite distinctive from a squall line (Maddox, 1981). Among its distinctive characteristics are a long-lived, near-circular cold cloud shield, large areas of light precipitation (with embedded, locally heavy precipitation), a mesoscale mid-to-upper tropospheric warm core, and a large-amplitude anticyclonic outflow perturbation in the upper troposphere that strongly modifies the larger-scale environment. Fritsch and Maddox (1981) have further described the upper-level structure of the MCC and have inferred (with numerical model support) that a mesoscale region of mean ascent in the mid-to-upper troposphere is a fundamental aspect of the MCC that explains many of the observed features.

The previously cited MCC studies have focused on the meso-α structure and the macroscale (>2500 km) environment of the MCC. While Maddox (1980) recognized the role of meso-β scale (25-250 km), intense convective systems in initiating the MCC and in continuing to produce locally heavy rainfall within the larger, mature MCC, no systematic study of the meso-β structure of the MCC has been made. In particular, given the consistent meso-α features of the MCC on the one hand, and the more capricious nature of convective scale processes on the other, what degree of generality can be drawn about the meso-β substructure and evolution of the MCC? This paper gives the initial results of a study with that objective in mind.

2. CASES STUDIED AND DATA UTILIZED

The MCCs investigated here occurred in an eight-day episode, 3-10 Aug 1977. The quasi-stationary synoptic pattern at 50 kPa during this period consisted of a strong low centered in the Hudson Bay region, a ridge off the west coast extending well into eastern Alaska, and a polar jet running southward in western Canada and turning basically zonal along the U.S.-Canadian border. A diffuse quasi-stationary surface front extended from the Nebraska region towards the Great Lakes and New England, with southerly low-level flow to the south of the front on the west side of the Atlantic subtropical high.

Each afternoon, convection originating on the eastern slopes of the Rockies, the High Plains and the Central Plains, underwent nocturnal intensification into one or more MCCs, which tracked eastwards as long-lived entities of enhanced convection (up to three days). Fig. 1 depicts the satellite-based tracks of the centroids of the convection associated with each MCC. (The darkened tracks indicate periods when the convection met Maddox's (1980) areal criteria for a mature MCC.) Cotton et al. (1981) analyzed the mountain generation and High Plains evolution of a north-south meso-β squall line on 4 Aug, and Wetzel et al. (1981) further documented its role in the formation of MCC number 2 in Fig. 1. Wetzel et al. (1981) examined the three-dimensional structure of systems 1 and 2 in as much detail as could be inferred from the synoptic data at 1200 GMT on 4 and 5 Aug, respectively (when both systems were several hours past their maximum intensity). In this paper, we look closer at the evolution of systems 1, 2, and 3, utilizing GOES IR imagery, NWS radar data (film from five sites, observation logs, summary charts, and manually digitized radar [MDR] digitial products), conventional surface and upper-air data, and hourly precipitation data.

3. THE MESO-β SUBSTRUCTURE OF THE MCCs

Figures 2-4 illustrate several important evolutionary features of MCCs 1, 2, and 3, respectively. Included in these figures are infrared GOES-east apparent blackbody isotherms of -40 and -62°C, meso-β scale clusters and lines of relatively strong convection, and approximate displacements of these features since the previous map time or over the previous three hours (if in existence for that long). The identification of the meso-β features was subjectively based primarily on NWS radar film, which was generally of a poor quality as far as quantitative intensity determination was concerned. However, the temporal resolution of the PPI data was generally excellent, so an amalgamation of intensity inferences, using all data sources, allowed the reliable identification of relatively strong meso-β scale echo entities that persisted for well over an hour. Each meso-β

[1] See Orlanski (1975) for a detailed discussion of scale terminology.

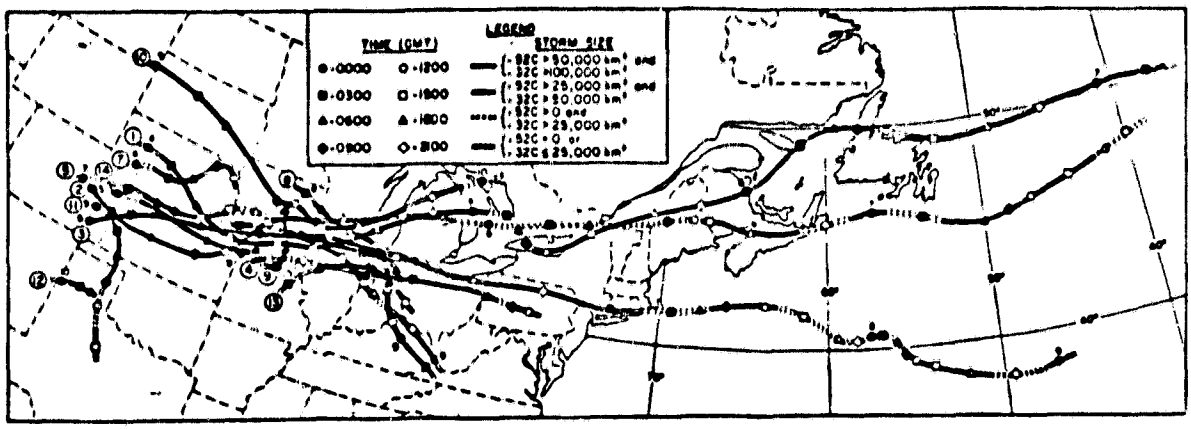

Figure 1. Tracks of the centroid of the fourt[illegible] MCCs which developed during the episode of 3-10 August 1977. The circled sequential numbers chronologically identify the systems, with the date given near the 0000 GMT symbol.

feature depicted may represent near-solid echo coverage, while at other times it may be a cluster or line of discrete echoes that maintains a meso-β cohesiveness. Omitted for the sake of clarity are other areas of weak echo, isolated echoes, and some meso-β regions of echo, if these seem to have had little influence on the MCC development.

Figure 2a shows some of the synoptic features at the time when the pre-MCC convection was beginning to organize, 0000 GMT 4 August. A weak 70 kPa shortwave extended from western Nebraska to the Texas panhandle, with the low-level jet in the same region. A surface trough was located along the lee side of the Rockies, with another dipping into southeastern Nebraska. An area of mid-level moisture and weak residual convection from the previous day extended from southern Missouri northwestward through eastern Kansas.

The satellite and radar map for 0300 GMT (Fig. 2b) depicts three meso-β convective complexes (A, B, C) in a north-south line in western Nebraska and Kansas. These had formed in the Wyoming and Colorado foothills along the trough shown in Fig. 2a and are typical of the orogenic convection induced by differences in the mountain plateau and plains diurnal heating cycle (Cotton et al., 1981). Complex A formed earliest and was most intense, producing the bulk of the cold cloud shield which met MCC criteria by 0200 GMT. Storms in this complex produced strong winds and large hail in western Nebraska. Another group of meso-β complexes (D, E, F) formed in a northwest-southeast orientation along the residual moisture axis in Fig. 2a. These were newer and less intense than the orogenic complexes, but were beginning to intensify rapidly as the faster eastward propagating orogenic line approached.

By 0500 GMT (Fig. 2c), complexes A and B had moved eastward and assumed meso-β squall-line characteristics. This was likely due to their propagating into the low-level jet region, thereby increasing the low-to-mid-tropospheric shear (50 kPa winds were fairly uniform, ~15 m s^{-1} and northwesterly). The motion of complexes A and B over the previous 3 hours (Fig. 2b,c) was confluent, perhaps steered by the confluent 70 kPa winds displayed in Fig. 2a for LIC, LBF and DDC. This confluence of meso-β convective complexes may be instrumental in forcing the development of the MCC. As the A-B meso-α line in Fig. 2b moved east and intersected the E-F meso-α line, the meso-β complexes nearest the region of intersection (A and F) intensified. The western portion of F merged into the northeast end of A, while the southeastern portion of F split into a right-moving severe storm that produced a 50 km hailswath and merged with the meso-β band E.

Over the next two hours, complexes A and B continued their confluence, merged, and overtook F, creating a single large meso-β (or small meso-α) band of intense convection by 0700 GMT (Fig. 2d). A 200 km track of severe surface winds accompanied the merging of these complexes. Complex D lost its discrete identify as it became lost in an expanding echo of uniform intensity that merged into the A-B-F band.

The maximum intensity of the MCC, as judged by the largest areal extent of the coldest enhanced IR contour (not shown), occurred at 0800 GMT. Despite the large cold cloud shield and weaker cells and patches of echo both ahead of and behind the intense meso-β echo depicted in Fig. 2d, nearly all of the hourly precipitation reports are confined to the depicted meso-β region.

By 1000 GMT (Fig. 2e), the single intense meso-β complex had fragmented into several smaller meso-β complexes. Whereas up until the time of maximum MCC intensity the meso-β complexes displayed a confluent tendency, in the weakening stage they displayed a difluent tendency, with the northern complexes propagating easterly, the southern ones more southeasterly. This difluent propagation may be due to further growth being forced at the boundary of the expanding surface meso-high, which intensified most rapidly during the period of concentrated meso-β convection at MCC maximum intensity. Another mechanism that might explain the difluent propagation is a difluent low-to-mid-tropospheric shear vector, where enhanced moist layer inflow relative to the moving complexes would favor growth in the difluent direction. The vector difference between the 30 kPa wind and the centroid of the surface,

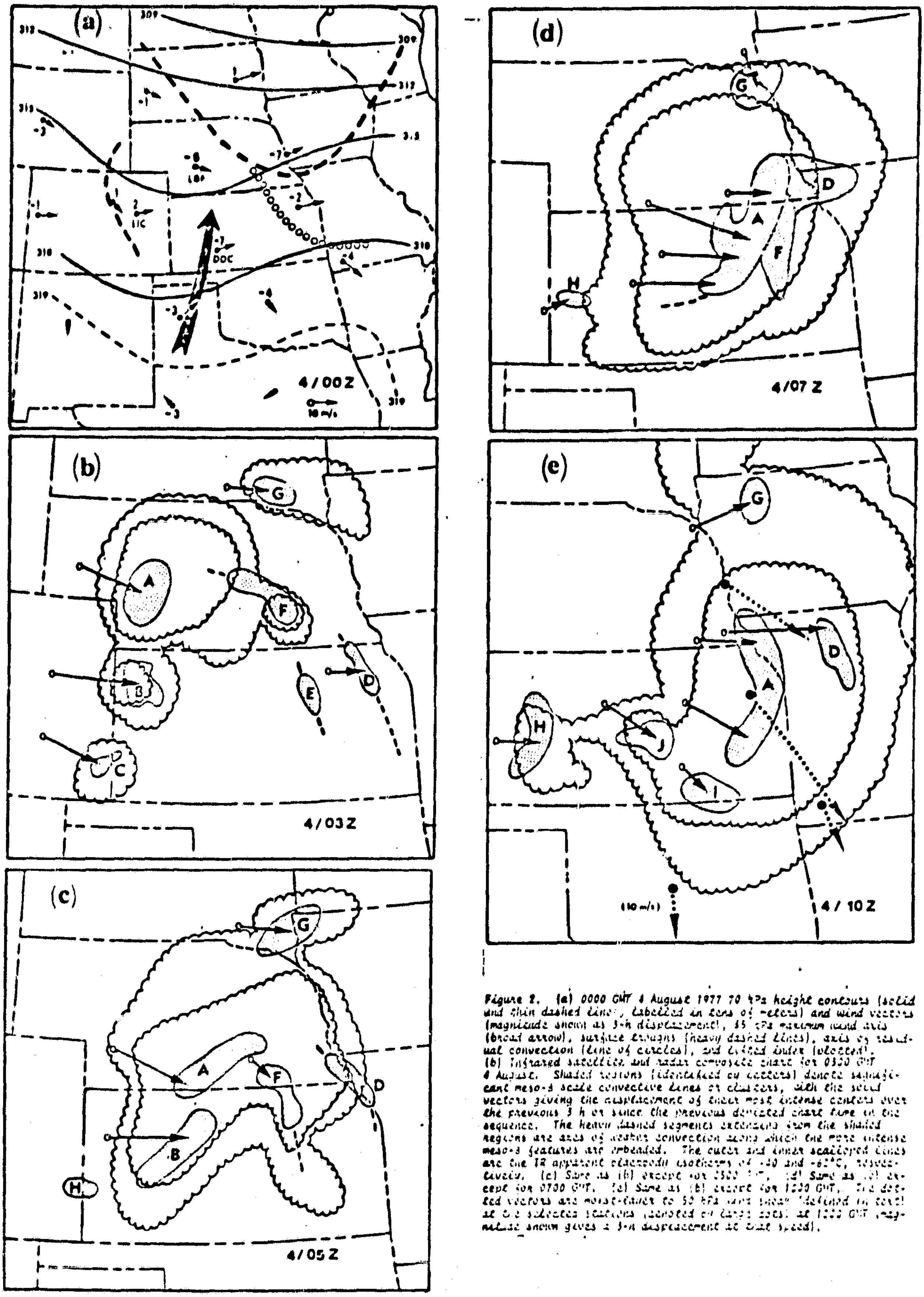

Figure 2. (a) 0000 GMT 4 August 1977 70 kPa height contours (solid and thin dashed lines, labelled in tens of meters) and wind vectors (magnitude shown as 3-h displacement), 35 kPa maximum wind axis (broad arrow), surface troughs (heavy dashed lines), axis of residual convection (line of circles), and lifted index (plotted). (b) Infrared satellite and radar composite chart for 0300 GMT 4 August. Shaded regions (identified by letters) denote significant meso-β scale convective lines or clusters, with the solid vectors giving the displacement of their most intense centers over the previous 3 h or since the previous depicted chart time in the sequence. The heavy dashed segments extending from the shaded regions are axes of weaker convection along which the more intense meso-β features are embedded. The outer and inner scalloped lines are the IR apparent blackbody isotherms of -30 and -62°C, respectively. (c) Same as (b) except for 0500 GMT. (d) Same as (c) except for 0700 GMT. (e) Same as (b) except for 1000 GMT. The dotted vectors are moist-layer to 50 kPa wind shear (defined in text) at the selected stations (denoted by large dots) at 1000 GMT (magnitude shown gives a 3-h displacement at that speed).

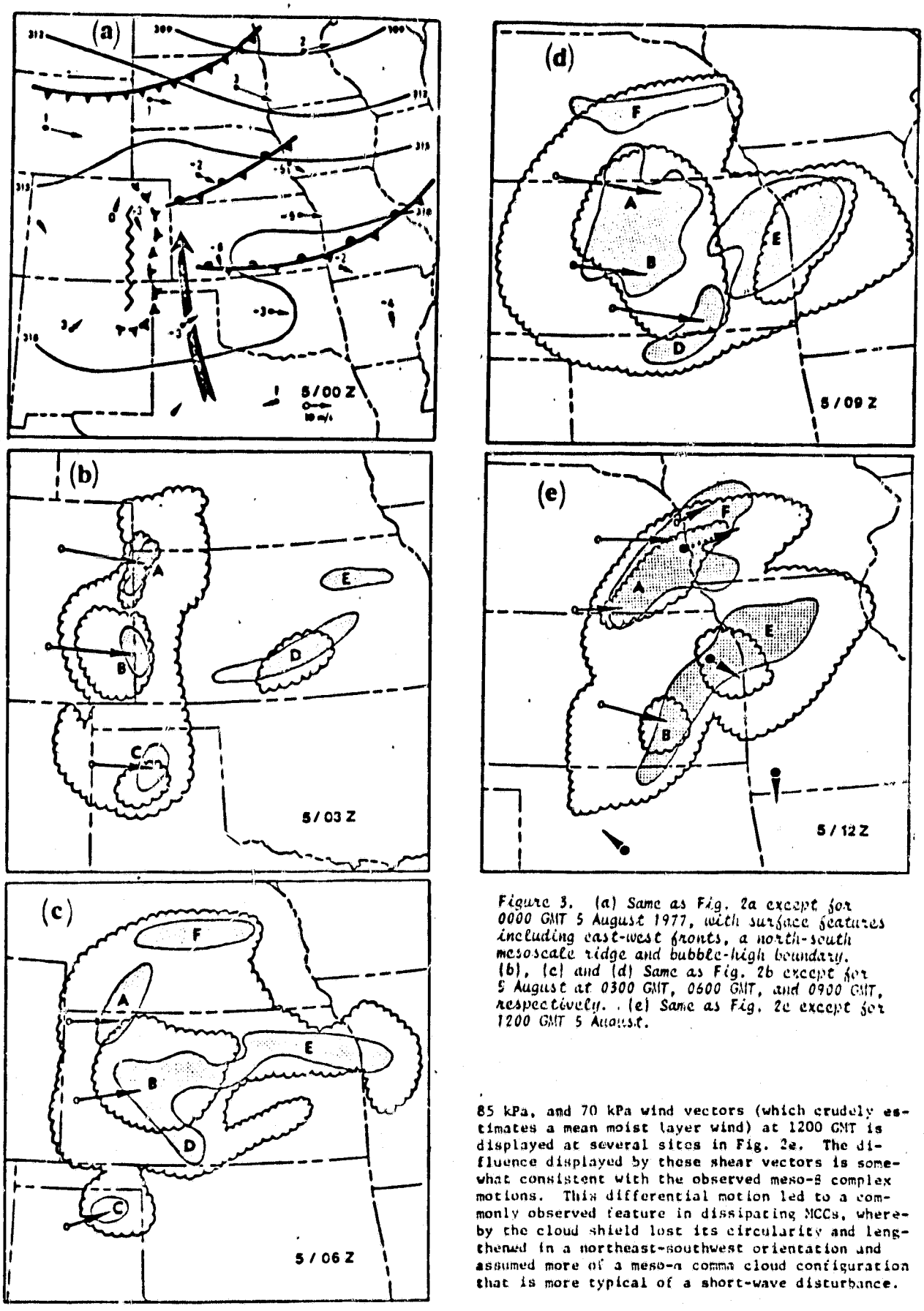

Figure 3. (a) Same as Fig. 2a except for 0000 GMT 5 August 1977, with surface features including east-west fronts, a north-south mesoscale ridge and bubble-high boundary. (b), (c) and (d) Same as Fig. 2b except for 5 August at 0300 GMT, 0600 GMT, and 0900 GMT, respectively. . (e) Same as Fig. 2c except for 1200 GMT 5 August.

85 kPa, and 70 kPa wind vectors (which crudely estimates a mean moist layer wind) at 1200 GMT is displayed at several sites in Fig. 2e. The difluence displayed by these shear vectors is somewhat consistent with the observed meso-β complex motions. This differential motion led to a commonly observed feature in dissipating MCCs, whereby the cloud shield lost its circularity and lengthened in a northeast-southwest orientation and assumed more of a meso-α comma cloud configuration that is more typical of a short-wave disturbance.

The next day's MCC, system 2 in Fig. 1, displayed similarities to, but also some significant differences from, MCC number 1. At the pre-MCC stage at 0000 GMT 5 August (Fig. 3a), the 70 kPa height field displayed only a very weak trough extending from northwest Colorado to Oklahoma. The low-level jet was again established in the Texas panhandle, and surface features consisted of a cold front advancing into Wyoming and South Dakota, stationary fronts through southern Nebraska and across southern Kansas into Illinois (the latter was the outflow boundary from the previous day's MCC as it tracked on eastward), and a strong meso-high on the Colorado and New Mexico High Plains, produced by the afternoon orogenic convective line. This meso-α north-south line of storms was similar to, but farther south than, the previous day's orogenic line.

By 0300 GMT (Fig. 3b), the orogenic line, consisting of three meso-β complexes (A, B, C), had moved eastward, with B producing severe surface winds and hail in southeast Colorado. New meso-β lines (D, E), oriented east-west, developed in Kansas, the southern one (D) occurring along the stationary front separating the cooler, moister wake of the previous day's MCC from the unmodified maritime tropical air to the south. This was one hour prior to MCC initiation, as determined by IR cloud shield area.

As the eastward moving meso-α orogenic line (A, B, C) intersected the western end of the newer meso-α east-west line (D, E), the meso-β complexes at the region of intersection (B, D) intensified rapidly, as was the case the day before. By 0600 GMT (Fig. 3c), the MCC was well established and centered on complex B, which merged with the western end of D, developed rapidly towards complex E to the east, and produced local hourly rainfalls of 60 mm. A new meso-β complex, F, developed in central Nebraska along the east-west stationary front shown in Fig. 3a.

The MCC had achieved maximum intensity and was beginning to weaken by 0900 GMT (Fig. 3d). A and B had merged and expanded into a large precipitation region, but not too intense. Complex D split off of B and, as with the southernmost complex in the previous day's weakening system, displayed a southeastward propagation. Complexes E and F, both originating as east-west lines, remained essentially stationary in the westerly steering flow as individual cells propagated eastward along the complexes. E developed in areal extent as the A-B complex approached it.

The squall-line characteristics displayed by the intense meso-β complex during the mature phase of the first MCC (see Fig. 2d) did not occur in MCC 2, probably because the low-to-mid tropospheric shear was not as strong (west-northwesterly 50 kPa wind of only 5-10 m s^{-1}). In the dissipation stage (1200 GMT, Fig. 3e), the A-B complex split, with B merging into E and A merging into F to give two weak meso-β bands with a squall-like configuration. The A-F complex propagated east-northeastward while the E-B complex moved southeasterly, again consistent with the difluent moist-layer to 50 kPa shear.

The third MCC in Fig. 1 had similarities with and differences from the previous two. The Wyoming-South Dakota cold front in Fig. 3a had advanced into northern Kansas and eastern Colorado by 0000 GMT 6 August. Two north-south waves of orogenic convection developed from the upslope conditions north of the front and were separated by about 4 h and 200 km. A mesoscale band of weak convection developed in a northeast-southwest orientation along the front in southern Nebraska and northern Kansas. By 0300 GMT (Fig. 4), the most intense meso-β complex of the first orogenic wave (A) had approached the weak frontal band (C) and intensified, followed shortly by the rapid intensification of meso-β complex B in the second orogenic wave, together producing the MCC. A and C merged into a meso-α band from southeast Nebraska to southwest Kansas and remained the most significant feature of the MCC as complex B weakened rapidly by 0600 GMT. The front apparently had a strong controlling influence on the organization of this MCC, as evidenced by the A-C complex remaining strongly tied to the frontal position, by less complex meso-β substructure and by little difluent propagation of meso-β features occurring with MCC dissipation.

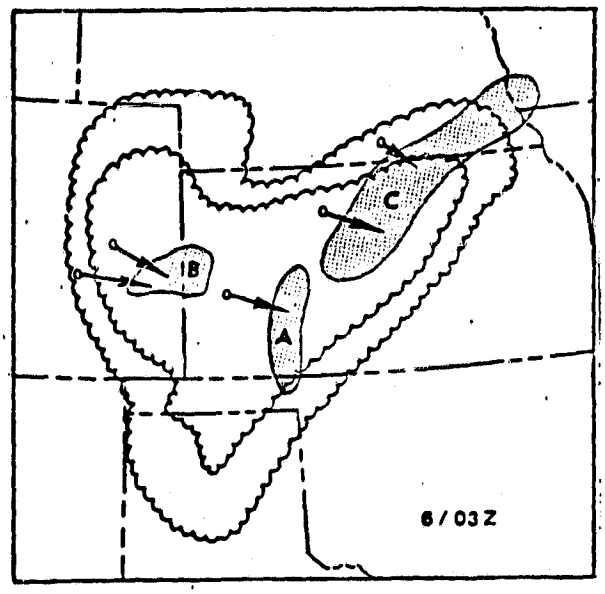

Figure 4. Same as Fig. 2b except for 0300 GMT 6 August 1977.

4. PRECIPITATION CHARACTERISTICS OF THE MCCs

Despite the large uniform cold cloud shield in an MCC the rainfall rates at a given time are far from uniform. Virtually all of the measurable hourly precipitation reports for the three MCCs studied occurred within the shaded meso-β regions indicated in Figs. 2-4 (and for intermediate hours not shown). At the most, the combined meso-β areas were less than half of the area within the -40°C isotherm, and substantial portions of the -62°C area were also rain-free. Even within the meso-β structures, the hourly reports show much variability that is characteristic of convective rain-

fall in general. An isohyet analysis for MCC 2 over Kansas (Fig. 5) illustrates the total storm variability (in which much of the temporal variability of traveling meso-β systems is smoothed out). Note that the three sites in central Kansas reporting less than 0.25 inches are within the -62°C area in Fig. 3d and are nearly in the center of the MCC. The most uniform and widespread hourly precipitation reports occurred in east central Kansas in conjunction with the quasi-stationary meso-β complex E in Fig. 3. Along with the controls on meso-β structure exerted by the front on MCC 3, discussed in Section 3, the front also apparently produced a more uniform precipitation distribution, both overall and for hourly periods, due to the reduced meso-β substructure complexity.

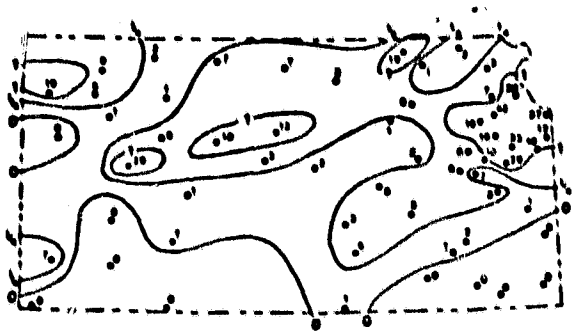

Figure 5. Isohyet analysis over Kansas for MCC number 2. Contours of 0, ½, and 1 inch are drawn. MCC total precipitation for hourly recording stations is plotted to the nearest tenths of inches.

Because of the sparse raingauge spacing in the western Plains, the nature of rainfall rate distribution within an MCC was estimated by compositing the observations from the 4, 5, and 6 August systems with respect to beginning, end, and maximum intensity times, all based on enhanced-IR criteria (Maddox, 1980). The resultant composite system is a mature MCC for nine hours with the maximum intensity occurring at the sixth hour. The measurable hourly precipitation amounts for eastern Colorado, Nebraska, Kansas, Oklahoma, and Missouri were stratified into various classes, with the percent of measurable precipitation reports meeting those thresholds plotted as a function of composite MCC time (Fig. 6). The plots are indicative of what fraction of the active rain areas are intense. The results suggest that from the time of MCC initiation to about an hour after maximum intensity, about 40-50%, 30%, and 15% of the active rainfall areas were having hourly rainfall rates exceeding 0.11, 0.25, and 0.50 in/hr, respectively. The total area of active rainfall could not be determined because of the unequal observation density across the region; hence, the increasing number of stations reporting rain from pre-MCC to termination time (plotted along the top of Fig. 6) represents an undetermined combination of both the areal expansion of rainfall with MCC growth and the tracking of the system into regions of higher observation density. Little confidence is placed in the curves for the pre-MCC stages because of the very low number of observations available from eastern Colorado, where many of the important meso-β com-

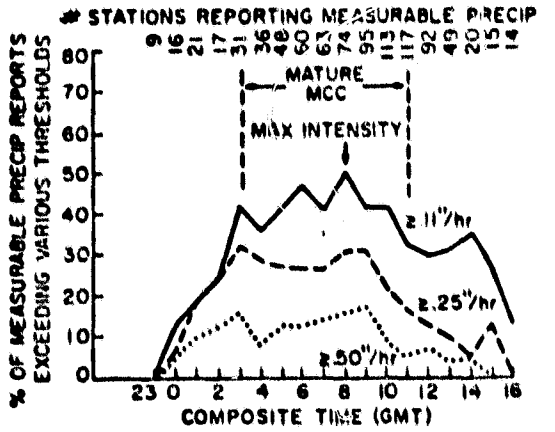

Figure 6. Composite MCC measurable precipitation intensity distribution. The composite system is based on hourly precipitation reports from eastern Colorado, Kansas, Nebraska, Oklahoma, and Missouri. The time of each system was normalized with respect to an idealized MCC beginning, maximum intensity, and end. The percentages of measurable reports exceeding 0.11, 0.25, and 0.50 in/hr are plotted as a function of composited MCC time, with the total number of measurable reports plotted at the top.

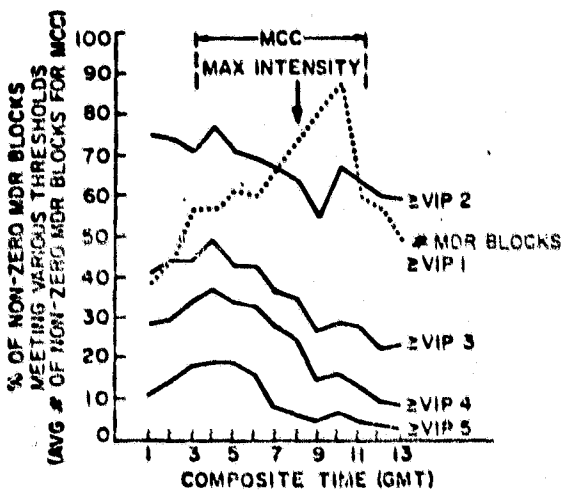

Figure 7. Composite MCC manually digitized radar intensity distribution. Compositing is the same as for Fig. 6, and included in the composite are all non-zero MDR blocks subjectively judged to be associated with the MCCs. Plotted are percentages of non-zero MDR blocks exceeding or equal to VIP levels 2, 3, 4, and 5, and the system-average number of non-zero blocks, as a function of composite time.

plexes were generated. The decreasing percentages of intense precipitation after maximum MCC intensity represent the decay of the meso-β complexes that support the meso-α system.

Figure 7 is a similar type plot of manually digitized radar (MDR) intensity distribution associated with the composite MCC. The plots

show that a maximum percentage of intense echoes occurs about the first hour or two after MCC initiation, suggesting that the severe weather potential is greatest in the early stages. However, the MDR intensities show significant steady decrease from the early stage maximum to after the maximum MCC intensity, while the intense precipitation percentages are steady or slightly increase during this period (Fig. 6). This is likely due to increased precipitation efficiency as the MCC region becomes saturated. The areal coverage of MCC precipitation, as implied by the dotted line in Fig. 7 showing the average number of non-zero MDR blocks, steadily increases to two hours after maximum intensity, then decreases sharply as the system begins to decay.

5. SUMMARY

From a detailed examination of three MCCs occurring in an episode of 14 total MCCs, the following conclusions are inferred:

1. The important meso-β scale complexes which give birth to the MCC tend to originate along larger, meso-α scale features, such as the lee-side of the Rockies, surface troughs or fronts, or regions of residual convection and mid-level moisture. The orogenic line of meso-β complexes is the most important, probably participating in most of the MCCs forming in western Kansas and Nebraska. It is not essential, however, as evidenced by those systems originating further east.

2. In all three cases, more than one meso-α scale feature as described above were important. The region of most intense meso-β convective development and MCC rapid growth is near the point where these meso-α features intersect.

3. The configuration of meso-β complexes appears to be somewhat random, unless controlling factors such as fronts or strong environmental shear force a preferred arrangement. The latter tends to produce meso-β squall-lines oriented perpendicular to the shear and also maintains the severe weather potential longer into the MCC life cycle.

4. In the absence of strong synoptic controlling influences (such as fronts), the decay of the MCC is characterized by (or perhaps caused by) the diffluent propagation directions of the meso-β elements.

5. The precipitation produced by an MCC is almost totally associated with the meso-β complexes. A widespread precipitation field does not occur on the scale of the meso-α cold cloud shield.

6. The potential for severe weather is greatest in the early MCC stage, while the percent area of intense rainfall (>0.50 in/hr) remains fairly steady until an hour or two after MCC maximum

ACKNOWLEDGMENTS

Dr. Peter J. Wetzel performed much of the preliminary analysis incorporated into this study. This research was supported under National Science Foundation Grant ATM-7908297, National Aeronautics and Space Administration Grant NSG-5341, and Office of Naval Research Grant N00014-79-C-0793.

REFERENCES

Cotton, W.R., R.L. George, and P.J. Wetzel, 1981: A long-lived mesoscale convective complex, Part I: The mountain generated component. Submitted for publication in Mon. Wea. Rev.

Fritsch, J.M., and R.A. Maddox, 1981: Convectively driven mesoscale weather systems aloft, Part I: Observations, Part II: Numerical simulations. J. Appl. Meteor., 20, 9-26.

Maddox, R.A., 1980: Mesoscale convective complexes. Bull. Amer. Meteor. Soc., 61, 1374-1387.

Maddox, R.A., 1981: The structure and life-cycle of midlatitude mesoscale convective complexes. PhD. thesis, Dept. of Atmos. Science, Colorado State Univ., Fort Collins, Colorado, 260 pp.

Means, L.L., 1944: The nocturnal maximum occurrence of thunderstorms in the midwestern states. Misc. Report No. 16, The Univ. of Chicago, 38 pp.

Miller, R.C., 1967: Notes on analysis and severe storm forecasting procedures of the Military Weather Warning Center. AWS Tech. Report 200 (available from Headquarters Air Weather Service, Scott AFB, Illinois), 94 pp.

Orlanski, I., 1975: A rational subdivision of scales for atmospheric processes. Bull. Amer. Meteor. Soc., 56, 527-530.

Porter, J.M., L.L. Means, J.E. Hovde, and W.B. Chappell, 1955: A synoptic study on the formation of squall lines in the north central United States. Bull. Amer. Meteor. Soc., 36, 390-396.

Wallace, J.M., 1975: Diurnal variations in precipitation and thunderstorm frequency over the conterminous United States. Mon. Wea. Rev., 103, 406-419.

Wetzel, P.J., W.R. Cotton, and R.L. McAnelly, 1981: A long-lived mesoscale convective complex, Part II: Morphology of the mature complex. Submitted for publication in Mon. Wea. Rev.